Dynamics and Historical Changes of the Petersen Ice Shelf and Epishelf Lake, Nunavut, Canada, Since 1959

Adrienne White

Thesis submitted to the
Faculty of Graduate and Postdoctoral Studies
in partial fulfillment of the requirements
for the M.Sc. Degree in Physical Geography

Department of Geography
Faculty of Arts
University of Ottawa

Supervisors:
Dr. Luke Copland (University of Ottawa)
Dr. Derek Mueller (Carleton University)

Thesis Committee:
Dr. David Burgess (Natural Resources Canada)
Dr. André Viau (University of Ottawa)

Abstract

This study presents the first comprehensive assessment of the Petersen Ice Shelf and the Petersen Bay epishelf lake, and examines their current characteristics and changes to their structure between 1959 and 2012. The surface of the Petersen Ice Shelf is characterized by a rolling topography of ridges and troughs, which is balanced by a rolling basal topography, with thicker ice under the surface ridges and thinner ice under the surface troughs. Based on thickness measurements collected in 2011 and area measurements from August 2012, the Petersen Ice Shelf has a surface area of 19.32 km^2 and a mean thickness of 29 m, with the greatest thicknesses (>100 m) occurring at the fronts of tributary glaciers feeding into the ice shelf. The tributary glaciers along the northern coast of Petersen Bay contributed an estimated area-averaged 7.89 to 13.55 cm yr^{-1} of ice to the ice shelf between 2011 and 2012. This input is counteracted by a mean surface ablation of 1.30 m yr^{-1} between 2011 and 2012, suggesting strongly negative current mass balance conditions on the ice shelf.

The Petersen Ice Shelf remained relatively stable until 2005 when the first break-up in recent history occurred, removing >8 km^2 of ice shelf surface area. This break-up led to the drainage of the epishelf lake once the ice shelf separated from the southern coast, providing a conduit through which the freshwater from the lake escaped. More break-ups occurred in summers 2008, 2011 and 2012, which resulted in a >31.2 km^2 loss in surface area (~63% of June 2005 area). While ephemeral regions of freshwater have occurred along the southern coast of Petersen Bay since 2005 (with areas ranging from 0.32-0.53 km^2), open water events and a channel along the southern coast have prevented the epishelf lake from reforming. Based on these past and present observations it is unlikely that Petersen Ice Shelf will continue to persist long into the future.

Acknowledgements

First, I would like to thank the various organizations that funded this research. Support for this project was provided by ArcticNet, Canada Foundation for Innovation, Ontario Research Fund, Canadian Space Agency's SOAR-E program, CRYO-EX, Carleton University, Fonds de recherche du Québec, the Garfield Weston Foundation, the Northern Scientific Training Program, National Sciences and Engineering Research Council of Canada (NSERC) Discovery Grant, the Polar Continental Shelf Project, Royal Canadian Geographical Society, and the University of Ottawa.

I would like to gratefully thank my supervisors Dr. Luke Copland and Dr. Derek Mueller for their guidance, inspiration, patience and providing me with the support to achieve my dream of seeing both the High Arctic and Antarctic. In addition I would like to thank Dr. Luke Copland for providing me with so many incredible opportunities to learn about glaciology in some of the most beautiful places on earth. I can't thank Luke enough for inspiring my love of travel and aviation, and for teaching me so much, from sliding steep scree slopes to avoiding bird strikes, and most importantly balance in life.

I would also like to thank Andrew Hamilton and Miriam Richer-McCallum for assistance with data collection and providing great company in the field. I would also like to thank Trudy Wohlleben for her support in the field and her mentorship. I would like to acknowledge the members of the Laboratory for Cryospheric Research for their advice, support and friendship. In particular, I would like to thank Wesley Van Wychen for his help with this study and Samantha Darling for being with me through the completion of this thesis. Thank you to my thesis committee members, Dr. André Viau and Dr. David Burgess, for their comments and suggestions which greatly improved the quality of this manuscript. I would also like to thank Faculty members including Sylvie Thériault for all her help and encouragement, as well as Jim McGrath for providing IT support.

Finally I would like to express my deepest thanks to my friends and family (my MLSI) for believing in me every step of the way. I am very grateful to my parents Richard White and Elisabeth Churcher who have always inspired in me what hard work and determination can bring. I am also grateful to Timothy Denton for providing the support for me to continue my education. I would like to thank Sue Warman for her kind words and encouragement. I want to thank my sister, Michelle White, her creativity, independence and determination are a huge inspiration. Last but certainly not least, I would like to thank Andy Snowdon, who listened to and encouraged me every day, and never for a second let me doubt myself. Thank you.

Table of Contents

List of Tables

List of Figures:

1. Introduction

The International Panel on Climate Change reported that atmospheric warming in the Arctic has been nearly twice that of the global average since the 1960s (Anisimov et al., 2007). According to the Arctic Climate Impact Assessment (ACIA) the average warming in areas north of 60°N has been 1-2°C since the temperature minimum in the 1960 and 1970s, and is projected to increase by 2° to 9°C by the year 2100 (McBean et al., 2005). Along with past increases in temperature, McBean et al. (2005) reported a probable increase in total precipitation (at a rate of 1% decade^{-1}), and a decrease in atmospheric pressure over the Arctic Basin, over the last century. As a result of this warming, the ACIA has also reported decreases in snow-cover extent (around a periphery of the Arctic), average sea ice extent (over the past 40 years), and multi-year sea ice (MYI) (in the central Arctic Ocean).

On Ellesmere Island, weather observations are available for Eureka since 1953. Based on this dataset Lesins et al. (2010) determined a mean annual surface warming of 3.2°C since 1972, with the least warming occurring in summer and a 10% increase in overall precipitable water since 1961, particularly in the spring, summer and fall. Along the northern coast of Ellesmere Island evidence for warming has been apparent through cryospheric changes such as the break-up of multi-year landfast sea ice (MLSI), and changes from perennial to annual lake ice cover (Mueller et al., 2009; Pope et al., 2012). Ice shelves located on the northern coast of Ellesmere Island have exhibited major changes over the past decade, including large-scale calving events, fracturing, and loss of freshwater lakes once dammed behind them (Copland et al., 2007; Mueller et al., 2003). While there is limited information concerning the relationship between climate and ice shelf stability in the Arctic, it is evident that climate is having a major impact on the Arctic cryosphere.

1.1 Arctic Ice Shelves

According to Dowdeswell and Jeffries (In press) an ice shelf is '*an ice mass of considerable thickness (>20 m) that is afloat on the ocean but attached to the coast. It is often of great horizontal extent (many km) and has, typically but not exclusively, a regularly undulating*

surface. An ice shelf can form by the seaward extension of a glacier or glaciers, or by formation of multiyear sea ice, or both, and thicken further by the accumulation of snow at the top surface and the accretion of ice from water at the bottom surface'.

Arctic ice shelves grow primarily via glacial input from grounded glaciers, and/or in situ growth of MLSI (sea ice that is attached to the coast and that has survived at least one melt season) (Lemmen et al., 1988). Secondary growth mechanisms include addition of mass through accumulation of snow and ice directly on the ice shelf surface, basal accretion of fresh, brackish, and sea water flowing below the ice shelf, and lateral accretion of MLSI along the fringe or seaward edges of the ice shelf (Jeffries, 1992a). After a calving event occurs, ice shelves commonly regenerate through the lateral accretion method (Jeffries, 1992a).

Ice shelves lose mass via surface and basal melt, and calving. Melting can occur on the surface of the ice shelf, and is strongly influenced by latitude and length of ablation season (Jeffries, 1992a). Calving events can produce ice islands (known as tabular icebergs in the Antarctic), which are distinguishable by their large size and typically undulating surface (consistent with the surface of their source ice shelf) (Koenig et al., 1952). Between 1946-1992, there were a total of ~600 ice island observations in the Arctic Ocean and surroundings (Jeffries, 1992a). The majority of these ice islands likely originated from the ice shelves of northern Ellesmere Island, particularly from the Ward Hunt Ice Shelf following calving events there in the 1960s (Spedding, 1977).

Ice shelves can be composed of different ice sources, such as glacial (classic ice shelf), sea ice (sea-ice ice shelf), or both (composite ice shelf), and all of these ice shelf types have been identified along the northern coast of Ellesmere Island (Dowdeswell & Jeffries, In press; Lemmen et al., 1988). For example, the Milne Ice Shelf can be considered a glacial ice shelf because it was formed primarily by glacial input from the Milne Glacier and surrounding glacier tributaries (Jeffries, 1986a). By contrast, the Ward Hunt Ice Shelf is considered to be an ice shelf formed by the growth of MLSI (Lemmen et al., 1988; Jeffries, 1991; Jeffries et al., 1988; Lyons et al., 1971). Both the sea ice and composite ice shelf types are uncommon in the Antarctic, and are one of the reasons why Arctic ice shelves are so unique.

1.2 Epishelf Lakes

According to Jungblut et al. (2012) '*epishelf lakes are an ecosystem type that occurs where ice shelves block the head of fiords and embayments, retaining a layer of freshwater (that has flowed in from terrestrial sources) over the marine water below*'. Epishelf lakes are formed as summer meltwater flows into a fiord or inlet and becomes dammed behind an ice shelf. A feature called a shallow ice-dammed lake is similar to an epishelf lake, except that it is dammed by MLSI. Because freshwater is less dense than ocean water, the freshwater remains as a permanently stratified layer, as deep as the draft of the ice shelf, overtop the salty marine water (Keys, 1977). A thick permanent ice cover over epishelf lakes protects the freshwater from wind-mixing, thereby maintaining its stratified structure. The lake ice also limits the amount of light that reaches the lake water below, thus creating a unique freshwater ecosystem. Because epishelf lakes are dependent upon the structural integrity of their adjacent ice shelf, changes in their existence is often used as indicator of changes in climate (Keys, 1977). The loss of epishelf lakes has major implications for the survival of rare cold-tolerant species of zooplankton that occupy these exclusive ecosystems (Jungblut et al., In press; Mueller et al., 2003; Veillette et al., 2008; Veillette et al., 2011).

1.3 Recent Ice Shelf and Epishelf Lake Changes in the Arctic

Approximately 4000 to 5500 yrs BP the ice shelves along the northern coast of Ellesmere Island began to form (Antoniades et al., 2011; England et al., 2008). According to radio-carbon dating studies, the sea-ice ice shelves (i.e. Serson and Ward Hunt ice shelves) formed first (Crary, 1960; Jeffries, 1992a; Lemmen et al., 1988), whereas the formation of glacial-ice ice shelves likely responded more slowly to climate deterioration (Lemmen et al., 1988). By the late 1800s and early 1900s, explorers such as Aldrich and Peary reported an extensive ice shelf fringe along the entire coast of Ellesmere Island, from Point Moss to Axel Heiberg Island (Jeffries, 1992a; Peary, 1907). This continuous fringe was termed the Ellesmere Ice Shelf (82-83°N, 64-90°W), and had a maximum area of ~8900 km² (Vincent et al., 2001). According to Veillette et al. (2008) there may have been up to 17 epishelf lakes dammed by the Ellesmere Ice Shelf at its maximum extent.

Prior to the 1950s, large scale disintegration decreased the area of the Ellesmere Ice Shelf into several individual shelves (including the Serson, Petersen, Milne, Ayles, M'Clintock, Ward Hunt, and Markham), and nine remaining ice-dammed lakes (including the Stuckberry, Moss, M'Clintock, Taconite, Ayles, Milne, Kulutingwak, Serson, and Philips) (Figure 1.1) (Jeffries, 1987; Koenig et al 1952; Veillette et al., 2008). In the 1960s several large calving events occurred, including massive losses from the Ward Hunt (which lost 596 km²), Ayles and M'Clintock ice shelves (Table 1.1) (Hattersley-Smith, 1966). After the 1960s, there was little change reported for the remainder of the 20th century (Jeffries & Serson, 1983; Mueller et al., 2003), except for 1980-1983 when Ward Hunt Ice Shelf calved an additional ~80 km² (Jeffries & Serson, 1983).

By the 21st century there were six major ice shelves remaining with a total area of ~1043 km² (Mueller et al., 2006). During the early 2000s, calving was limited to one event at the Ward Hunt Ice Shelf when ~6 km² of ice broke away from the ice shelf (Mueller et al., 2008). This event resulted in the complete freshwater drainage of Disraeli Fiord, the epishelf lake dammed behind the Ward Hunt Ice Shelf, when vertical fracturing through the ice shelf provided a conduit through which the lake could drain (Mueller et al., 2003). Large-scale collapses began in 2005 when the Ayles Ice Shelf was entirely lost (87 km^2), followed by a calving event of 12.6 km² from the Petersen Ice Shelf (Copland et al., 2007). The Petersen underwent further calving in 2006/07 with an area loss of 8 km² (Copland, 2009). In summer 2008, the next massive collapse took place when the Ward Hunt Ice Shelf lost 42 km², the Serson Ice Shelf calved 122 km², and the Markham Ice Shelf collapsed entirely (50 km²) (Mueller et al., 2008). In total, by the end of summer 2008 these multiple calving events lead to a combined loss of 23% of total remaining ice shelf area since the early 2000's, leaving behind 720 km² of ice shelf and one remaining epishelf lake behind the Milne Ice Shelf (Mueller et al., 2008; Veillette et al., 2008).

1.4 Research Rationale

The recent break up of ice shelves along the northern coast of Ellesmere Island has been linked to climate warming and to the loss of MLSI. The importance of MLSI as a protective barrier for ice shelves was apparent in 2005, when the Petersen Ice Shelf lost 20% of its area

within days of a break out of 1020 km² MLSI from Yelverton Bay (Copland et al., 2007). Since then, this MLSI has not reformed (Pope et al., 2012). These changes are of particular concern for the stability of the remaining Petersen Ice Shelf, yet no prior studies regarding the dynamics, physical characteristics or historical changes of this ice mass exist. This limits the ability to understand how the ice shelf is changing and to predict how it will react to climate forcing in the future. Furthermore, a study of the drainage of Disraeli Fiord (behind the Ward Hunt Ice Shelf) highlighted the importance of ice shelf integrity and stability in maintaining epishelf lakes (Mueller et al., 2003). Studies of the characteristics and recent changes of other Arctic epishelf lakes are limited and therefore the presence and recent changes to the Petersen Bay epishelf lake, in conjunction with changes to the ice shelf, will be investigated. This will place recent change to the freshwater layer into context of ice shelf changes.

1.5 Thesis Objectives

The overall objective of this thesis is to improve understanding of the historical changes, dynamics, and characteristics of the Petersen Ice Shelf and Petersen Bay epishelf lake, together with the relationships between these features. This is undertaken by:

1. Completing the first comprehensive survey of the Petersen Ice Shelf by quantifying historical changes in its areal extent (from 1950s to 2012), current thickness, and mass balance.
2. Confirming the existence and recent changes to the epishelf lake behind the Petersen Ice Shelf via SAR (synthetic aperture radar) backscatter analysis.

This research contributes to a broader project run by the University of Ottawa (Dr. Luke Copland) and Carleton University (Dr. Derek Mueller) that is improving understanding of ice shelf dynamics and the conditions leading to ice shelf collapse along the northern coast of Ellesmere Island.

1.6 Thesis Format

This thesis is presented in article format, with two manuscripts intended for publication. Chapter 2, 'Dynamics and Historical Changes of the Petersen Ice Shelf, Nunavut, Canada' and Chapter 3, 'An Analysis of Recent Changes to the Petersen Bay Epishelf Lake (1992-2012)' were both written by Adrienne White as separate manuscripts that will be submitted to a publication such as '*Journal of Glaciology*' or '*Journal of Geophysical Research*'. Luke Copland and Derek Mueller supervised and assisted with field work, data collection, and editing, and will be credited with secondary authorship in both manuscripts. Speckle tracking results were processed by Wesley Van Wychen in Chapter 2. Chapter 4 provides a general conclusion that summarizes the results presented in Chapters 2 and 3. The figures and tables are presented at the end of their respective chapters, but references cited throughout the entire thesis are listed after Chapter 4.

Table 1.1: Ellesmere Island ice shelf calving and fracture events from 1961-2011 (adapted from Table 1 in Copland, 2009).

Date	Ice Shelf	Event	Loss	Source
1961-1962	Ward Hunt Ice Shelf	Calving	596 km² or 50%	Hattersley-Smith, 1963
1982-1983		Calving	~80 km²	Jeffries & Serson, 1983
2000-2002		Calving	~6 km²	Mueller, 2003
2008		Calving	42 km²	Copland, 2009
2011		Calving	39 km^2	Kealey et al., 2011
2008	Markham Ice Shelf	Collapse	50 km² (Entire ice shelf)	Mueller et al., 2008
1962-1966	Ayles Ice Shelf	Calving	15 km²	Jeffries, 1986
2005		Collapse	87 km² (Entire ice shelf)	Copland et al., 2007
1955	Serson Ice Shelf[a]	Calving	no data	Jeffries, 1992a
2008		Calving	122 km² or 60%	Mueller et al., 2008
2011		Calving	32 km^2	Kealey et al., 2011
2005	Petersen Ice Shelf	Calving	12.6 km² or ~20%	Copland et al., 2007
2006-2007		Calving	8 km²	Copland, 2009

[a]Serson Ice Shelf was known as the Alfred Ernest Ice Shelf in literature prior to 2006

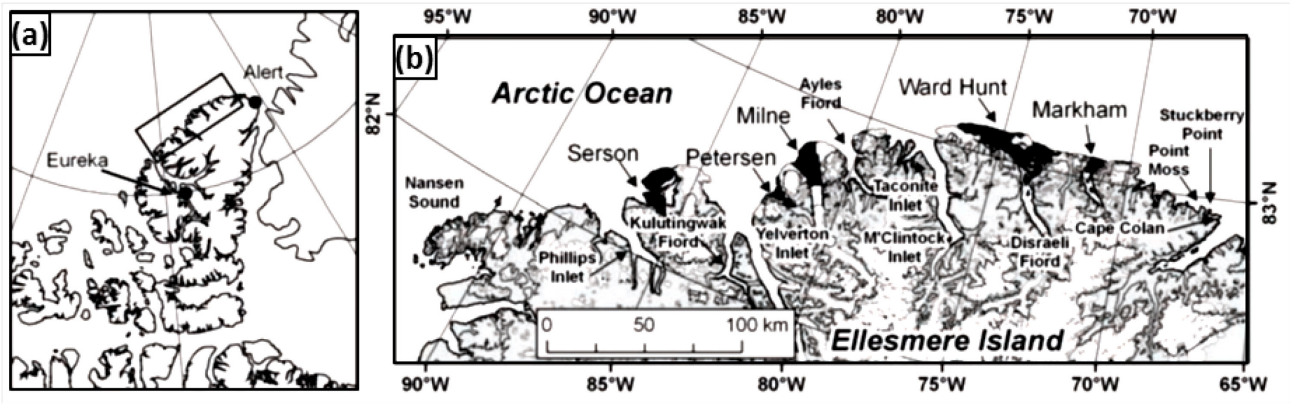

Figure 1.1: (a) Map showing the location of northern Ellesmere Island; (b) Map of the northern coast of Ellesmere Island showing the location of the ice dammed/epishelf lakes and ice shelves (shown in black) as of June 2008. Image adapted from Veillette et al. (2008).

2. Dynamics and Historical Changes of the Petersen Ice Shelf, Nunavut, Canada

2.1 Introduction

Ice shelves are features that occur at the boundary of coastlines and sea ice, and are found in the Antarctic and High Arctic. Arctic ice shelves are typically defined as a thick (>20 m) mass of floating ice that is attached to a coast, and are typically characterized by an undulating surface of ridges and troughs produced from winds and accentuated via meltwater ponds (Hattersley-Smith, 1957; Dowdeswell & Jeffries, In press). Arctic ice shelves form from glacier input and/or accretion of multi-year sea ice (MYI), and continue to gain mass by accumulation of snowfall and basal freeze-on (Dowdeswell & Jeffries, In press). Ice shelves can be composed of different ice sources, such as glacial (classic ice shelf), sea ice (sea-ice ice shelf), or both (composite ice shelf) (Dowdeswell & Jeffries, In press; Lemmen et al., 1988). Antarctica is dominated by classic ice shelves (glacial ice), which develop via the seaward extension of glaciers and ice streams that extend up to hundreds of kilometers from a point grounded on land (Dowdeswell & Jeffries, In press). In contrast, Arctic ice shelves are formed via growth of multi-year landfast sea ice (MLSI) (e.g., Ward Hunt Ice Shelf), glacial input (e.g., Milne Ice Shelf), or a composite of both (e.g., Serson) (Jeffries, 1991; Jeffries et al., 1988; Lemmen et al., 1988; Lyons et al., 1971).

While ice shelves are found in both the Arctic and Antarctic, they differ in scale, composition and distribution. Typically Antarctic ice shelves are much larger than Arctic ice shelves; for example, the Ross and Ronne ice shelves in the Antarctic are 10^5 km^2 in area and hundreds of meters thick, whereas the largest ice shelf in the Arctic is the Ward Hunt Ice Shelf on northern Ellesmere Island with an area (in 2003) of ~443 km^2 (Dowdeswell & Jeffries, In press; Mueller et al., 2003).

The distribution of ice shelves in the Arctic and Antarctic differs greatly. In the Antarctic, ice shelves fringe ~55% of the coast, while ice shelves in the Arctic are restricted to far northern areas such as Greenland, the Eurasian Arctic, and the northern coast of Ellesmere Island (Dowdeswell, In press; Dowdeswell & Jeffries, In press). The ice shelves along the northern coast of Ellesmere Island began to form 4000 to 5500 yrs BP (Antoniades et al., 2011; England et al., 2008). According to radio-carbon dating the sea-ice ice shelves (e.g., Ward Hunt) formed first, while the glacial ice shelves likely responded more slowly to a cooling

climate and formed later (Crary, 1960; Jeffries, 1992a; Lemmen et al., 1988). At the turn of the 20th century, expeditions led by Aldrich and Peary reported the first observations of an ice fringe, known as the Ellesmere Ice Shelf, along the entire coast of Ellesmere Island, from Point Moss to Axel Heiberg Island, with an estimated area of ~8900 km^2 (Figure 2.1a) (Vincent et al., 2001). Prior to the 1950s the area of the Ellesmere Ice Shelf was reduced into several individual ice shelves (Jeffries, 1987; Koenig et al., 1952). During the 1960s there were several calving events that included large losses from the Ward Hunt (596 km^2 between 1961 and 1962), Ayles (15 km^2 lost between 1962 and 1966) and M'Clintock ice shelves (~15 km^2 lost between 1962 and 1966) (Hattersley-Smith, 1966; Jeffries, 1986). For the remainder of the 20th century there was little change observed, with the exception of the Ward Hunt Ice Shelf which calved an additional 40 km^2 between 1982 and 1983 (Jeffries, 1982; Jeffries & Serson, 1983; Mueller et al., 2003).

By the start of the 21st century six ice shelves remained, comprising the Ward Hunt, Markham, Ayles, Serson, Milne and Petersen ice shelves, with a total area of ~1,043 km^2 (Mueller et al., 2006). There was one calving event (6 km^2 loss) between 2000 and 2002 at the Ward Hunt Ice Shelf, which was also associated with widespread fracturing and the drainage of a floating layer of freshwater (epishelf lake) to the landward side of the ice shelf (Mueller et al., 2003). By August 2005 large-scale collapses began to occur, resulting in the complete loss of the Ayles Ice Shelf (87 km^2) and a calving event at the Petersen Ice Shelf (12.6 km^2) (Figure 2.1b) (Copland et al., 2007). The summer of 2008 was a particularly active summer with collapses occurring at the Ward Hunt (42 km^2), the Serson (122 km^2) and the complete loss of the Markham Ice Shelf (50 km^2) (Figure 2.1c) (Mueller et al., 2008). The last major break-up of the Ellesmere ice shelves was reported during the summer of 2011 when the Serson lost an additional 32 km^2 and the Ward Hunt lost 39 km^2. This resulted in the total area of the Ellesmere ice shelves to be reduced to 563 km^2 by the end of 2011, approximately 54% of the total area in 2005 (Figure 2.1d) (Kealey et al., 2011).

2.1.1 Research Rationale and Objective

The recent break up of ice shelves along the northern coast of Ellesmere Island has been linked to climate warming and to the loss of MLSI (Copland et al., 2007). The importance of

MLSI as a protective barrier for ice shelves was apparent in 2005, when the Petersen Ice Shelf lost 20% of its area within days of a break out of 1,020 km² of MLSI from adjacent Yelverton Bay (Copland et al., 2007). Prior to 2005, the MLSI in Yelverton Bay may have been up to 70 years old (Copland et al., 2007; Pope et al., 2012) but since then it has only reformed occasionally as a fringe in front of the Petersen Ice Shelf (Pope et al., 2012). These changes are of particular concern for the stability of the remaining Petersen Ice Shelf, yet no prior studies regarding the dynamics, physical characteristics or historical changes of this ice mass exist. This limits the ability to understand how and why the ice shelf is changing, and to predict how it will react to current and future climate forcing.

The main objective of this paper is to conduct the first comprehensive survey of the Petersen Ice Shelf by quantifying historical changes in areal extent (from 1950s to 2012), current ice thickness and surface mass balance. In addition, the importance of glacial ice input will be determined using speckle tracking of Radarsat-2 image pairs to derive glacier motion.

2.1.2 Study Site

The Petersen Ice Shelf (unofficial name) (82°31' N, 81°45' W) is located on the northern coast of Ellesmere Island and occupies Petersen Bay, which opens towards the west into Yelverton Bay (Figure 2.2). The study site includes the ice shelf, a fringe of MLSI on the west side of the ice shelf, two tributary glaciers (Glaciers 1 and 2) and the remaining ice cover of Petersen Bay. The ice shelf is up to 17 km long and 12 km wide with an approximate area in 2000 of 51.2 km² (Mueller et al., 2006). The surface of Petersen Ice Shelf is characterized by elongated troughs and ridges, with mixed orientations at the front and a north-west/south-east orientation at the back. Based on the 2009 ASTER image shown in Figure 2.2 there appears to be curved moraines towards the front of the ice shelf. Six glaciers flow towards Petersen Bay: three along the northern edge and three along the southern edge of the bay (Figure 2.2). However, only two of these glaciers are currently connected to the northern side of the ice shelf (Glacier 1 and Glacier 2 in Figure 2.2). An epishelf lake (~4.6 km^2 in 1992), a freshwater layer dammed by the draft of the ice shelf and permanently stratified over marine water below, existed along the southern coast of the ice

shelf until a break-up event in 2005, which drained the freshwater from this area. Since this drainage event, the southern coast of Petersen Bay has been covered by first-year sea ice (FYI) and MYI (see Chapter 3). There are also two rock islands located in the south-central portion of the ice shelf.

2.1.2.1 Climate

There are few long-term climate records for Ellesmere Island, although weather observations are available for Eureka (~300 km southwest of Petersen Ice Shelf) since 1953. According to the measurements collected in Eureka (1954-2007), the average annual air temperature is -19.1°C (Lesins et al., 2010). Temperatures since 1954 demonstrated a decreasing trend (total of ~2°C) until the 1970s. Except for a brief cooling period in the early 1980s, temperatures have been warming consistently (total of 3.2°C) since 1972 (Lesins et al., 2010). An automatic weather station in Purple Valley (Figure 2.2) has been recording surface temperatures since June 3, 2009. Since this time, the maximum surface air temperature recorded has been 20.1°C (July 18, 2012), and a minimum surface air temperature of -50.1°C (February 7, 2011).

2.2 Methods

To assess the characteristics and recent changes of the Petersen Ice Shelf, this study used a combination of fieldwork and remote sensing measurements to investigate three main objectives: area changes, ice thickness, and mass balance. During fieldwork in May 2011 and 2012, field sites were accessed via snowmobile from a base camp in Purple Valley (82°28.983'N, 80°59.983'W), approximately 10 km to the east of the ice shelf. Area changes of the ice shelf were assessed from 1959 to 2012. Measurement of the ice thickness also included the derivation of basal topography and ice core analysis. Mass balance investigations included ground-based ablation measurements and the use of remote sensing data to determine surface motion across the front of tributary glaciers to estimate mass inputs. In addition, the results of this study will provide information about the future stability

of the ice shelf and a baseline against which future monitoring studies can compare their results.

2.2.1 Quantifying Temporal Area Changes

Changes in the areal extent of the Petersen Ice Shelf were determined using georectified aerial photographs (partial coverage in 1959, 1974 and 1984), optical satellite imagery from Landsat 7 (1999) and ASTER (2001-2003 and 2005-2010), and Radarsat-2 satellite imagery (2011 and 2012) (Table 2.1). For the aerial photographs, multiple vertical (nadir) images were acquired from the National Air Photo Library in Ottawa, Canada, in TIFF format at a resolution of 1200 dpi (dots per inch). The 1959 photographic set had the most extensive coverage, excluding only the back of the ice shelf, while the 1974 and 1984 images covered only the very front of the ice shelf. The air photographs for each year were cropped and converted to grayscale and then mosaicked to create one continuous image for each year. Areas with missing coverage are assumed to have not changed for the purposes of this study.

Both the aerial photography and satellite imagery were georeferenced against a master image (ASTER L1B, July 16, 2009) to ensure alignment of all scenes used in the study. The images were processed in ArcGIS 9.3.1 by first projecting the data (WGS 84, UTM Zone 17N), and then performing a shift to align the image to the master image. Where necessary, the images were then georectified using between 10 and 16 ground control points (GCPs) while attempting to maintain an RMSE less than the pixel size of the image. The GCPs were applied to areas of stable exposed land, and were as widely distributed across the image as possible (Table 2.1). Because the 1974 and 1984 air photographs had limited land coverage, distinctive, stable meltponds on the surface of the ice shelf were also used to provide GCPs. A first order polynomial interpolation was used to transform the photographs and complete the georectification. The air photographs have higher geolocation RMSEs than the satellite imagery with values of 33.25 m (1959), 23.67 m (1974) and 38.22 m (1984). The RMSE for satellite imagery geolocation was lower with values of 14.66 m (2001), 15.45 m (2002) and 14.93 m (2003). The average RMSE for all scenes was 23.36 m. For satellite imagery which only required shifting into place by alignment with stable features in the base image, rectification with GCPs was not required and therefore no RMSE was recorded.

The changes in ice shelf area between scenes were measured in ArcGIS 9.3.1 by digitizing a polygon that delineated the ice shelf extent in each image and then calculating the area of each extent. The characteristic undulating topography of the ice shelf surface guided the discrimination between ice shelf and other ice types. In this study, the area of the ice shelf was calculated using only the contiguous ice mass, which did not include ice detached from the main ice shelf even if it was still attached to the coast. By differencing the total area of the polygon between each year of study, the temporal change in ice shelf extent was determined.

2.2.2 Quantifying Ice Thickness

A Pulse EKKO Pro 250 MHz Ground Penetrating Radar (GPR) system (Sensors and Software Inc.) was used to measure ice thickness across the Petersen Ice Shelf via a reflection type survey in May 2011. A time window of 1500 ns was set for the GPR, enabling identification of a maximum ice depth of ~190 m, while the sampling interval was set to 0.40 ns, and the antenna separation was 0.40 m. The GPR system was custom-fitted into a sled and towed behind a snowmobile at ~20 km hr^{-1}. A grid-like pattern was followed where possible, but steep local topography and safety considerations prevented this pattern in some locations, particularly near the ice shelf front. A secondary survey was also conducted on the ice shelf to examine changes in thickness across the surface ridge and trough topography of the ice shelf on a smaller scale. A single frequency StarGPS receiver was connected to the DVL and used to record the position of each GPR trace.

The GPR data was processed in EKKO View Deluxe Version 1.4 (Sensors and Software Inc.) and converted to ice thickness in IcePicker Release 4 (Sensors and Software Inc.). In EKKO View Deluxe, a DEWOW time filter was first applied as a signal saturation corrector (Sensors & Software, 2003). A trace difference was then applied to the data to enhance rapidly changing features (e.g., changes in ice thickness) and suppress flat-lying and constant features (e.g., background noise). Repeat traces, which occurred while the GPR was immobile, were deleted.

IcePicker Release 4 was used to pick the snow-ice interface and bed reflections to derive ice thicknesses using the following equation:

$$T = \sqrt{\left(\frac{\left(t + \frac{s}{0.3}\right)}{2}\right)^2 V_I - \frac{s^2}{4}} \quad \textbf{(1)}$$

where T is ice thickness (m), t is two way travel time (ns), s is the antenna separation (0.40 m in this study) and V_I is the electromagnetic wave velocity (m ns^{-1}) of the material. Based on previous studies using GPR to determine thickness in sea ice across Yelverton Bay and glacial ice on the Milne Ice Shelf, an electromagnetic wave velocity of 0.20 m ns^{-1} was selected for snow, 0.15 m ns^{-1} for sea ice, and 0.17 m ns^{-1} for ice shelf ice (Mortimer, 2010; Pope et al., 2012). Pope et al. (2012) verified the accuracy of the 0.15 m ns^{-1} value by comparing GPR-derived thickness measurements to borehole measurements. Mortimer (2010) derived the 0.17 m ns^{-1} value by conducting a common midpoint survey on the Milne Fiord epishelf lake. The snow to ice (i.e., near surface) and ice to underlying water (i.e., basal) interfaces were processed separately to isolate ice thickness data.

The errors associated with GPR system resolution and reflection picking were summed to determine the total error for the ice thicknesses recorded across Petersen Ice Shelf. The GPR system resolution is typically 10% of the transmitted wavelength, (Bogorodsky et al., 1985), which accounts for an error of ±0.07 m for a 250 MHz GPR system. To examine reflection picking error a cross point analysis was conducted, which involved determination of the difference between ice thicknesses derived from independent transects that crossed within 2 m of each other (Figure 2.3; Table 2.2). A total of 16 cross points were identified in the 2011 dataset, 12 across the ice shelf and four over the epishelf lake. The cross points from the ice shelf provide a range of error between 0.1 and 11.7% of the ice thickness, with a mean error of 3.9%. For the epishelf lake, error between transects ranged from 7.8 to 23.9% of the ice thickness with a mean error of 17.4%. To provide conservative error estimates for use in

calculations of mass flux from the tributary glacier, the maximum error of 11.7% of the ice shelf thickness was applied.

Processed radargrams obtained through measurements with the PulseEKKO Pro GPR provided a visual check on the effectiveness of the system. At most locations the radargrams showed a distinct boundary at the snow-ice and ice-ocean interfaces, facilitated by the strong dielectric contrast between these layers. However, signal attenuation occurred intermittently across the thinner areas of the ice shelf, primarily in the eastern third. To investigate the causes of this attenuation, a small rectangular (400 m long and 100 m wide) grid survey was conducted in this region (Figure 2.4). The grid consisted of 4 long transects and 7 shorter perpendicular lines. In May 2012 a 13.24 m ice core was also extracted from the top of a ridge within this grid where basal reflections were weak. The temperature profile along the core was measured by drilling into it as the ice was extracted and inserting thermometers every 10 cm. The ice core was then sawed into 10 cm segments, bagged and analyzed for bulk salinity. Within 24 hours of extraction, the ice core segments were photographed and melted for conductivity and temperature measurement with a YSI Pro Plus multi-parameter water quality meter. Conductivity was converted to salinity using the calculation by Fofonoff and Millard (1983). Visual observation of each core segment was also conducted to examine characteristics such as colour, cloudiness, and bubble size, shape and pattern.

2.2.3 Mass Balance

To measure surface mass balance, a total of four 3 m long ablation stakes were drilled into the ice shelf surface and one tributary glacier (Glacier 2) in May 2011. In May and June 2012, two of the four ablation stakes were re-measured to determine annual surface lowering. The value for surface lowering was converted to units of water equivalent (w.e.) by using an ice density of 0.90 g cm^{-3}.

2.2.3.1 Ice Motion: Differential GPS

To obtain ground-based velocity measurements, a Trimble R7 dGPS receiver was used to determine the change in position of two ablation stakes between May 2011 and May/July

2012. In 2011 the dGPS antenna was mounted on the top of each ablation stake and recorded every 15 seconds for a minimum of 30 minutes. In May and July 2012 the ablation stakes were re-measured with the same protocol, while an occupation time of 20 minutes was used for the stake on the tributary glacier. The dGPS data was processed in static mode using the precise point positioning (PPP) service of Natural Resources Canada, which provides an estimated horizontal positional accuracy of ~2-3 cm and eliminates the need for a local base station.

2.2.4 Ice Motion: Speckle Tracking

Speckle tracking is a remote sensing technique that uses a two-dimensional cross-correlation algorithm to estimate the relative motion of ice masses from pairs of coherent SAR imagery (Short & Gray, 2004; Short & Gray, 2005; Van Wychen et al., 2012). In this study, a speckle tracking script developed in MATLAB by Dr. Laurence Gray of the Canadian Centre for Remote Sensing (Short & Gray, 2005) was used to estimate the surface motion across tributary glaciers 1 and 2 (Figure 2.2). The SAR imagery applied in this study included a pair of single look complex (SLC) Radarsat-2 Ultrafine Wide images that were acquired on a repeat 24 day orbit (April 25th and May 19th, 2012). The images were acquired prior to the melt season to ensure that the surface properties of the ice (i.e., coherence) remained similar between acquisitions. The surface displacement was determined in both azimuth and range directions using image chip sizes of 301 pixels (~600 m) for both components of motion, which enabled calculation of total motion. These chip sizes are default values used in processing of other high Arctic imagery, and were deemed appropriate for the size of the glaciers investigated here (Van Wychen, pers. comm., 2012). A 1:250 000 Canadian Digital Elevation Dataset (CDED) for Nunavut, resampled to a 100 m grid spacing, was applied to the output of the image cross-correlation to remove the topographic component of the slant range displacement, and therefore facilitate the conversion to ground range displacement. The displacements in range and azimuth were calibrated over areas with zero motion such as rock outcrops. Velocities were calculated based on this calibration and converted to annual values (Short & Gray, 2005; Van Wychen et al., 2012).

Errors from the final speckle tracking output arise from mismatches, where cross correlation finds a better match with an incorrect area, rather than the actual match. This type of error normally occurs in areas of phase decorrelation due to changes in surface features (e.g., snowfall, wind distribution, melt) and along shear margins where phase may change substantially over a period of 24 days due to rapid changes in surface motion. Obvious erroneous points were identified and deleted manually in ArcGIS where flow direction did not follow the surrounding topography and/or where flow vectors changed dramatically (in magnitude or direction) or were inconsistent with adjacent vectors (Van Wychen et al., 2012).

A final raster velocity map was generated in ArcGIS using an inverse distance weighting (IDW) algorithm on the point velocity values derived from the speckle tracking. IDW algorithm provides a conservative approach to interpolation as it does not allow new values to exceed those in the original dataset (ArcGIS, 2009). The IDW algorithm produced the raster with a 50 m resolution, using a fixed search window of 250 m to create each pixel raster value. Error was calculated by the apparent motion derived from 43,994 speckle tracking matches over stable bedrock outcrops. The mean error using this method was 5.09 m yr^{-1} with a standard deviation of 3.65 m yr^{-1}.

The velocity derived from speckle tracking was combined with ice thickness measurements to estimate the mass input from Glaciers 1 and 2 to the ice shelf. Because no thickness data was available for Glacier 1, three flux scenarios were generated with assumed depths of 50 m, 75 m, and 100 m derived from the GPR measurements on Glacier 2. Flux gates were defined along the boundary of Glaciers 1 and 2 where they meet the ice shelf, with Glacier 1 separated into six 250 m segments, and Glacier 2 into eight 250 m segments (Figure 2.5). Due to the lack of thickness measurements the GPR point(s) nearest to each 250 m segment for Glacier 2 was used to determine a mean thickness based on a linear interpolation (Figure 2.5). The velocity across each segment was determined by calculating the mean of the nearest velocity points (within 40 m) to each flux gate (Figure 2.5). For each 250 m segment the following equation was used to determine ice flux (Q):

$$Q = ((V * 0.8) - V_{error})(h - h_{error})(W) \quad \textbf{(2)}$$

Where V is surface velocity, V_{error} is velocity error, h is ice thickness, h_{error} is ice thickness error and W is column width (250 m). A multiplication factor of 0.8 was used to convert surface velocity to depth-averaged velocity based on the theoretical measurements outlined by Paterson (1994). Because the velocities for Glacier 2 used in this calculation were within the margin of error (5.09 m yr^{-1}), velocity error was not accounted for in the flux calculation. The mass from each segment was summed to determine the ice flux along the total 1500 m flux gate at Glacier 1 and 2000 m flux gate at Glacier 2. It should be noted that the flux calculations are based on wintertime velocities (April 25 to May 19, 2012).

2.3 Results

2.3.1 Area Changes

2.3.1.1 Area Changes: 1959 to 1999

A 1.5 km^2 cumulative increase in total ice shelf area occurred between 1959 (48.40 km^2) and 1999 (48.87 km^2) (Figure 2.6; Table 2.3). This increase is largely attributable to an advance of the ice shelf front due to a ~250 m advance in the north-western portion of Glacier 1 (Figure 2.2). The increase in extent may also be attributed to the development of widening fractures visible in the 1999 image. Along the southern margin of the ice shelf, to the east of the islands, there was a 0.76 km^2 decrease in area between 1959 and 1999.

The years from 1999 to 2005 represented a period of little change to the ice shelf (-1.41 km^2 to +0.96 km^2). However, since 2005 there have been more dramatic changes in extent than have ever previously been observed; the following sections describe years when annual losses have been >2 km^2.

2.3.1.2 Area Changes: Summer 2005

An 8.06 km^2 reduction in ice shelf area was measured between June 3, 2005 (48.92 km^2) and July 24, 2006 (40.84 km^2). This was the first major break up of the Petersen Ice Shelf during

the period of study, and accounted for a loss of 16.5% of total area as a result of disintegration of the ice shelf front. This loss primarily occurred between August 5-18, 2005, at the same time as the loss of >690 km^2 of 55-60 year old MLSI from Yelverton Bay (Copland et al., 2007). This included the MLSI which existed at the front of Petersen Ice Shelf (Pope et al., 2012). Little change was observed along the southern margin of the ice shelf, although a channel from the epishelf lake to the ocean appeared to open in this region at this time and allow freshwater from the epishelf lake to completely drain away. The drainage of the lake was confirmed through backscatter analysis of SAR data, which showed a shift from high backscatter (>6 dB) consistent with freshwater ice to lower backscatter values consistent with sea ice (see Chapter 3; Veillette et al., 2008).

Through observations made with Radarsat-1 data, changes in the ice shelf and epishelf lake were analysed on March 18, August 18, August 23 and September 26, 2005 (Figure 2.7). The Radarsat-1 scene from March 18, 2005, shows the ice shelf prior to break up, with the ice shelf intact, the epishelf lake contained (characterized by bright backscatter in the SAR image), a large fracture in the MLSI at the front of the ice shelf and one through the center of the ice shelf (running north-south) (Figure 2.7a). The fracture through the center of the ice shelf was first observed in the 1999 image, but had remained static since then.

According to the Radarsat-1 data from August 18, 2005, the MLSI, once identifiable by a rolling surface containing thin linear melt-ponds (relative to the ice shelf), had disappeared and open water (appearing smooth and dark in the SAR imagery) became visible (Figure 2.7b). The front of the ice shelf had disintegrated into hundreds of pieces up to 0.48 km^2 in area. A meandering open water channel appeared along the southern margin of the ice shelf, between the ice shelf and the land, leading from the epishelf lake to the head of Petersen Bay. Areas of open water were also observable in the epishelf lake at the rear of Petersen Bay, identifiable by a smooth dark texture on the Radarsat-1 image.

By August 23, 2005, the Radarsat-1 image showed that an ice island measuring 6.47 km^2 had calved along the pre-existing north-south fracture near the front center of the ice shelf (Figure 2.7c). Pack ice filled the majority of the bay at the front of the ice shelf at this time.

The ice island appeared to rotate away from the ice shelf toward the south-west, with a wide opening (~250 m) between the ice shelf and the island at the northern end of the fracture, but it abutted against the ice shelf at the southern tip of the crack. However, complete break away of the ice island was prevented by the pressure of the pack ice which had moved south-east by September 26, 2005 (Figure 2.7d). The pressure applied by the motion of the pack ice caused the fracture to be closed and the ice island to freeze back in place.

2.3.1.3 Area Changes: Summer 2008

Petersen Ice Shelf underwent a second major break up when its area reduced from 40.97 km^2 to 31.98 km^2 between July 19, 2007 and August 22, 2008, as measured in the ASTER L1B satellite scenes. The 8.99 km^2 loss occurred in the summer of 2008 and marked a 21.9% reduction in the remaining ice shelf area. This loss primarily occurred due to calving at the seaward front of the ice shelf (in summer 2008) along the pre-existing fracture, causing the release of the ice island that was trapped at the terminus in September 2005. The break along the fracture caused a release of ice islands with individual areas up to 0.9 km^2 (those that were visible in the August 22, 2008 ASTER image). The 2008 satellite image also showed the entire front of Petersen Bay as open water, including the epishelf lake to the south of the ice shelf. A clear open water channel is visible between the coastline and the ice shelf in August 2008, as in 2005, connecting the epishelf lake to the ocean and preventing any chance of freshwater layer reformation. The ice loss from Petersen Ice Shelf in 2008 coincided with further loss of MLSI remnants from Yelverton Inlet by September 2005 (Pope et al., 2012).

2.3.1.4 Area Changes: Summer 2011

Between April 1, 2011 and February 3, 2012 the surface area of Petersen Ice Shelf decreased from 30.29 km^2 to 24.81 km^2, a total loss of 5.48 km^2. These losses primarily occurred in summer 2011, from both the front and southern coast of the ice shelf, resulting in an 18% reduction in remaining area. A loss of 3.63 km^2 occurred at the seaward front, including the separation between the main ice shelf and a remnant piece on the north-west corner of the ice shelf along the edge of the Cape Evans Ice Cap. Losses along the southern edge of the ice

shelf amounted to 2.67 km^2 and subsequently led to expansion of the ice shelf-free zone along the southern coast of Petersen Bay. This expansion occurred predominantly in the north-west section of the southern coast.

2.3.1.5 Area Changes: Summer 2012

Radarsat-2 imagery from August 24, 2012 revealed a loss of 5.49 km^2 (22% reduction) from the Petersen Ice Shelf compared to the end of summer 2011, resulting in an ice shelf area of 19.32 km^2. This loss, which occurred predominantly at the back of the ice shelf, resulted in the production of several large ice islands up to ~1.13 km^2 in surface area. The Radarsat-2 image also revealed open water surrounding the ice shelf, including the southern coast of Petersen Bay and across the outlet into Yelverton Bay. Following this break-up, the remaining ice shelf area was limited to the region adjacent to the termini of Glacier 1 and Glacier 2, extending southward toward the large island in the central region of Petersen Bay.

2.3.2 Ice Shelf Thickness

The mean thickness of the Petersen Ice Shelf was 29 m in spring 2011, with a standard deviation of 24 m (Figure 2.8; Table 2.4). The thickness increased with proximity to the two tributary glaciers. This was particularly true for Glacier 2, which ranged in thickness between 34 and 106 m and had a mean thickness of 70 m. Away from the glacier termini ice thicknesses were less, ranging between <1 m and 72 m, with a mean of 23 m. The sea ice (previously lake ice; see Ch3) to the south of the ice shelf had a mean thickness of 0.8 m and standard deviation of 0.2 m. The thicker areas of the sea ice were located in the eastern portion of the southern coast (at the back of the ice shelf), where the mean thickness measured ~0.9 m.

2.3.3 Ice Core Analysis

From the ice surface down to ~3.0 m, the ice shelf core was characterized by clear ice with small (<1 mm) bubbles scattered throughout (Figure 2.9a). The bulk salinity in this section of the core was near zero (Figure 2.9c) and the temperature was relatively stable throughout at

approximately -15^{0}C (Figure 2.9d). From 3.0 to ~5.5 m, rounded bubbles were slightly larger (1- 3 mm) and the ice was slightly cloudy. The bulk salinity remained <1 psu and the temperature increased to -10^{0}C. From 5.5 m down the remainder of the core (to 13.24 m), the ice was white with vertical trains of elongated connected bubbles and a lamellae crystal structure that became apparent at a depth of ~7 m. This transition in ice type is reflected in the salinity profile, where the salinity goes up to >2 psu at a depth of 5 to ~6 m. From 10.7 m to 11.15 m particles of debris were apparent in the core and a layer of slush was found at 11.11 m with an extremely high salinity of >79 psu. At the base of the core, bubble trains became longer, larger and transformed into vertical brine channels between 11 m and 13 m. The effect of the concentration of brine in these channels is shown in the profile, where salinity peaked with >4 psu at 12 m depth (Figure 2.9c). The temperature peaked at the base of the core at ~-5^{0}C. It should be noted that this ice core did not penetrate the full ice shelf thickness.

2.3.4 Surface and Basal Topography

The GPR data that had strong basal reflections were combined with the GPS elevations (accuracy ~±5 m) to derive surface and basal topography (Figure 2.10). Traces that did not have a detectable bottom-trace were filtered out of the dataset. The rolling topography was gradual at the back of the ice shelf and steeper in the central and outer portions of the ice shelf. The results display a connection between thicker surface ice and thicker basal ice, or in other words high surface ridges correlating to deep basal ridges (Pearson's r=0.659, n=12,920, p <0.0001).

2.3.5 Surface Mass Balance

Losses from the Petersen Ice Shelf due to calving were measured as changes in extent (above), but this yielded only partial mass balance information as it did not account for gains and losses at the base of the ice shelf due to melting and/or freeze-on. To complement this, the surface mass balance and flux from Glaciers 1 and 2 was measured. The P2 ablation stake indicated surface ablation of 1.42 m yr^{-1} (1.28 m w.e. yr^{-1}) between May 17, 2011 and May 11, 2012, and motion towards the south by 9.46 m (Figure 2.11). At the back of the ice

shelf, the P1 ablation stake showed 1.19 m yr^{-1} (1.07 m w.e. yr^{-1}) of surface lowering and motion towards the south east by 4.18 m.

2.3.6 Glacier Tributary Surface Velocities and Mass Flux

Figure 2.11 shows the surface velocities of the ice shelf and tributary glaciers between April 25 and May 19, 2012, standardized to values of m yr^{-1}. The speckle tracking velocities determined within 50 m (one pixel spacing) of the ablation stakes (P1 and P2) showed differences in velocity within the range of error. At ablation stake P2, the nearest speckle tracking point displayed movement of 7.6 m yr^{-1} with a bearing of 177.3°, while the ablation stake moved 9.03 m yr^{-1} with a bearing of 184.7°. At P1 (at the eastern side of ice shelf), the nearest speckle tracking point moved 9.6 m yr^{-1} with a bearing of 55.8°, while the dGPS at the ablation stake recorded 4.05 m yr^{-1} with a bearing of 154.6°. The difference in bearing between the velocity vector and the ablation stake measurement was 7.4° at P2, and 98.8° at P1. These differences are likely attributed to the error limits of the speckle tracking method and to the difference in time scale between the measurement dates for the ablation stakes (>1 year) and speckle tracking (<1 month).

The velocity of the main trunk of Glacier 1 varied between 1 and 87 m yr^{-1}, with a mean of 33 m yr^{-1} and standard deviation of 21 m yr^{-1} (Figure 2.11). The velocities at the boundary between Glacier 1 and the ice shelf ranged between 0.3 and 77 m yr^{-1} with a mean of 20 m yr^{-1} and standard deviation of 12 m yr^{-1}. Along the main trunk of Glacier 2, surface velocities derived from speckle tracking ranged from 1 m yr^{-1} to 98 m yr^{-1} with a mean of 14 m yr^{-1} and a standard deviation of 10 m yr^{-1}. The area of the ice shelf directly adjacent to the terminus of Glacier 2 had velocities that ranged from 1 to 29 m yr^{-1} with a mean of 7 m yr^{-1} and standard deviation of 5 m yr^{-1}. In combination with the GPR thickness measurements collected at the terminus (Figure 2.5), the total flux into the ice shelf from Glacier 2 was estimated at 556,119 m^3 yr^{-1}. If this mass is distributed evenly across the February 2012 ice shelf area (24.8 km^2), it would equate to an ice thickness of 2.24 cm yr^{-1}. Because of lack of thickness measurements at Glacier 1, three flux scenarios were generated with assumed depths of 50 m (lower bound), 75 m (similar to Glacier 2), and 100 m (upper bound) along the 1500 m long

flux gate. Assuming a 50 m thickness, the total flux from Glacier 1 would be 1,402,705 m^3 yr^{-1} (5.65 cm yr^{-1} equivalent ice shelf thickness). With thicknesses of 75 m and 100 m, the mass flux from Glacier 1 would be 2,104,058 m^3 yr^{-1} (8.48 cm yr^{-1}) and 2,805,410 m^3 yr^{-1} (11.31 cm yr^{-1}), respectively.

2.4 Discussion

2.4.1 Area Changes Across the Petersen Ice Shelf (1959 to 2012)

Over the past 53 years the greatest area changes for the Petersen Ice Shelf occurred in summer 2005 (-8.07 km^2), summer 2008 (-8.99 km^2), summer 2011 (-5.48 km^2), and summer 2012 (-5.49 km^2). The break up in summer 2005 coincided with the loss of 690 km^2 of MLSI from the Yelverton Bay region directly in front of the Petersen Ice Shelf, as well as the complete loss of the nearby Ayles Ice Shelf (87 km^2). According to a study of the Ayles Ice Shelf by Copland et al. (2007), climatic factors leading to its break-up included the occurrence of the second highest number of positive degree days (PDD) on record (over the period 1948 to 2006), an early start to the 2005 melt season, a long-term reduction in freezing degree days (FDDs), temperatures almost continuously above the long term mean (1948-2006), and particularly warm temperatures in July 2005 (2.1^{0}C above average). Copland et al. (2007) also related the loss to record low sea ice extent (21% below 1979-2000 average and 7% below previous record low in 2002) (Serreze et al., 2007), and noted the loss of the Nansen and Sverdrup ice plugs (which had previously only broken up twice since 1961) (Alt & Wilson, 2006). Copland et al. (2007) also determined that during the first two weeks of August 2005 offshore and along-shore winds along northern Ellesmere Island were unusually strong (up to 25 m s^{-1}), which when combined with the westward flowing Beaufort Gyre would remove the typical support from pack ice and MLSI against the coast of northern Ellesmere Island. Without the protection from MLSI, ice shelves are vulnerable to calving due to thermal and mechanical erosion from waves, as well as collisions with mobile pack ice (Copland et al., 2007). Furthermore, without sea ice at the front of an ice shelf, ice islands are able to separate from the ice shelf along pre-existing fractures. These factors likely contributed to the calving of the Petersen Ice Shelf.

In 2008, when the Petersen experienced its next large break-up (8.99 km^2), simultaneous break-ups occurred at the Ward Hunt (42 km^2), Markham (50 km^2, entire ice shelf) and Serson (122 km^2) ice shelves (Copland, 2009). These changes were accompanied by unusually warm temperatures recorded on Ward Hunt Island of up to 20^0C in summer 2008 and open water along the northern coast of Ellesmere Island. Furthermore, remnants of MLSI in Yelverton Bay and Inlet were removed and replaced with FYI (Pope et al., 2012).

In summer 2011, Petersen Ice Shelf underwent a reduction in area of 5.48 km^2. During the time of this calving event in 2011, losses to the Serson (32 km^2) and Ward Hunt (39 km^2) ice shelves also occurred. According to air temperature data from Eureka weather station (http://www.climate.weatheroffice.gc.ca/climateData/canada_e.html), 2011 had the warmest mean summer temperature since 1947. The mean summer (June to August) air temperature at Eureka in 2011 was 1.84^0C higher than the recorded mean summer temperature in 2009. MODIS summer imagery from August 2011 shows open water conditions along the northern coast of Ellesmere Island, thus exposing the ice shelves, including the Petersen Ice Shelf, to the effects of wind and wave action.

The last recorded loss of the Petersen Ice Shelf occurred in summer 2012, with a reduction in area of 5.49 km^2. With the exception of summer 2011, summer 2012 had the highest mean summer temperature (6.4°C) since 1947, based on the June to August daily air temperature data from the Eureka weather station. MODIS imagery from July and August 2012 reveal open water condition along the northern coast of Ellesmere Island, while Radarsat-2 imagery (August 24, 2012) shows open water surrounding the ice shelf in Petersen Bay. The warm summer temperatures and open water conditions, observed in previous break-up years, would have facilitated the calving events observed from the Petersen Ice Shelf in August 2012.

2.4.2 Ice Shelf Thickness Measurements

This study provides the first thickness measurements of the Petersen Ice Shelf and epishelf lake. The mean thickness of the Petersen Ice Shelf in 2011 was 29 m, with a maximum thicknesses of 106 m. The thickest areas of the ice shelf occurred in the central regions,

particularly at the front of the Glacier 2 tributary. The spatial distribution of ice thicknesses on the Petersen is similar to that of the Milne Ice Shelf, where the mean ice thickness is ~55 m and the thickest regions (~94 m) are located where a tributary glacier enters the ice shelf (Mortimer et al., 2012). This indicates the importance of glacial input to the form of the Petersen Ice Shelf, and likely its persistence (despite large recent losses) compared to the recent complete collapse of many surrounding ice shelves without current glacier inputs (e.g., Ayles, Markham). The thinnest regions (<20 m) of Petersen Ice Shelf are along its seaward edge and particularly along its southern margin adjacent to the former epishelf lake region. Similar patterns were observed at the rear of the Milne Ice Shelf adjacent to the Milne Epishelf Lake (Mortimer, 2010). Based on the observed area changes and iceberg production patterns, it is this southern margin which is currently deteriorating the most, and according to the definition provided in the introduction, this region is now becoming too thin to meet the formal classification of an ice shelf.

2.4.3 Basal Ice Characteristics

The results presented here indicate that GPR reflections were prevalent in the thicker regions of Petersen Ice Shelf, but that many thinner regions lacked bottom reflections, especially across the eastern half of the ice shelf. The secondary small-scale grid survey that was conducted in this area produced bottom reflections along the ridges, but no reflections in the troughs. However, elsewhere in the eastern section of the ice shelf there were large areas where bottom reflections were also absent along ridges. Past studies have attributed weak or missing bottom reflections on other Arctic ice shelves to signal attenuation caused by saline intrusion into basal ice, such as at the Ward Hunt Ice Shelf (Hattersley-Smith et al., 1969; Narod et al., 1988; Prager, 1983). In particular, weak soundings at the western Ward Hunt Ice Shelf were attributed to brine inclusion in the basement ice with a mean bulk salinity of 2.22 ±0.6 psu (Jeffries and Sackinger, 1988; Lyons et al., 1971). Given that the bulk salinity below a depth of 5-6 m identified in our ice core on the Petersen Ice Shelf was >2 psu, it is likely that this is the cause of the signal attenuation there.

2.4.4 Basal Ice Topography

In addition to thickness measurements, this study is the first to use a combination of terrestrial GPR and GPS data to examine the basal topography of Petersen Ice Shelf. There has been little previous research to describe the detailed basal topography of Arctic Ice Shelves. In the airborne GPR study by Narod et al. (1988), they determined that the basal topography of the Milne Ice Shelf was essentially flat and therefore did not mirror the rolling ice shelf surface. However, it is likely that the lack of detailed surface topography, high survey speeds (~215 km hr^{-1}) and spreading of the radar wave in the method used by Narod et al. (1988) averaged out much of the topographic detail that was observed with the method presented here. This has important implications for understanding ice shelf properties as Narod et al. (1988) concluded that the rolls on the ice shelf surface were formed strictly by surface processes and that the stresses resulting from incomplete isostatic compensation were too low to cause the basal topography to adjust to the surface topography. This runs contrary to the original hypothesis proposed by Hattersley-Smith (1957), stated that while the rolling surface is likely formed by wind and further enhanced by meltwater ponds, the basal topography would be proportionately thinner beneath toughs and thicker below ridges because the ice shelf is floating and in isostatic equilibrium. Hattersley-Smith (1957) further explained that the ice is not rigid enough to support a rolling topography without a reciprocating basal topography. Based on the variations in basal topography of the Petersen Ice Shelf measured in this study, the theory of Hattersley-Smith (1957) is better supported than that of Narod et al. (1988).

2.4.5 Surface Mass Balance

Petersen Ice Shelf has experienced significant losses in extent since 2005, with a loss of >31.23 km^2 between 2005 and 2012 (~63% of the June 2005 area). While the ice shelf continues to receive mass from two tributary glaciers, at an ice thickness equivalent of 7.89 to 13.55 cm yr^{-1} from Glacier 1 and 2.24 cm yr^{-1} from Glacier 2, these inputs are far less than the mean surface ablation of 1.18 m w.e. yr^{-1} measured in 2011/2012. Compared to previous studies of surface mass balance at the Milne and Ward Hunt ice shelves, the rate of surface lowering at the Petersen Ice Shelf is relatively high. From 1989-2003 Braun et al. (2004)

calculated surface lowering of 0.07 m w.e. yr^{-1} for the Ward Hunt Ice Shelf, while measurements conducted by Mortimer (2011) produced a mean surface lowering of 0.37 m w.e. yr^{-1} for the Milne Ice Shelf (2008-2009).

Given that there is currently no evidence for net basal freeze-on due to the repeated recent breakups of the Petersen Bay epishelf lake (see Chapter 3), this ablation rate can be assumed to reflect current annual losses from the ice shelf. It is also likely that melted ice is actually lost from the ice shelf, as opposed to redistributed across the surface, due to the consistency in meltpond size between years. If this ablation rate is extrapolated across the entire ice shelf area (30.3 km^2 in April 2011) and combined with the calculated inputs from Glacier 1 and 2 (7.89 to 13.55 cm yr^{-1}), this equates to a mass loss of 3.54×10^7 to 3.71×10^7 m^3 yr^{-1}. Assuming this rate remains constant over time, and neglecting any losses from calving, the ice shelf would no longer exist by the year 2034-2036. This estimate is in line with the prediction by Hattersley-Smith et al. (1955) that the northern Ellesmere ice shelves would be completely lost by 2035 (based on ablation measurements from 1953 to 1954).

2.5 Conclusion

In conclusion, it is clear that large scale reductions of the Petersen Ice Shelf have occurred since the turn of the 21st century, in conjunction with the losses of other ice shelves along the northern coast of Ellesmere Island and the loss of MLSI in Yelverton Bay and Yelverton Inlet. Analysis of historical aerial photography and satellite imagery revealed general stability from 1959 to 2003, followed by a series of break-ups in summers 2005, 2008, 2011 and 2012, and the expansion of epishelf lake area throughout the last decade. The events of 2005 were fundamental in a series of changes to Petersen Bay; long-term climate warming and the loss of the protective MLSI in Yelverton Bay likely led to the break up at the front of Petersen Ice Shelf (8.07 km^2). In turn, it appears that this also led to the opening of a channel along the southern coast which resulted in the drainage of the epishelf lake, causing it to switch from a fresh to a marine water environment. The continued presence of late-summer open water and a drainage channel along the southern coast have prevented the reformation of the freshwater lake system since then.

Petersen Ice Shelf represents the remains of the greater Ellesmere Ice Shelf that developed under past colder conditions, necessary for ice growth and stability. While the precise relationship between climate and Arctic ice shelf stability requires further investigation, it is apparent that the ice shelves are breaking up in response to warming air temperatures ($+0.37^{0}$C decade^{-1} along the northern coast of Ellesmere Island between 1948 and 2006) and the presence of new open water regions along their fronts (Copland et al., 2007). Recent satellite-based observations released by the NSIDC (2012) indicate that low sea ice extents have continued since 2007, with 2012 representing the lowest extent on record (760 000 km^2 below 2007 record low). Based on these past and present observations it is unlikely that Petersen Ice Shelf, along with other Arctic Ice Shelves, will continue to persist long into the future.

Table 2.1: List of remotely sensed imagery used in the analysis of ice shelf area changes. All images were georeferenced against the 2009-07-16 ASTER image (WGS 84, UTM Zone 17N).

Sensor	**Resolution (m)**	**Date**	**Image ID**	**GCPs**	**RMSE (m)**
Air Photograph	6.61	1959-08-13	A16724: 63, 64	10	33.25
Air Photograph	2.25	1974-07-11	A23943: 55, 57,58, 60	16	23.67
Air Photograph	2.11	1984-07-23	A26535: 160, 162, 171	11	38.22
Landsat-7 ETM+	29.55	1999-07-07	L71060246_24619990707	NA	NA
ASTER Level 1B	14.25	2001-05-23	AST_L1B_00305232001222836	13	14.66
ASTER Level 1B	15.08	2002-06-19	AST_L1B_00306192002213131	13	15.45
ASTER Level 1B	15.93	2003-07-03	AST_L1B_00307032003224929	13	14.93
ASTER Level 1B	14.21	2005-06-03	AST_L1B_00306032005221820	NA	NA
ASTER Level 1B	14.21	2006-07-24	AST_L1B_00307242006221851	NA	NA
ASTER Level 1B	16.21	2007-07-19	AST_L1B_00307192007230820	NA	NA
ASTER Level 1B	18.68	2008-08-22	AST_L1B_00308222008000337	NA	NA
ASTER Level 1B	15	2009-07-16	AST_L1B_00307162009204121	NA	NA
ASTER Level 1B	17	2010-07-02	AST_L1B_00307022010231419	NA	NA
ASTER Level 1B	14.21	2010-07-19	AST_L1B_00307192010221901	NA	NA
Radarsat-2 UF	2.24	2011-04-01	20110401_203928_r2_u78__hh	NA	NA
Radarsat-2 UFW	2.40	2012-02-03	20120203_205610_r2_u3w2__hh	NA	NA
Radarsat-2 FQW	7.65	2012-08-24	201120824_203523_r2_fq9w_qp	NA	NA

Table 2.2: Ground penetrating radar cross point error analysis of ice shelf and lake ice thicknesses (see Figure 2.3 for location of cross points).

Cross Point ID	Ice Shelf Area	Total Ice Thickness Error (m) (including system resolution error of 0.07 m)	Mean Ice Depth (m)	Relative Error (%)
1	Front	0.38	4.35	8.75
2	Front	0.10	5.57	1.80
3	Front	0.26	4.83	5.39
4	Front	0.17	5.03	3.38
5	Front	0.09	0.77	11.69
6	Front	0.16	38.18	0.42
7	Front	0.23	18.71	1.23
8	Front	1.26	11.49	10.97
9	Central	0.18	43.75	0.41
10	Central (Glacier 2 front)	0.08	75.03	0.11
11	Central	0.20	12.40	1.61
12	Rear (at lake boundary)	0.09	1.15	7.83
13	Lake Area	0.12	0.85	14.20
14	Lake Area	0.21	0.88	23.86
15	Lake Area	0.20	0.85	23.67
16	Central	0.74	53.64	1.38

Table 2.3: Petersen Ice Shelf area changes from 1959 to 2012.

Time period (Year/Month)	Time interval (# of years)	Total ice shelf area (km^2)	Total area change (km^2)
1959/08 – 1974/07	14.9	48.37	-0.03
1974/07 – 1984/07	10.0	48.42	+0.05
1984/07 – 1999/07	15.0	49.87	+1.45
1999/07 – 2001/05	1.9	48.88	-0.99
2001/05 – 2002/05	1.0	49.36	+0.48
2002/05 – 2003/07	1.1	50.32	+0.96
2003/07 – 2005/06	1.9	48.9	-1.41
2005/06 – 2006/07	1.1	40.84	-8.07
2006/07 – 2007/07	1.0	40.97	+0.13
2007/07 – 2008/08	1.1	31.98	-8.99
2008/08 – 2009/07	0.9	32.08	+0.10
2009/07 – 2010/07	1.0	30.68	-1.40
2010/07 – 2011/04	0.8	30.29	-0.38
2011/04 – 2012/02	0.8	24.81	-5.48
2012/02 – 2012/08	0.6	19.32	-5.49

Table 2.4: Petersen Ice Shelf thickness statistics, determined from GPR measurements in spring 2011.

Statistic	**Value**
# of Traces	12746
Minimum (m)	0.01
Maximum (m)	106.26
Mean (m)	28.52
Median (m)	23.56
Standard Deviation (m)	23.99
Upper Quartile (m)	47.40
Lower Quartile (m)	5.14

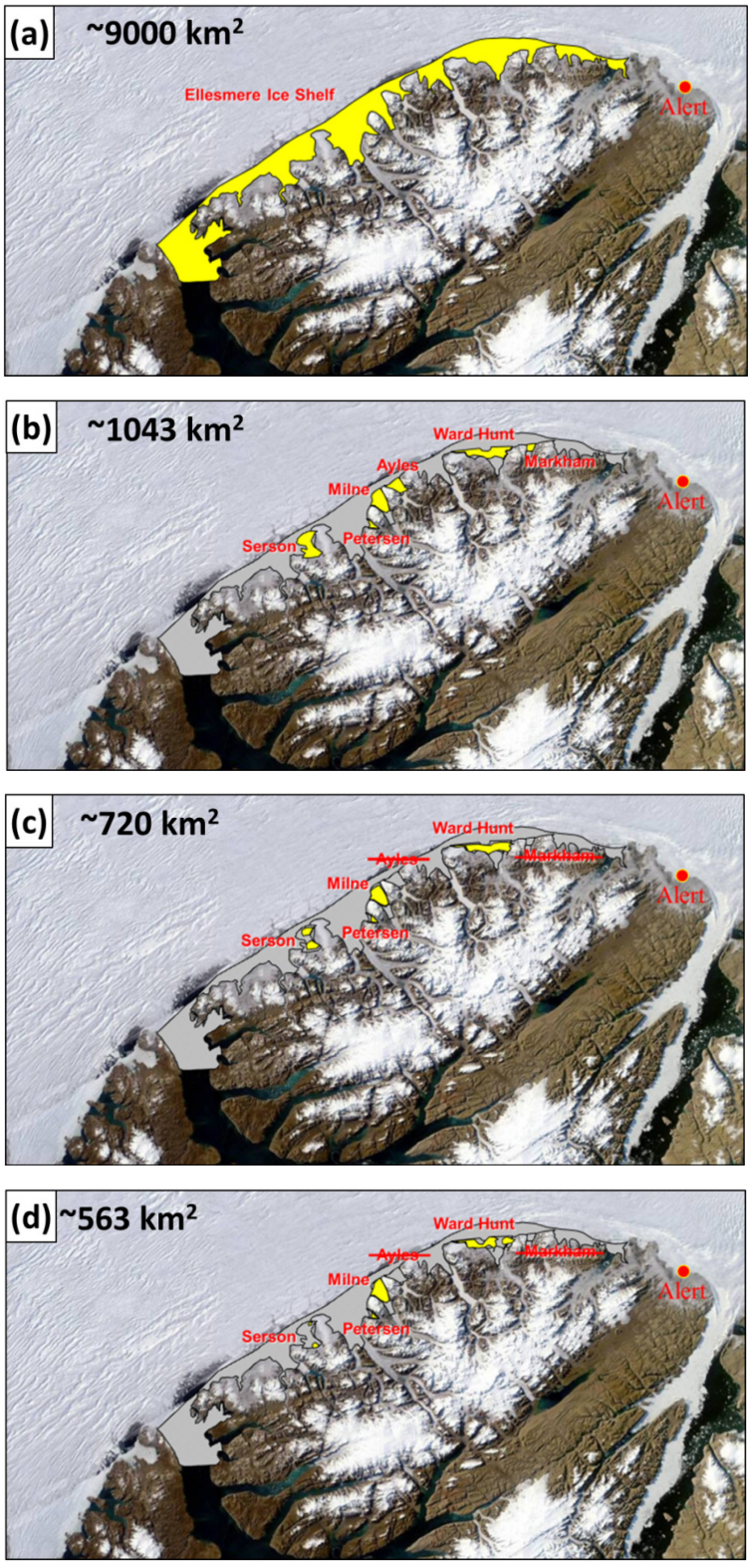

Figure 2.1: Annotated summer MODIS image (NASA) of the northern coast of Ellesmere Island, showing the change in ice shelf area since the beginning of the 20th century: (a) 1906; (b) July 2005; (c) September 2008; (d) September 2011.

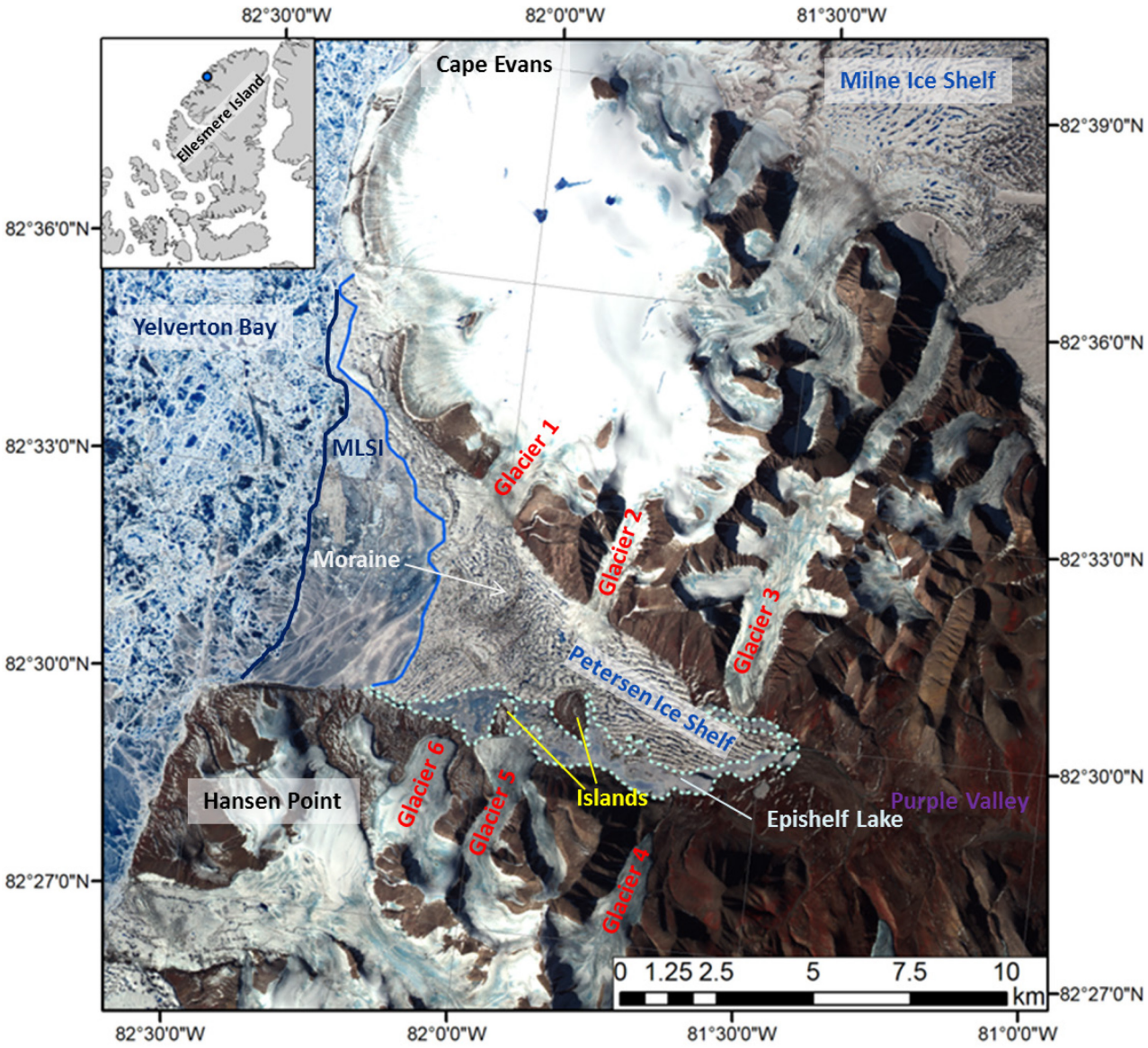

Figure 2.2: Study area map of Petersen Bay overlain on an ASTER L1B satellite scene from 2009-07-16. The image is also annotated with glacier names used in this study. Inset: Blue dot indicates location of Petersen Ice Shelf on Ellesmere Island.

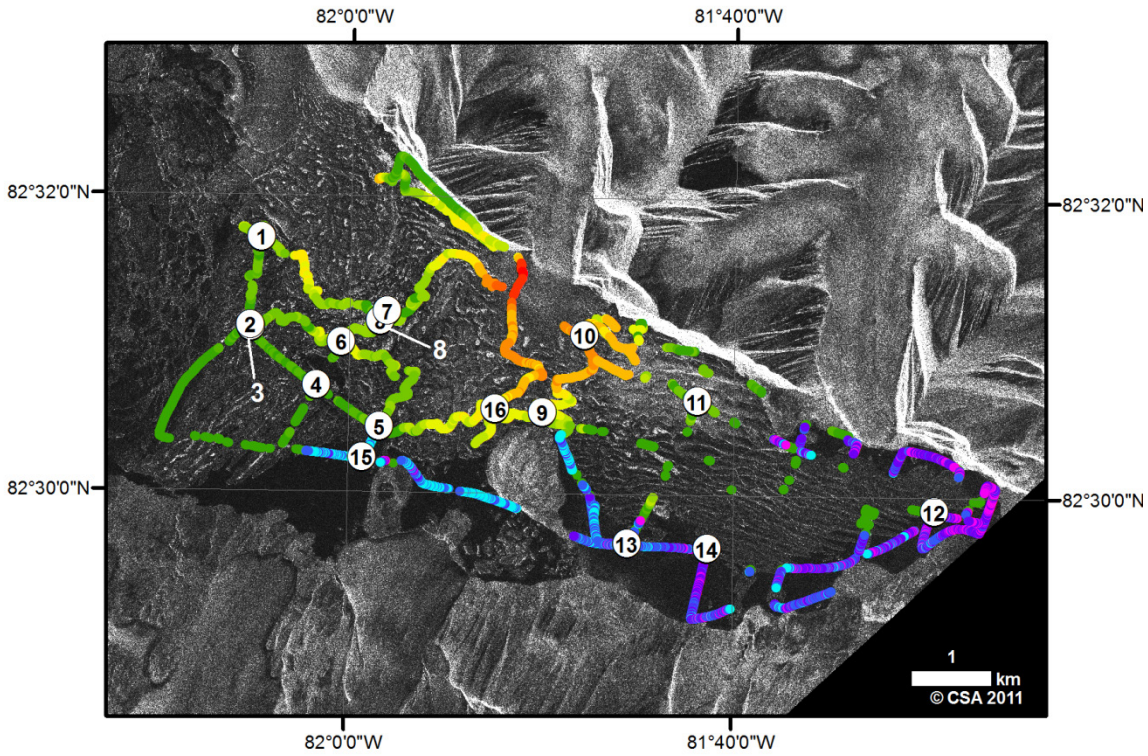

Figure 2.3: Cross point sites selected for evaluation of the accuracy of ground penetrating radar measurements collected in May 2011 across the Petersen Ice Shelf and adjacent lake area. The numbers denote the ID provided in Table 2.2 (overlaid on a Radarsat-2 Ultrafine HH image, 2011-04-01).

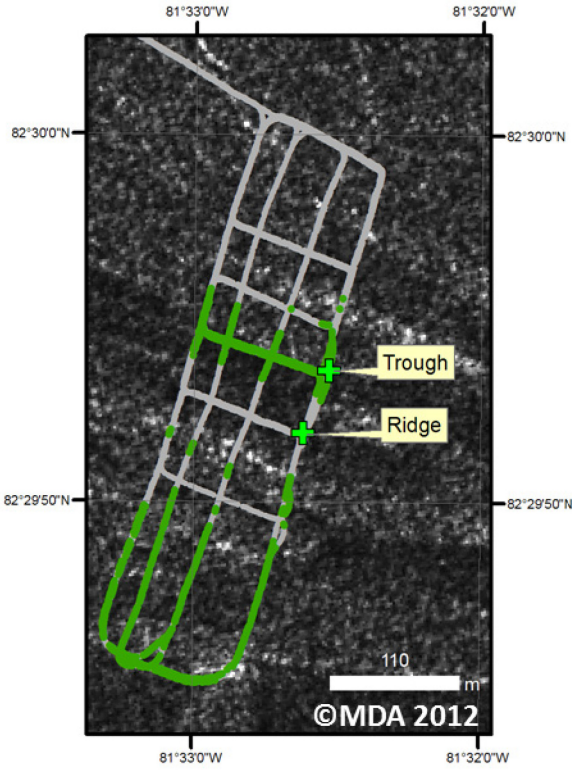

Figure 2.4: Radarsat-2 Ultrafine HH scene (2012-02-03) overlaid with the location of the small grid GPR survey conducted in May 2012. Green represents areas where bottom reflections were recorded, while the grey represents the grid. Processed traces reveal ice thicknesses of >5 m. Crosses indicate the position of one ridge where an ice core was extracted, and one trough where ice thickness was measured.

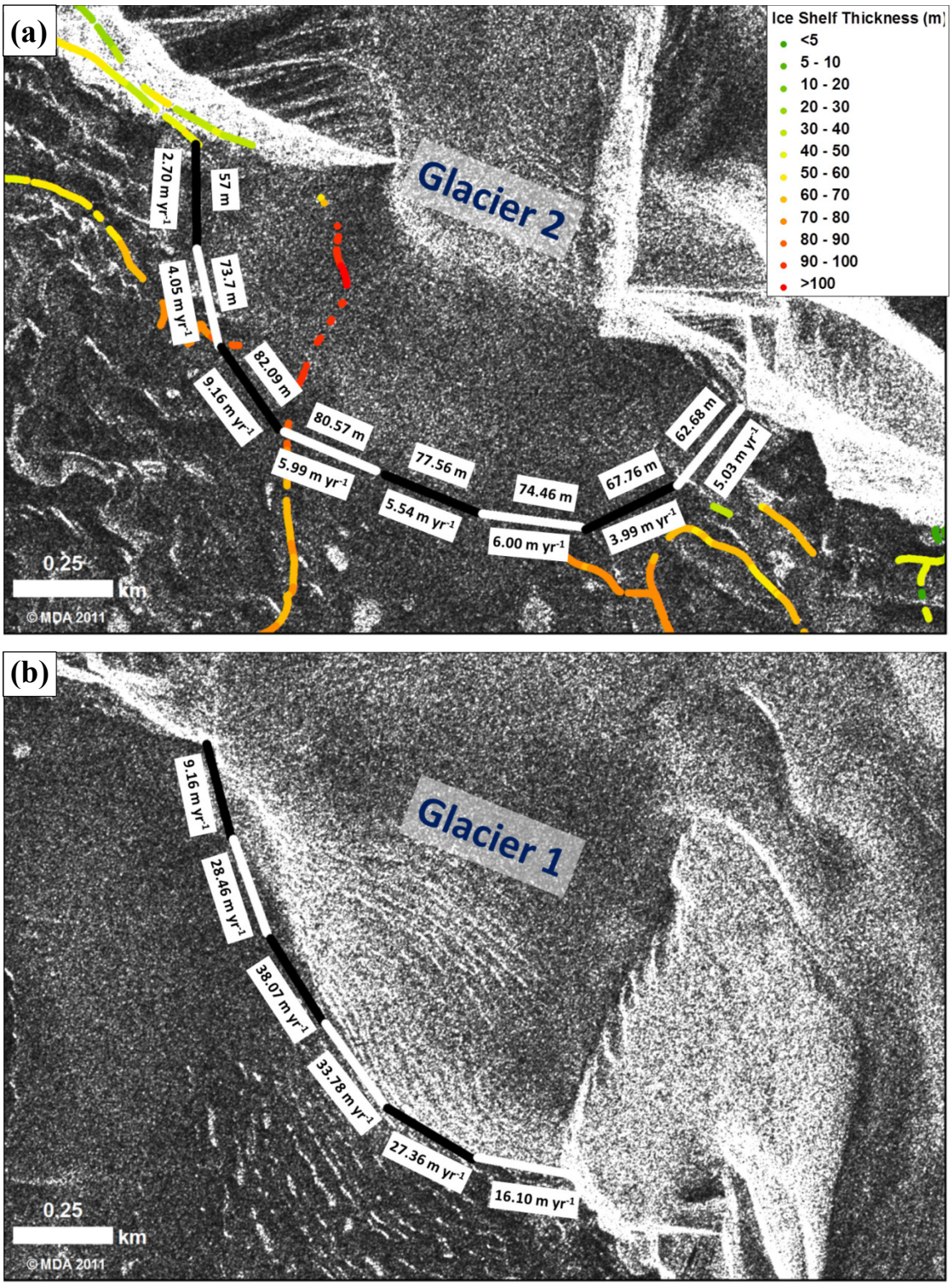

Figure 2.5: Flux gates across the front of tributary glaciers feeding into Petersen Ice Shelf, represented by 250 m segments (black and white line) with average thickness (interpolated from ground penetrating radar measurements) and average velocities (derived from speckle tracking) for each segment: (a) Glacier 2; (b) Glacier 1. Annotations overlaid on a Radarsat-2 Ultrafine HH image: 2011-04-01, 20:39:28.

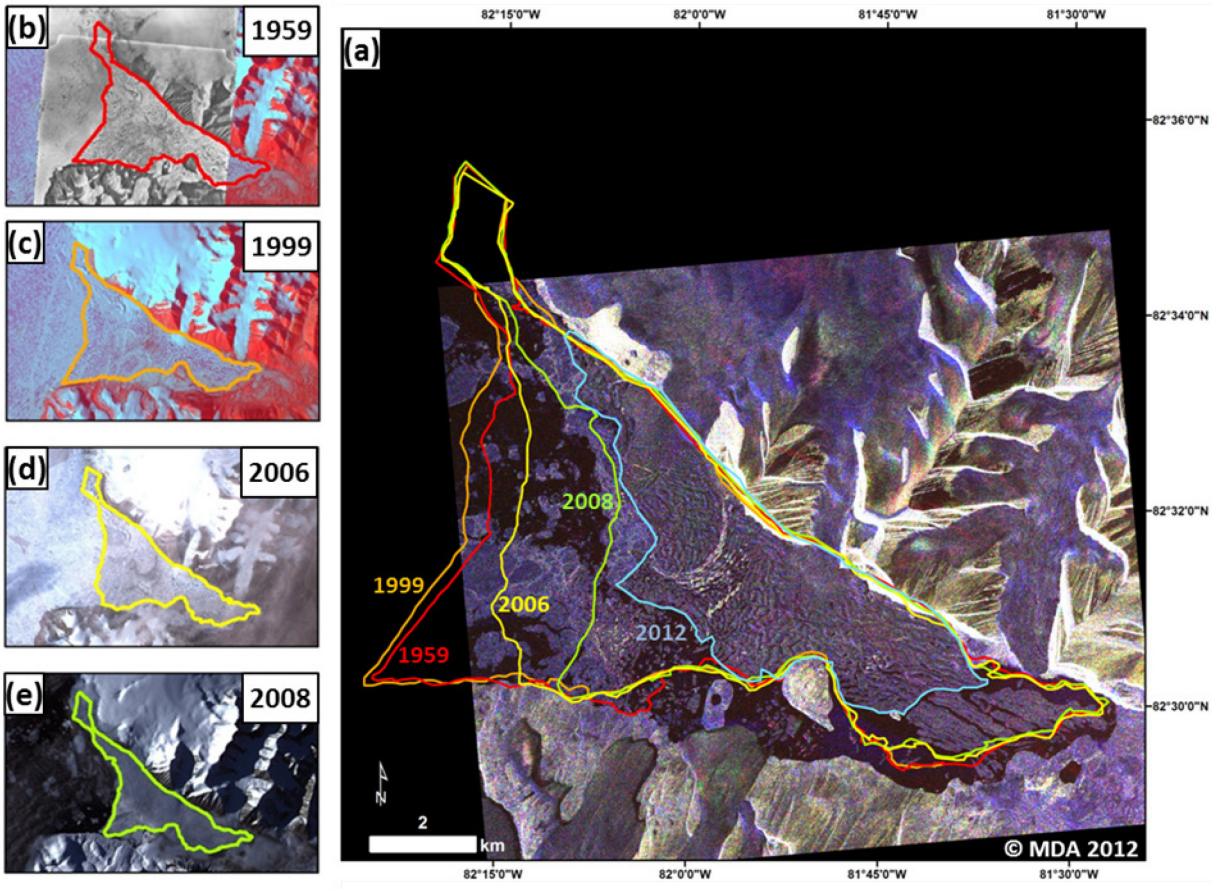

Figure 2.6: Petersen Ice Shelf extent changes through time: (a) Radarsat-2 Wide Fine Quad-Pol (2012-02-03) with annotations of major changes through time; (b) Aerial photograph (1959-08-13) with Landsat ETM+ (1999-07-07) as background; (c) Landsat ETM+ (1999-07-07); (d) ASTER L1B (2006-07-24); (e) ASTER L1B (2008-08-22).

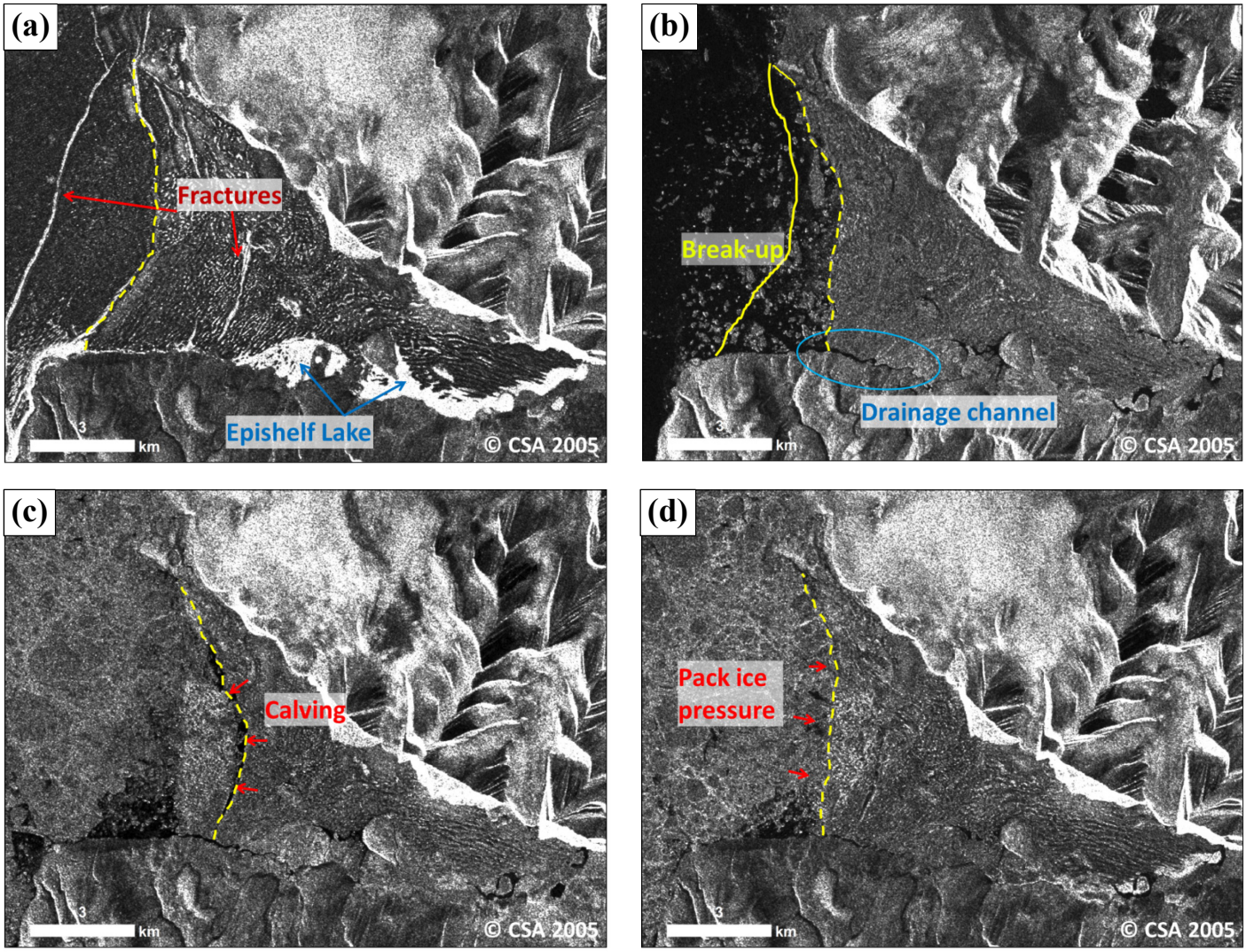

Figure 2.7: Annotated Radasat-1 Standard imagery (12.5 m resolution) describing the changes that occurred at Petersen Ice Shelf in summer 2005: (a) 2005-03-18, (b) 2005-08-18, (c) 2005-08-23, (d) 2005-09-26.

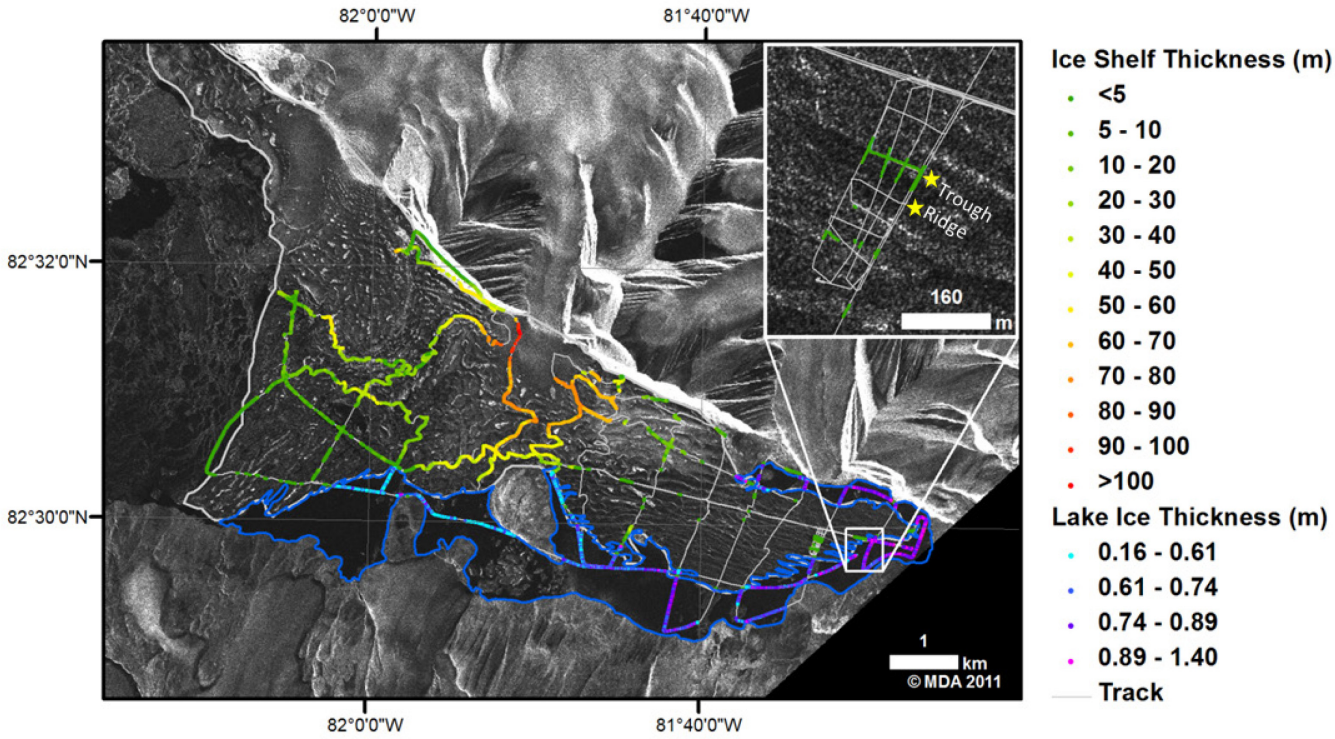

Figure 2.8: Ice thicknesses across Petersen Ice Shelf and the adjacent lake area (outlined in blue), derived from GPR surveys conducted in May 2011, overlaid on a Radarsat-2 Ultrafine Wide HH image (2012-02-03). Inset map shows a small-scale grid survey that was completed where GPR reflections were intermittent. Ice shelf and lake ice thicknesses were calculated with a radio-wave velocity of 0.17 and 0.15 m ns^{-1} respectively. The depth of snow was calculated using a radio-wave velocity of 0.20 m ns^{-1}, and was subtracted from the total profile thickness to determine ice thickness alone.

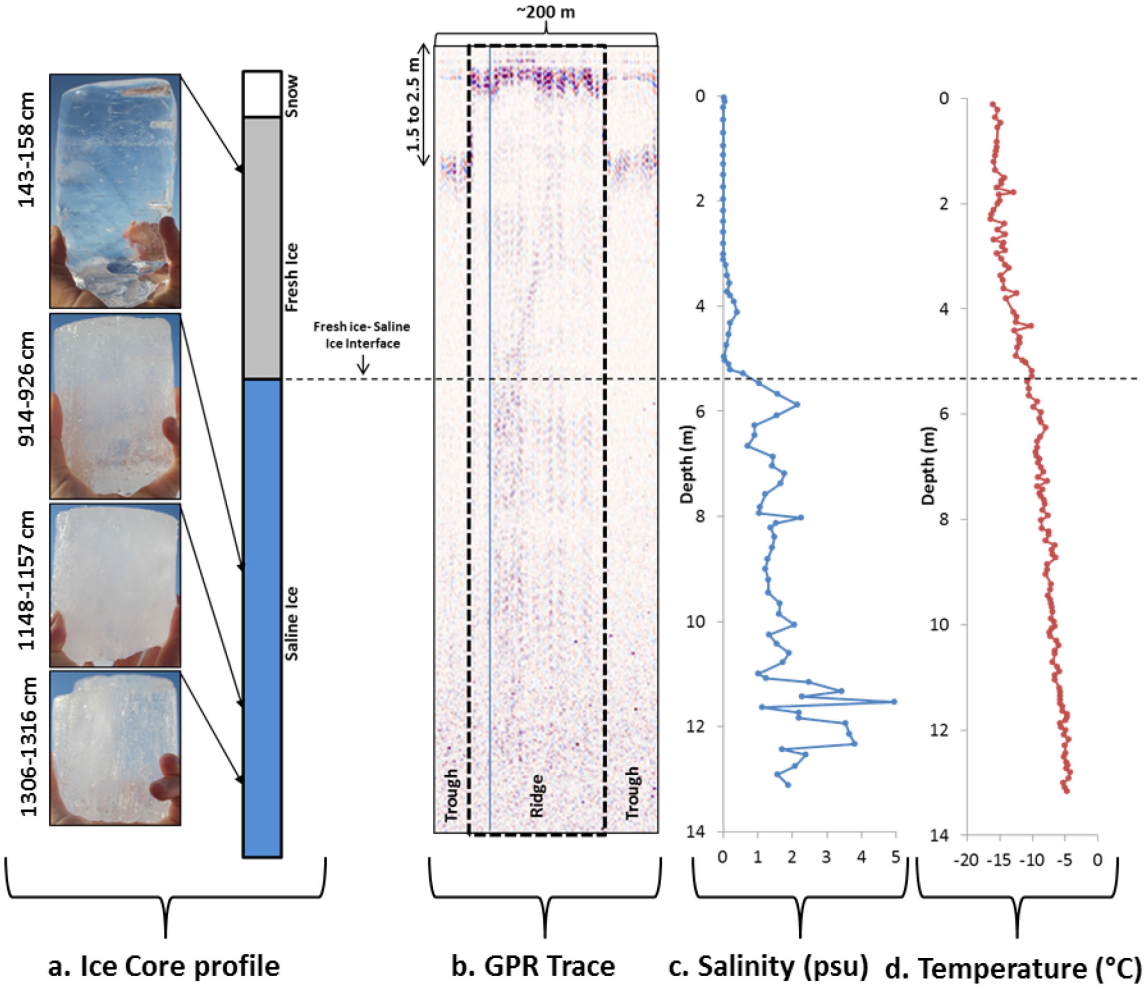

Figure 2.9: Vertical ice stratigraphy analysed from a 13.24 m core extracted from a ridge of Petersen Ice Shelf (82°29'51.6457"N, 81°32'36.4992"W): (a) Ice core profile and photographs of core segments, (b) Radargram showing a 118 m long transect collected in May 2012 during the small grid survey at the back of the ice shelf (see inset of Figure 2.8). Ridges and troughs are separated with a dashed line, while the blue vertical line indicates the point on the transect where the core was extracted, (c) Salinity measurements measured with melted core segments, (d) field measurements of internal ice core temperatures (every ~10 cm) recorded immediately after each core segment was extracted.

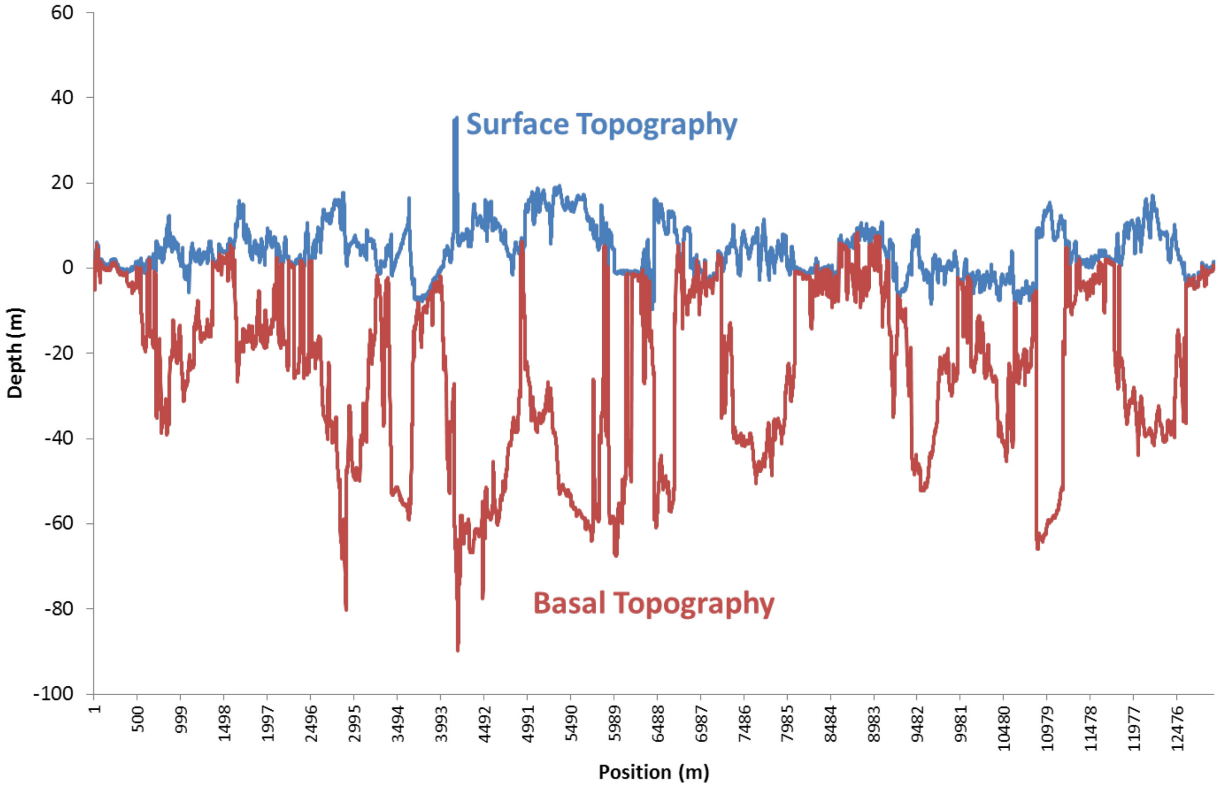

Figure 2.10: Surface and basal topography of the Petersen Ice Shelf in 2011, derived from GPS heights and all GPR traces that had a basal reflection.

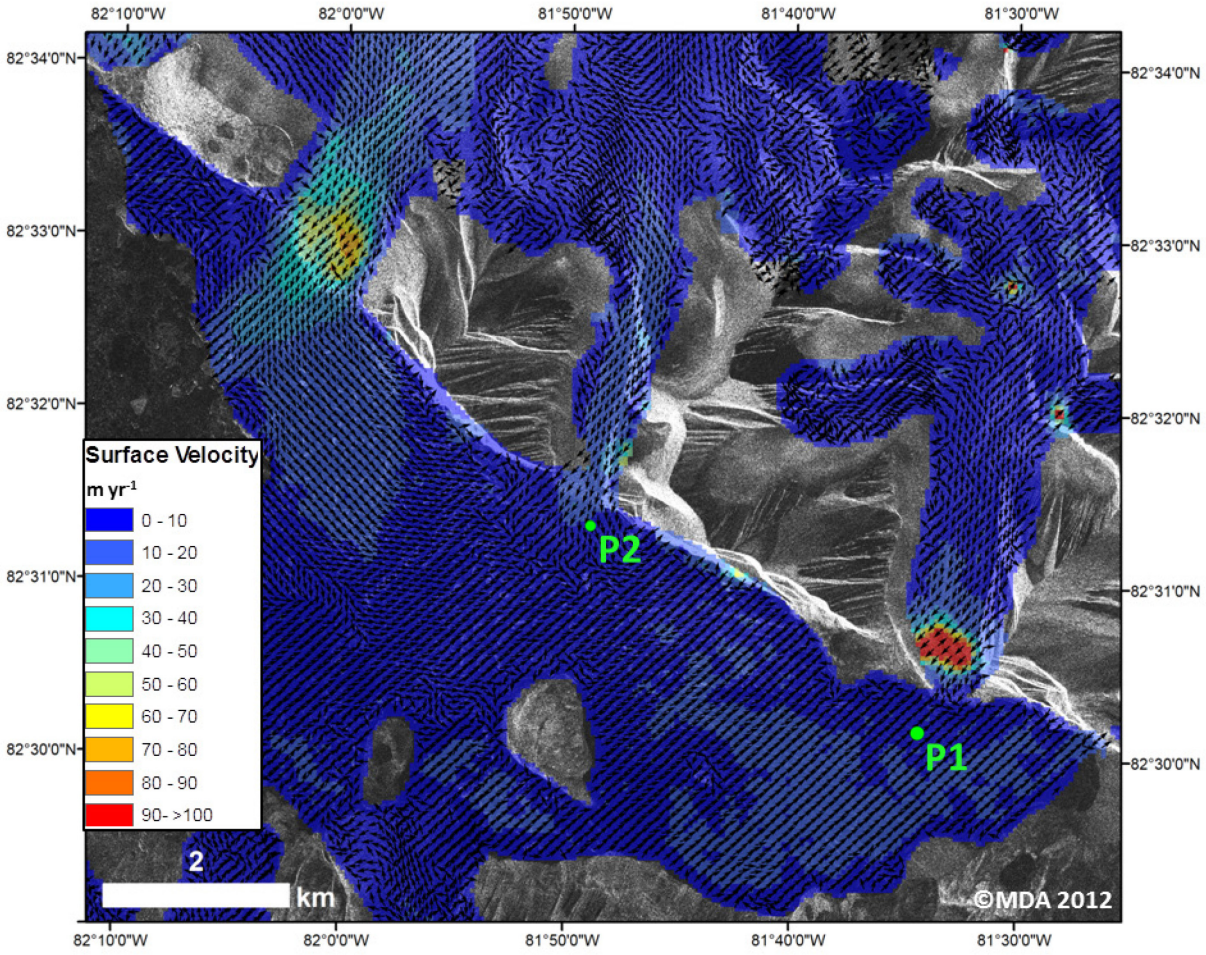

Figure 2.11: Surface velocities of Petersen Ice Shelf and surrounding glaciers derived from speckle tracking of Radarsat-2 Ultrafine HH scenes (April 25 to May 19, 2012), overlaid on a Radarsat-2 Ultrafine Wide HH image (2012-02-03). P1 and P2 represent the ablation stakes measured over the 2011/12 field seasons. Pixel spacing between velocity vectors is approximately 100 m.

3. An Analysis of Recent Changes to the Petersen Bay Epishelf Lake (1992 to 2012)

3.1 Introduction

Since the 1950s, annual Arctic (between 60° and 90° N) surface air temperatures have increased by >2°C (AMAP, 2011). In response to the warming temperatures, seasonal and perennial sea ice has been declining since 1953, with an acceleration in decline since 1996 (Comiso et al., 2008; Stroeve et al., 2007). The decrease in sea ice and subsequent open water conditions along the northern coast of Ellesmere Island, in combination with warmer temperatures and high winds, has been associated with the dramatic loss of Canadian Arctic ice shelves (Copland et al., 2007). Ice shelves are thick masses (>20 m) of floating landfast ice that formed along the northern coast of Ellesmere Island up to 5500 yrs BP, and had an estimated area of ~9000 km^2 at the turn of the 20^{th} century (England et al., 2008; Jeffries, 1992b; Vincent et al., 2001). Over the last century they have experienced a loss of >90% in areal extent, and an additional >40% loss since 2005 (Kealey et al., 2011; Mueller et al., 2006).

Studies are limited about the effects of Arctic ice shelf loss, particularly on epishelf lakes, a unique type of lake that is structurally dependent on these cryospheric features. An epishelf lake is a unique water body that forms where a layer of relatively low density freshwater, underlain by higher density marine water, becomes dammed at the head of fiords and embayments behind an ice shelf (Figure 3.1a; Jungblut et al., In press; Veillette et al., 2008; Veillette et al., 2011). The freshwater typically originates from summer meltwater which flows into the fiord or inlet from terrestrial sources such as snowmelt. A perennial ice cover on the epishelf lake surface prevents mixing by winds, thus allowing the freshwater layer to remain permanently stratified over the marine water below (Veillette et al., 2008). Recent studies have highlighted the importance of epishelf lakes as unique habitats for microbial ecosystems due to their vertical segregation between layers of fresh, brackish and marine water (Veillette et al., 2011). For example, the Milne Fiord epishelf lake provides a habitat for diverse microbial communities of Eukarya, Eubacteria, Archaea, and viruses (Veillette et al., 2011). Furthermore, zooplankton communities of freshwater, brackish and marine taxa

have been identified down the water column of both Disraeli Fiord (behind the Ward Hunt Ice Shelf) and the Milne Fiord epishelf lake (Van Hove et al., 2001; Veillette et al., 2011).

The existence of an epishelf lake is strongly dependent upon the thickness and structure of its adjacent ice shelf. Because the ice shelf behaves as a dam, preventing freshwater from draining into the ocean, changes in its thickness can result in a thinning of the freshwater layer. If the structural integrity of an ice shelf is compromised (e.g., due to fracturing or calving), the epishelf lake can be lost entirely (Figure 3.1b). For example, the epishelf lake in Disraeli Fiord, Ellesmere Island, drained away completely when the Ward Hunt Ice Shelf fractured in the early 2000s (Figure 3.1c & 3.1d; Mueller et al., 2003). Leading up to this drainage event (from 1967 to 1999) the Ward Hunt Ice Shelf had thinned by 13 m (27%) (Vincent et al., 2001). Between 2000 and 2002 vertical fracturing occurred all the way through the Ward Hunt Ice Shelf, providing a conduit through which the freshwater drained (Mueller et al., 2003). As a result of this drainage event, the epishelf lake was lost as well as the biota found in this unique ecosystem.

Over the past 54 years, many epishelf lakes along the northern coast of Ellesmere Island have disappeared in conjunction with ice shelf losses (Veillette et al., 2008). Using 1960 Canadian National Topographic Systems maps, with coverage along the 450 km coastline of northern Ellesmere Island, Veillette et al. (2008) identified 17 potential epishelf lake sites that may have been retained by the 'Ellesmere Ice Shelf' (a continuous permanent ice fringe that was observed by the Peary expedition in 1906). By 1960, the Ellesmere Ice Shelf had disintegrated, leaving behind remnant ice shelves in fiords, thus reducing the number of potential epishelf lakes to nine. After subsequent ice shelf break-ups, Veillette et al. (2008) used synthetic aperture radar (SAR) backscatter analysis to identify epishelf lakes with mid-winter standard and fine-beam Radarsat-1 scenes from 2005-2007. In-situ salinity and temperature profiles were collected, and previous profile data were assessed to confirm the presence of freshwater stratification in the Milne, Ayles, and Markham fiords (Figure 3.2). By comparing histograms of backscatter with the field measurements, Veillette et al. (2008) determined that ice-dammed lakes had bright radar returns that typically exceeded -6.0 dB, while sea ice and ice shelf ice demonstrated a lower backscatter. By applying this threshold

to the SAR scenes, they concluded that only one deep epishelf lake remained behind the Milne Ice Shelf in 2008 while nine ice-dammed lakes were present since 1960 across the northern coast of Ellesmere Island. Shallow ice-dammed lakes have a freshwater layer <5 m deep and represent the transition from epishelf lake to an open fiord or bay (Jungblut et al., In press). These freshwater lakes have a shallow depth because their ice shelf dam is lacking and/or it is dammed by thin multi-year landfast sea ice (MLSI) (Jeffries, 1992a; Jungblut et al., In press). While Veillette et al. (2008) were able to identify potential epishelf lake areas during the presence of the 'Ellesmere Ice Shelf', and identify the last existing epishelf lake detectable in SAR scenes from 2005, no information regarding the presence of epishelf lakes prior to that date exists for the Petersen Bay area. Indeed, this method has yet to be applied to analyze the extent of any epishelf lakes using earlier SAR data (e.g. 1990s).

The objectives of this study are to determine if an epishelf lake existed in Petersen Bay, and if so, how this lake has changed over time using SAR imagery. Backscatter analysis of SAR scenes will be used to observe historical changes since 1992, and validated with ice cores and conductivity-temperature-depth (CTD) profiles collected since 2008. These results will be used to examine how the Petersen Bay epishelf lake has responded to changes in the Petersen Ice Shelf, and further our understanding of the relationship between these features.

3.1.1 Study Area

Petersen Bay is located on the northern coast of Ellesmere Island, Nunavut, between Hansen Point and Cape Evans, and to the west of the Milne Ice Shelf (Figure 3.2). This bay contains the Petersen Ice Shelf (82°31'N, 81°56'W), which is currently connected to the northern coast of the bay. The area between the ice shelf and southern coastline contains the area where an epishelf lake would be expected, and is the area under investigation in this study. Previous work in this region is very limited. In a study by Mueller et al. (2006) the dimensions of the ice shelf and surrounding features were reported. According to observations based on synthetic aperture radar satellite data from 2000, the Petersen Ice Shelf had a length of 17 km and a width of 12 km, with MLSI at its front of >100 km^2, and a lake area of 7.3 km^2. In a study by Copland et al. (2007) that focused on the collapse of the

Ayles Ice Shelf, changes to the Petersen Ice Shelf in August 2005 were also mentioned and included a reported loss of 12.6 km^2 from the terminus, or 20% of its total area.

3.2 Methods

3.2.1 Field Measurements

Field measurements were completed in Petersen Bay in spring (April/May) 2008, 2009, 2011 and 2012. CTD profiles were collected to determine the characteristics of the water below the lake ice cover, and ice cores were extracted to measure the temperature profile and salinity throughout the ice and to distinguish between fresh water and salt water ice. Furthermore, ground penetrating radar (GPR) measurements were used to determine the thickness of the lake ice. The results of the field measurements were used to validate the results of the remote sensing analysis.

3.2.1.1 Ice Core Measurements and CTD Profiles

CTD profiles and ice cores were extracted across the Petersen Bay lake area at four different sites (Figure 3.3). Site 1 is located towards the rear of the ice shelf along its southern shore. Site 2 was selected to examine changes adjacent to an island that borders the lake area and the ice shelf. Site 3 is located at the rear of the bay in what appears to be the most protected portion of the lake (far from the outlet). Site 4 was selected to examine the lake area beyond the island, towards the outlet of the bay.

A Kovacs Mark II ice coring system (with an internal diameter of 8.8 cm) was used to drill through the ice cover and extract the ice cores, after which a Kovacs ice thickness gauge was lowered into the borehole to measure the ice thickness. The ice cores were laid out in a sled and photographed, and an electric drill was used to insert probe thermometers into holes drilled into the centre of the core every 10 cm. An ice saw was then used to slice the core into 10 cm sections, which were individually packaged into double plastic bags and labelled accordingly. Within 24 hours of extraction the cores were photographed again and visually assessed for ice crystal type, colour, cloudiness, and bubble inclusions. In May 2012 the cores were melted and and a YSI Pro Plus multiparameter probe (used in spring 2012) was

used to measure their temperature-corrected conductivity. In previous years, the conductivity of the cores were measured with an XR-420-CTDm (RBR Global Ltd.) in 2008, an Oakton PCS Testr 35 in 2009 and an EC meter model 2052 in 2011. Conductivity was converted to salinity using the calculation by Fofonoff and Millard (1983).

An RBR XR-420-CTDm (in 2008) or XR-620-CTDm (in 2009, 2011 and 2012) profiler was lowered into the water beneath each borehole and used to determine the conductivity, temperature and depth characteristics of the underlying water column. To conduct the profile, a 1 Hz (in 2008) or 6 Hz (in 2009, 2011 and 2012) sampling period was set. Before lowering the profiler, the probe was left in the water to equilibrate for at least one minute. The measurements collected on the downcast were used in this study.

3.2.1.2 Ground Penetrating Radar Measurements

To measure ice thickness, a reflection type survey was conducted with a PulseEKKO Pro 250 MHz GPR system in May 2011, custom-fitted into a sled and towed behind a snowmobile at ~20 km hr^{-1}. Because the GPR was also being used to measure the thickness of the adjacent ice shelf, a time window of 2500 ns was set for the system, enabling measurement up to a maximum ice depth of ~190 m. The sampling interval was set to 0.4 ns, while the antenna separation was 0.40 m. A digital video logger (DVL) connected to the GPR displayed the reflections as they were collected, which allowed for periodic confirmation that the GPR was operating correctly. A single frequency GPS receiver (StarGPS) was connected to the DVL and recorded the position of every trace.

The GPR data was processed in EKKO_View Deluxe Version 1.4 (Sensors and Software Inc.) and converted to ice thickness in IcePicker Release 4 (Sensors and Software Inc.). In EKKO_View Deluxe, a DEWOW time filter was first applied to the trace data to remove the low frequency rise typical at the start of GPR traces, also known as signal saturation correction (Sensors & Software, 2003). A trace difference was then applied to the data, which replaced each trace with the difference between the trace and the previous one (Sensors and Software, 2003). This enhanced rapidly changing features (e.g, changes in ice

thickness) and suppressed flat-lying and constant features (e.g., background noise). Finally, areas of repeat traces were deleted when the snowmobile was immobile.

Following the filtering and trace deletions in EKKO_View Deluxe, the remainder of the processing was completed in IcePicker Release 4 to pick the bed reflections and derive ice thicknesses using the following equation:

$$T = \sqrt{\left(\frac{\left(t + \frac{s}{0.3}\right)}{2}\right)^2 V_I - \frac{s^2}{4}} \quad \textbf{(1)}$$

Where T is ice thickness (m), t is two way travel time (ns), V_I is the electromagnetic wave velocity of the material (m ns^{-1}), and s is the antenna separation (0.40 m in this study). In this study an electromagnetic wave velocity of 0.200 m ns^{-1} was selected for snow, and 0.150 m ns^{-1} was selected for ice. These wave velocities were selected based on the study by Pope et al. (2012), in which the same 250 MHz PulseEKKO Pro GPR system was used to determine the thickness of both multi-year ice (MYI) and first-year ice (FYI) in Yelverton Bay (at the outlet of Petersen Bay). In combination with borehole and snow pit measurements, Pope et al. (2012) determined that wave velocities of 0.150 m ns^{-1} and 0.200 m ns^{-1} were most appropriate for determining the thickness of sea ice and the overlying snow pack, respectively. The wave velocity for ice is further supported by Kovacs and Morey (1978), who measured MLSI near Narwhal Island, Alaska with a 625 MHz GPR system and used wave velocities of 0.156 and 0.157 m ns^{-1}. Similarly, Nyland (2004) used a 200 MHz GPR system to determine FYI thickness with wave velocities of 0.154 to 0.167 m ns^{-1}. With the wave velocities for ice and snow determined, the snow to ice and ice to underlying water interfaces were processed separately to produce separate measures of the snow and ice thicknesses across the study area.

To separate the GPR traces of the ice shelf from the epishelf lake, a polygon was traced around the extent of the epishelf lake using an ultrafine Radarsat-2 image from April 1, 2011. The GPR traces were clipped to this epishelf extent. The extent of icebergs in the lake were

also traced and used to clip the GPR measurements in these areas, to segregate the lake ice from surrounding ice types.

3.2.2 Remote Sensing

3.2.2.1 SAR Backscatter Analysis

Backscatter analysis is an effective method for identifying floating lake ice in winter due to the vertically oriented tubular bubbles within it, and the strong dielectric contrast across the ice-water interface. These unique lake ice characteristics cause a double bounce reflection which causes the incident energy to return to the sensor at the same angle that it was originally transmitted, resulting in a bright backscatter (Jeffries et al., 1994; Jeffries, 2002). In contrast, sea ice will have dark backscatter caused by volume scattering (due to bubbles within an order of magnitude in size of the radar wavelength, and surface roughness) and absorption of energy within the saline ice (Onstott & Shuchman, 2004).

The analysis of backscatter patterns in SAR imagery was used to determine if the ice cover adjacent to the ice shelf in Petersen Bay is currently, or was previously, perennial freshwater ice. This was then used to infer the presence or absence of an epishelf lake (Veillette et al., 2008). To complete this analysis, ERS-1, Radarsat-1, and Radarsat-2 SAR images were used that were acquired when there was no influence from surface melt (January to May; Table 3.1). The ERS-1 and Radarsat-1 satellite data were provided by the Alaska Satellite Facility (ASF), and the Radarsat-2 data was acquired through the SOAR-E program from the Canadian Space Agency (CSA). The satellite data was calibrated to a normalized radar cross section (σ^0) in a linear power scale to standardize the images for quantitative analysis. MapReady software version 3.0.6, provided by ASF (http://www.asf.alaska.edu/downloads/software_tools) was used to calibrate the Radasat-1 and ERS-1 satellite data. For the Radarsat-2 satellite data, a look-up table (LUT) is included with the product which allows the conversion from DN to σ^0:

$$\sigma^0 = (DN)^2/A^2 \quad \textbf{(2)}$$

where DN is the digital number (0-65535) and A is the gain value corresponding to the range sample.

In the study by Veillette et al. (2008), backscatter analysis was used to examine long-term changes to epishelf lakes and ice-dammed lakes along the entire northern coast of Ellesmere Island. In this study it was determined that lakes typically had a return >-6 dB in satellite SAR scenes, while sea ice and ice shelf ice had much lower values. To test if this threshold would be appropriate in the current study, a transect of values across the lake ice, ice shelf, and sea ice were extracted from a Radarsat-1 Fine beam image from 2008-02-14 that was acquired closest to an April 2008 CTD profile (at site 1 in Figure 3.3) which recorded the presence of lake ice and underlying freshwater. The mean return across each ice type was compared to the threshold presented by Veillette et al. (2008) and assessed for suitability. Based on the mean return of −5.16 dB for the lake ice, -12.50 dB for the ice shelf and -17.92 dB for the sea ice, the <-6 dB value was determined as a suitable threshold limit and therefore applied in this study (Figure 3.4).

To assess the presence of lake ice, all values above the established threshold of -6 dB were extracted from the SAR imagery. To do this a polygon was traced along the southern coast of Petersen Bay and the southern extent of Petersen Ice Shelf to include the entire potential lake area in each satellite scene (1992 to 1995, and 1997 to 2012) in ESRI ArcMap 9.3.1. All pixels within the polygon above the threshold were counted and this was multiplied by the pixel size to determine the area detected as epishelf lake in each satellite image. Due to the nature of SAR, this polygon contained speckle which may have reduced the overall area identified as epishelf lake ice. The statistics for this study were conducted with the σ^0 values in a linear power scale, with these values converted to a logarithmic scale (dB) in the results.

To determine if the changes observed in the above analysis were uniform across the lake or varied by region, six sites were examined across the southern coast of Petersen Bay where high backscatter consistent with an epishelf lake had been detected in 1992. As can be seen in Figure 3.5, sites A and B were located in the western portion of the former epishelf lake

area. Site C was located adjacent to the island while sites D and E were set in the eastern portion of the former lake area. Site F was placed at the back of the ice shelf. Each site, represented as a 0.07 km^2 polygon in ArcGIS 9.3.1, was used to extract the backscatter for each year of study.

3.2.2.2 Analysis of Aerial Photography and Optical Satellite Imagery

To place changes in the epishelf lake cover detected with SAR imagery into context, aerial photography and optical satellite imagery was assessed to monitor related changes to the Petersen Ice Shelf, including the sea ice at the front of the ice shelf, open water events along the southern coast, and input from tributary glaciers into the lake area (Table 3.2). The ice shelf is easily distinguished from adjacent sea ice due to its characteristic rolling surface topography, while the southern part of Petersen Bay contains smooth ice characteristic of lake or young sea ice. Vertical aerial photographs were obtained from the National Air Photo Library (Ottawa, Ontario), in TIFF format at resolution of 1200 dpi. Two photographs were acquired from August 1959, and were cropped, converted to grayscale and mosaicked. The mosaicked photograph was georeferenced to a cloud-free ASTER L1B scene (July 16, 2009) that was used as the master image against which all other imagery was aligned. A total of 10 ground control points (GCPs) were used for this process, distributed evenly across the image on stable land areas. The final root mean square error for the georeferenced aerial photo mosaic was 33.25 m. An extensive search for all ASTER L1B imagery of the study area was conducted online (http://reverb.echo.nasa.gov/reverb/). The ASTER imagery underwent the same georeferencing procedure as the aerial photography when alignment did not match with the master image.

3.2.2.3 Open Water Events

The status of the Petersen Bay ice cover was evaluated for open water from 1992 to 2012. ASTER imagery was used to visually inspect the southern coast for open water, while SAR imagery was used to determine movement of icebergs within the epishelf lake region (Table 3.3). The production of new icebergs comes from the rear of the ice shelf and the tributary glacier to the south. If icebergs moved in the southern coastal area by at least 50 m (beyond

the pixel size of the image), then it was assumed that open water had occurred. Using this information the lake ice cover in each summer season was classified as open, partial, or not open. If information was ambiguous or missing, then the lake ice cover was classified as 'not open' to provide a conservative record of the lake ice changes.

3.3 Results

3.3.1 Ice Core Measurements

Ice cores collected through the entire ice cover from four sites across the southern coast of Petersen Bay indicate variations in bulk salinity inconsistent with an epishelf lake cover in 2009, 2011 and 2012 (Figure 3.6). Ice cores extracted in 2009 from sites 1, 2 and 3 ranged in thickness from 0.124 to 0128 m. All three cores displayed a fresh layer (<1 psu) from the surface downwards, then transitioned into saline ice (by approximately 0.035 to 0.057 m). While the thickness of the three ice cores in 2009 is consistent with medium to thick FYI, the distinction in salinity and temperature between the upper and lower portions of the ice cores is consistent with ice that has survived at least one melt season (World Data Center A for Glaciology, 1978; Johnston & Timco, 2008). While the ice at all three sites is consistent with medium to thick FYI, the clear demarcation between fresh and saline ice is indicative of brine expulsion in MYI, meaning that the ice is most likely second year sea ice (SYI) (Johnston & Timco, 2008; Wadhams, 2000). The SYI likely developed from remnant ice floes that remained during open water conditions the previous melt season, as observed in ASTER L1B imagery from August 22, 2008 (Figure 3.7a). The presence of sea ice confirms the loss of the fresh epishelf lake water, and the new presence of marine water below. This provides validation for the backscatter analysis, where dark backscatter was observed across the entire southern coast in the Radarsat-2 imagery from February 2, 2009 (Section 3.5).

The ice core collected at site 1 in 2011 showed a slight increase in salinity with depth, although the salinity remained below 1 psu throughout the core profile (Figure 3.6). The temperature profile displayed a gradual increase in temperature with depth from -3°C at the surface to -0.4°C at the base. Direct observation of the core indicated bubble-free ice and the presence of vertical veins from the top of the core down to 0.024 m. The remainder of the

core was cloudy and had bubbles throughout, up to 1 cm in diameter. The occurrence of vertical veins at the top of the core is likely due to the presence of brine inclusions (Wadhams, 2000). Based on the thickness of the ice and the lack of demarcation between ice types, the ice core is most consistent with thick FYI formed over one winter (World Data Center A for Glaciology, 1978; Johnston and Timco, 2008). ASTER L1B imagery further supports this claim, as open water can be observed along the southern coast on July 19, 2010 at the location of site 1 (Figure 3.7b).

The ice cores collected from the four sites in spring 2012 demonstrated only slight variability in thickness, salinity and temperature between each other (Figure 3.6). Each ice core showed a gradual increase in core temperature with values ranging from -7.9^{0}C at the surface, to -0.8^{0}C at the base. Salinities in all the cores indicated upper layers with <1 psu, transitioning to slightly higher salinity levels (~2 psu) towards the base of the core. All of the cores were also similar in terms of their stratigraphy, with the near surface characterized by cloudy ice with large rounded bubbles. These surface characteristics are consistent with snow ice (or white ice), which is formed when enough snow falls on the ice cover during formation to depress it below the water surface, thus causing fracturing and water to rise to the surface through the snowpack (Adams & Roulet, 1980). This process results in snow ice which tends to have small spherical bubbles and a whitish appearance (Duguay et al., 2002). This snow ice layer is followed by a thicker layer of clear ice with small bubble trains throughout (Figure 3.8). This layer eventually transitions into increasingly cloudier ice and elongated bubbles, followed by the basal ice characterized by cloudy ice with small rounded bubbles. The salinity of the ice core profiles is consistent with MYI, while its linear temperature gradient and thickness is consistent with medium to thick FYI close to its winter state (in May) (World Data Center A for Glaciology, 1978; Johnston et al., 2003). Based on these observations it is likely that the ice cover is second-year sea ice, and therefore indicates that at least a portion of the sea ice along the southern coast remained since summer 2011.

3.3.2 CTD Measurements

A CTD profile collected at site 1 in April 2008 revealed a freshwater layer (<2 psu) down to 1.2 m, followed by a brackish layer (<17 psu) down to 5.6 m, reaching the halocline by ~7 m (Figure 3.9a). However, in 2009 CTD profiles showed sea water (salinity ~30 psu) throughout the entire water column, which confirmed the loss of the freshwater layer present in 2008 (Figure 3.9b). In 2011 and 2012 the CTD profiles recorded a shallow (<4 m) layer of freshwater at the surface, a depth too shallow to be consistent with an epishelf lake (where freshwater is >5 m) (Figure 3.9c, 3.9d & 3.10) (Jungblut et al., In press). This depth of freshwater is, however, consistent with the depth of a shallow ice-dammed lake.

The CTD profiles collected at all four sites in 2012 suggests that the water below the ice cover has a relatively thin, brackish layer, compared to the marine water below (Figure 3.9d & 3.10). At each site the brackish layer existed down to a depth of ~3 m, after which the salinity increased by ~2 psu to values consistent with ocean water for the remainder of the vertical profile.

3.3.3 GPR Measurements

According to the 2011 GPR measurements, the ice cover across the lake area had a mean thickness of 0.86 m, standard deviation of 0.32 m, and ranged from <0.25 m to 1.40 m. Slightly thicker areas (consistently over 0.70 m) occurred at the back of the embayment, in the region of site 3 (Figure 3.11). The presence of this thicker ice was confirmed with in situ ice coring, where ice measured 1.42 m at site 3, compared to 1.21 m, 0.97 m and 1.09 m at sites 1, 2 and 4, respectively. In-situ measurements also showed that site 3 had a more shallow snow depth of 43 cm, compared to a range of 53 to 58 cm at sites 1, 2 and 4. The thicker ice in this region may be attributed to thinner snow cover, slightly fresher water directly under the ice ranging from 17.1 to 21.2 psu compared to the other sites which ranged from 22.7 to 33.2 psu at site 1, 22.5 to 30.6 psu at site 2, and 20.3 to 26.9 psu at site 4, and shallow water depths (<15 m).

3.3.4 Satellite Image Analysis

3.3.4.1 Tributary Glacier Changes

In the 1959 aerial photograph of Petersen Bay the ice shelf appeared to extend across the bay to join the southern coastline to the west side of the islands (Figure 3.12a). At this time the tributary glacier in this region extended northward and terminated against the eastern-most island (Figure 3.13a). Remnant shelf ice was visible along the terminus of the glacier, distinguished by the rolling surface topography. Since 1959 the floating terminus of this glacier has decreased in extent (Figure 3.13a), and by 2007 the shelf ice extending to the east and west of the tributary glacier had gone (Figure 3.13b vs. 3.13c). In August 2008 the remaining shelf ice calved away from the glacier terminus during an open water event, and icebergs became distributed to the east and west side of the glacier tongue, which was no longer in contact with the island (Figure 3.13d). Again, in July 2010 an open water event occurred and further disintegration at the front of the tributary glacier occurred, causing additional icebergs to drift to the front and east of the terminus (Figure 3.13e). Radarsat-2 imagery acquired in 2011 does not show further break-up of the terminus, although fracture development is apparent across the remaining floating ice front, perpendicular to the flow of the glacier (Figure 3.13f). The icebergs dispersed in previous years appear to have drifted further to the east. Finally, in Radarsat-2 imagery from February 2, 2012, an additional portion of the floating area of the tributary glacier terminus has broken away and more icebergs have dispersed to the east (Figure 3.13g). Because this imagery was acquired in winter 2012, it is likely that the last of these reported changes occurred in summer 2011.

3.3.4.2 Open Water Events

Based on the lack of movement of icebergs throughout the lake area from March 1992 to March 2005, it is likely there was no open water during this 13 year period. By summer 2005, however, two large ice floes in the lake area showed evidence of motion (~130 m) between August 18 and 23. Lake ice cover was still visually detected in the SAR scenes in summer 2005, so this year was classified as partially open water (Table 3.3). No iceberg motion was observed between SAR scenes from July 2006 and July 2007, indicating that summer 2006 likely had no open water. The status of open water could not be assessed for

summer 2007, due to lack of image data. On August 22, 2008, an ASTER L1B satellite scene shows large areas of open water and sea ice break-up near the former tributary glacier along the southern coast (Figure 3.7a & 3.13d). Because ice cover was still present, the summer 2008 season was classified as partially open water. Based on ASTER satellite data acquired in July 2009 and July 2010, iceberg motion was observed. One iceberg that appeared to have broken off the tributary glacier rotated and moved ~476 m to the southeast between these satellite scenes, so summer 2009 was classified at partial open water. Open water was also visible in the July 2010 image, particularly around the islands in the central region of the lake area (Figure 3.12e), so 2010 was considered open water. Based on the motion of icebergs throughout the lake area between April 2011 and February 2012, the summer 2011 season was considered partially open water. With data limited to an ASTER scene from July 15, 2012, the summer 2012 scene was conservatively classified at partial open water.

In summary, based on the classification of open water events from 1992-2012, it would appear that open water events did not occur from 1992 until summer 2005. Since the 2005 melt season, partial open water and completely open water events have occurred every year, with the exception of summer 2007 that could not be classified due to insufficient data.

3.3.5 Backscatter Analysis

3.3.5.1 Backscatter Validation for Ice Types

To validate the effectiveness of backscatter analysis in identifying lake ice vs sea ice, the field measurements from field site 1 (Figure 3.3) were compared with backscatter analysis at site E (Figure 3.5), which are both located in the same region on the southeast side of the lake. In 2008, a CTD profile detected fresh and brackish water down to 5.6 m. The backscatter analysis from site A had a mean backscatter value of -4.8 dB, 1.2 dB above the threshold for freshwater used in this study. Therefore, the high backscatter was consistent with the presence of freshwater in this location. By 2009, when the CTD profile was saline throughout the water column (~30 psu), the backscatter across this site decreased to -15 dB, well below the -6 dB threshold for the presence of epishelf lake ice. The ice core collected from site 1 in 2009 (Figure 3.3) confirmed the presence of sea ice, therefore providing

further evidence that an epishelf lake was absent at that time. Based on this field validation, it is reasonable to assume that backscatter values >-6 dB are indeed evidence for a lake in Petersen Bay.

3.3.5.2 Temporal Lake Area Change

According to the spaceborne SAR imagery available prior to the 2000s (1992 to 1999), an epishelf lake occupied the area along the southern coast of Petersen Bay, extending to the eastern and northeastern coast (Figure 3.12b). For each year from 1992 to 1999 (excluding 1996 due to lack of data), the area of the epishelf lake detected through SAR backscatter analysis ranged from a minimum of 3.11 km^2 in 1995 to a maximum area of 5.21 km^2 in 1994 (Figure 3.14). The largest fluctuation in the area of epishelf lake occurred between 1994 and 1995 when the lake area lost 2.10 km^2.

From 2000 to 2004 the area fluctuated between 3.32 km^2 and 4.09 km^2. By March 2005, however, there was a drop in epishelf lake area to 2.46 km^2 from 3.94 km^2 in 2004. This was followed by a marked drop in area from 2005 to 2006 when the epishelf lake area decreased to 0.53 km^2 (Figure 3.12c, 3.12d, & 3.15). From 2006 to 2012 the area of higher backscatter indicative of an epishelf lake (>-6 dB) remained low, ranging from 0.02 km^2 to 0.66 km^2 (Figure 3.12d to 3.12f).

3.3.5.3 Subregional Backscatter Analysis

Until 2005 all study sites shown in Figure 3.5 had mean backscatter values above the -6 dB threshold, but after this time the strength of the backscatter was no longer uniform across the lake. Between 2005 and 2006, sites A, B, C, D and F all demonstrated a drastic decrease in mean backscatter (from ~1.4 dB to ~-11 dB). Site E, however, maintained a mean backscatter of -2.37 dB, well above the -6 dB threshold. Visual assessment of the calibrated Standard Radarsat-1 HH scene shows an area of high backscatter in the region of site E, with an area of ~0.7 km^2. A round area measuring 0.09 km^2 in the center of this region appears dark, and appears to be a sea ice floe based on observations from an ASTER L1B scene from July 24, 2006. In an ASTER L1B image from July 14, 2009, a major source of terrestrial

drainage flowed off the southern coast, into the site E region (Figure 3.16). A large alluvial fan to the south of this location supports evidence for long-term surface runoff in this particular area.

By January 26, 2007, Radarsat-1 imagery showed a decrease in backscatter at site E to ~−11dB, consistent with the loss of freshwater ice. However, sites D and F had an increase (to −5.1 and -4.8 dB respectively) in their returns above the freshwater threshold, while all other sites had returns below -10.76 dB. The presence of lake ice at site D and site F may have come from the freshwater at site E in the previous year, although this remains unclear. In 2008, site 5 became the only region with high backscatter returns (~-4.8 dB), while all other sites remained low. Once again, freshwater at site 5 likely originated from terrestrial drainage into this area.

3.4 Discussion

In 1959, the Petersen Ice Shelf occupied the majority of Petersen Bay, including the southern coast, with the exception of an area in the southeast region of the bay which may have been covered by lake ice. As the ice shelf began to decrease in area from the 1950s onward, the lake area was able to expand to occupy the areas once filled by the ice shelf. By 1992, the epishelf lake had an area of 4.6 km^2. From 1992 to 1999, the lake area ranged from 3.11 to 5.21 km^2, but the lake was always present. Based on the backscatter analysis by sub-region, the strong returns (>-6 dB), indicative of epishelf lake, were generally consistent across the lake until 2005.

In summer 2005, Petersen Ice Shelf underwent its first major break-up with a loss of 8.07 km^2 (Figure 3.17). This loss, along with the simultaneous loss of the entire Ayles Ice Shelf, occurred in tandem with the loss of MLSI from Yelverton Bay, which was thought to have provided a protective buffer for the ice shelves (Copland et al., 2007). Copland et al. (2007) also associated the 2005 ice shelf break ups with exceptional climatic conditions that year, including the early onset of the melt season, the second highest number of positive degree days since 1948, particularly warm temperatures in the month prior to the break up (2.1^{0}C

above the 1948-2006 average), and strong offshore and along shore winds (~90 km hr^{-1}). After this first major break-up, the Petersen Ice Shelf no longer provided a viable dam and the epishelf lake drained, likely along the southern coast of the bay where the ice shelf became detached from the coastline (Figure 3.18). This detachment was first detected in Radarsat-1 imagery from August 2005, when a meandering channel became apparent between the ice shelf and the southern coastline, providing a conduit for freshwater to escape. This type of drainage is reminiscent of the meandering channel that formed along the center of the Ward Hunt Ice Shelf in 2002, which provided a conduit for the drainage of the epishelf lake from Disraeli Fiord (Figure 3.1; Mueller et al., 2003). Based on the likely assumption that Petersen Epishelf Lake contained a rare ecosystem similar to the epishelf lakes at the Milne and Ward Hunt ice shelves (Van Hove et al., 2001; Veillette et al., 2011), the loss of this habitat would have resulted from the drainage.

The loss of the Petersen Bay epishelf lake was also supported via backscatter analysis and verified by ice core and CTD profiles. Based on the returns from SAR imagery between 2000 and 2004, the lake area with backscatter values consistent with the presence of an epishelf lake remained relatively consistent (ranging from 3.32 km^2 to 4.09 km^2). By 2005 the area of epishelf lake decreased to 2.46 km^2, and in 2006 decreased to 0.53 km^2. By examining the fluctuations in radar returns by sub-region, it was apparent that a large portion of the lake drained in 2005. However, an ephemeral freshwater region appeared to reform in the southeast part of the lake since 2005, at the edge of an alluvial fan where a major source of drainage can be observed in optical satellite imagery. This presence of this freshwater region was verified by field measurements in summer 2008, but didn't appear to be present between 2009 and 2012 when open water conditions began to occur throughout the summer months (Figure 3.7). Open water in the lake area would facilitate mixing via winds and would therefore prevent the freshwater from stratifying. This is supported by the results from a CTD profile from the ephemeral region in 2009 which showed a salinity of ~30 psu from the surface to the base of the profile. The loss of the lake was likely influenced by open water conditions in summer 2008 when a clear channel, once again, formed along the southern coast between the ice shelf and the land. Ice core analysis in 2009 confirmed the presence of sea ice in three different areas of the former epishelf lake area. The transition from

ephemeral freshwater regions to marine water and sea ice in Petersen Bay followed the second major break up to the Petersen Ice Shelf (-8.99 km^2) in summer 2008 and a large scale open water event in the former lake area. The break-up of the ice shelf also coincided with the second major loss of MLSI from Yelverton Bay in summer 2008 (Pope et al., 2012).

Since 2009, our remote sensing, ice core and CTD data suggest that the entire area formerly occupied by the epishelf lake has remained a marine environment. The vast open water event that occurred in summer 2010 also supports this interpretation. The ice cores extracted from several sites in May 2012 indicated a salinity profile consistent with MYI but with a thickness consistent with thick FYI, and was therefore classified as SYI. The CTD profiles collected in May 2012 detected a brackish 1 to 2 m deep layer across the lake area, which suggests that freshwater inflow from land continues to feed into the bay and may become impounded by the thin periphery of the ice shelf and sea ice at the outlet of the bay. This freshwater inflow comes from terrestrial snow and ice-melt runoff, as well as surface melt of the ice shelf itself (Gibson & Andersen, 2002). Although this thin brackish layer exists, it is not deep or fresh enough to be considered an epishelf lake.

3.5 Conclusions

The current state of the former lake in Petersen Bay, as of May 2012, includes a MYI cover with a mean thickness of 0.86 m. The water below the ice cover is characterized by ~3 m of brackish water followed by the marine water below, likely fed by freshwater runoff from the surrounding coastline. The lake has seen predominantly open water in the summers since 2005, reflecting a new ice regime in this area. It is likely that any chance of epishelf lake regeneration is disabled by these open water events. Under the present climate it is unlikely that Petersen Ice Shelf will regenerate, and therefore it is unlikely that the epishelf lake will ever form again. Similar to the drainage of the epishelf lake at Disraeli Fiord, the loss of the epishelf lake in Petersen Bay likely marks the loss of a unique ecosystem that may have provided a distinctive habitat for freshwater and marine water biota (Jungblut et al., In press).

Table 3.1: Image information for SAR data used in this study.

Sensor & Beam Mode	Date (YYYY-MM-DD)	Pixel Size (m)
ERS-1 Standard	1992-03-16	12.5
ERS-1 Standard	1993-05-19	12.5
ERS-1 Standard	1994-05-18	12.5
ERS-1 Standard	1995-02-24	12.5
Radarsat-1 ScanSAR Wide B	1997-02-11	50
Radarsat-1 ScanSAR Wide B	1998-02-06	50
Radarsat-1 Standard 7	1998-04-16	12.5
Radarsat-1 ScanSAR Wide B	1999-01-08	50
Radarsat-1 ScanSAR Wide B	2000-02-02	50
Radarsat-1 ScanSAR Wide B	2001-01-06	50
Radarsat-1 ScanSAR Wide B	2002-02-06	50
Radarsat-1 ScanSAR Wide B	2003-01-11	50
Radarsat-1 ScanSAR Wide B	2004-12-07	50
Radarsat-1 Standard 1	2005-03-18	12.5
Radarsat-1 Standard 1	2006-01-14	12.5
Radarsat-1 Fine 1	2007-01-26	6.25
Radarsat-1 Fine 1	2008-02-14	6.25
Radarsat-2 Wide 3	2009-02-02	12.5
Radarsat-2 Wide 3	2010-03-03	12.5
Radarsat-2 Ultrafine 78	2011-04-01	2.23
Radarsat-2 Ultrafine 3 Wide 2	2012-02-03	2.40
Radarsat-2 Ultrafine 3 Wide 2	2012-03-22	3.23

Table 3.2: Image information for aerial photographs and optical satellite scenes used in this study.

Sensor	Date (YYYY-MM-DD)	Resolution (m)	Number of GCPs	RMSE (m)
Aerial Photograph[1]	1959-08-13	6.6	10	33.25
ASTER Level 1B	2002-08-14	15	NA	NA
ASTER Level 1B	2003-07-03	15	13	14.93
ASTER Level 1B	2005-03-06	15	NA	NA
ASTER Level 1B	2005-08-18	15	NA	NA
ASTER Level 1B	2005-08-23	15	NA	NA
ASTER Level 1B	2006-07-24	15	NA	NA
ASTER Level 1B	2007-07-14	15	NA	NA
ASTER Level 1B	2008-08-22	15	NA	NA
ASTER Level 1B	2009-07-16	15	NA	NA
ASTER Level 1B	2009-07-21	15	NA	NA
ASTER Level 1B	2010-07-02	15	NA	NA
ASTER Level 1B	2010-07-19	15	NA	NA
ASTER Level 1B	2012-07-15	15	NA	NA

[1] Image IDs: A16724-63 & A16724-64

Table 3.3: Open water events recorded in Petersen Bay from 1992 to 2012 (with the exception of 2007).

Time Period	Sensor	Date	Evidence	Open Water Status
March 1992 to March 2005	ERS-1 (Standard) ERS-1 (Standard) ERS-1 (Standard) ERS-1 (Standard) Radarsat-1 (Standard 7) ASTER L1B ASTER L1B Radarsat-1 (Standard 1)	1992-03-16 1993-05-19 1994-05-18 1995-02-24 1998-04-16 2002-08-14 2003-07-03 2005-03-18	Icebergs to the west of the islands and to the east of the tributary glacier remain motionless and show in situ melting.	No open water
Summer 2005	Radarsat-1 (Standard 7) Radarsat-1 (Standard 1)	2005-08-18 2005-08-23	Ice floe (~0.17 km^2) in the eastern region of the lake moved ~130 m to the north. Bright backscatter and rough texture throughout lake area suggest presence of ice cover.	Partial open water
Summer 2006	ASTER L1B ASTER L1B	2006-07-24 2007-07-14	Icebergs throughout lake area remain motionless.	No open water
Summer 2008	ASTER L1B	2008-08-22	Open water throughout lake area. Icebergs breaking away from tributary glacier and flowing to the east and west.	Partial open water
Summer 2009	ASTER L1B ASTER L1B	2009-07-21 2010-07-02	Areas of open water around islands in 2009 image. Iceberg (0.03 km^2) from tributary glacier rotated and moved ~476 m to the southeast.	Partial open water
Summer 2010	ASTER L1B	2010-07-19	Open water visible in satellite imagery.	Open water
Summer 2011	Radarsat-2 (Ultrafine 78) Radarsat-2 (Ultrafine 3, Wide 2)	2011-04-01 2012-02-03	Iceberg motion throughout lake area.	Partial open water
Summer 2012	ASTER L1B	2012-07-15	Open water visible in several areas of the lake. Ice shelf break-up and new icebergs evident in lake area.	Partial open water

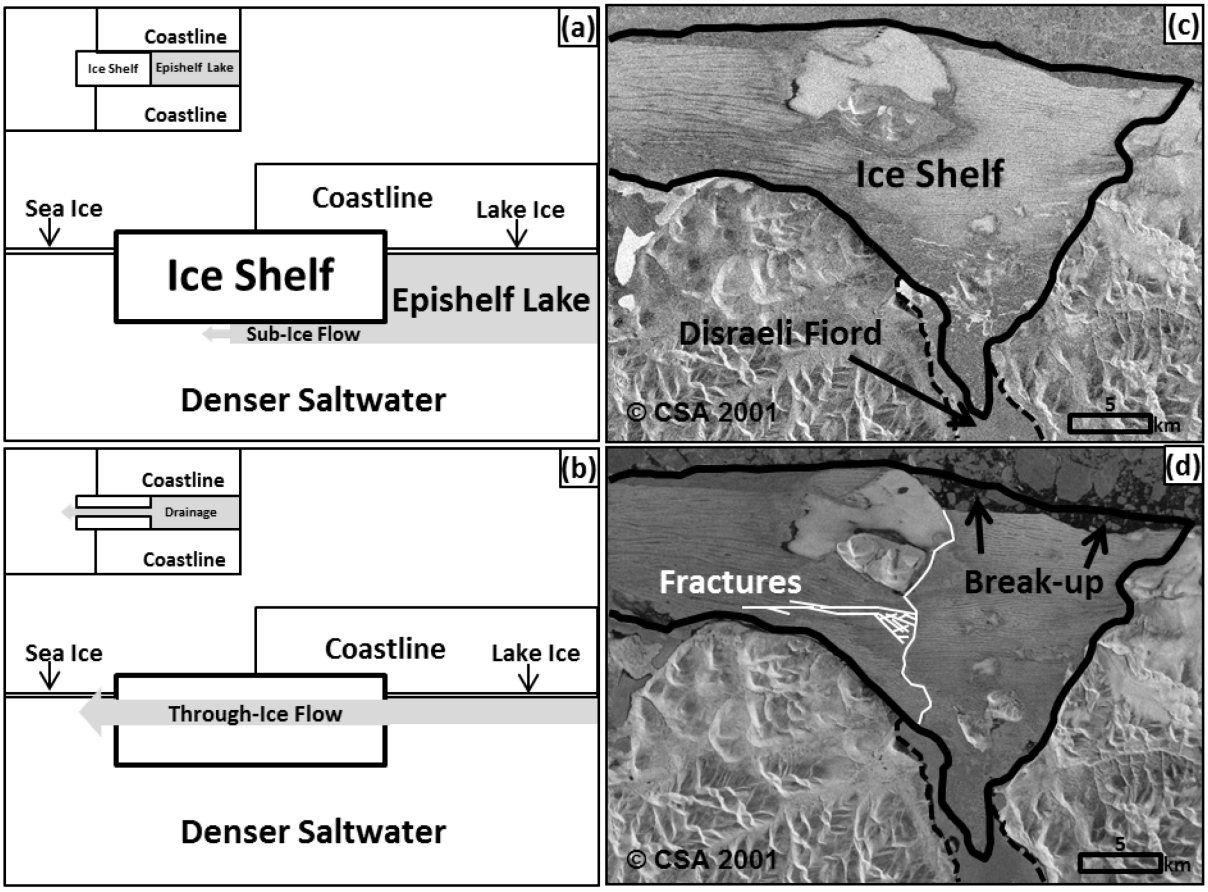

Figure 3.1: (a) Cross-section schematic of a typical, stable epishelf lake. Inset: Plan view of typical stable epishelf lake; (b) Cross-section schematic of epishelf lake drainage via fractures in the ice shelf. Inset: Plan view of epishelf lake drainage via fractures in the ice shelf; (c) Radarsat-1 SAR scene from October 2001 of the Ward Hunt Ice Shelf damming the epishelf lake known as Disraeli Fiord; (d) Radarsat-1 SAR scene from August 2002 which shows fracture formation in the ice shelf cover, allowing the freshwater to drain from Disraeli Fiord. (Figures 3.1a & 3.1b adapted from Mueller et al., 2003).

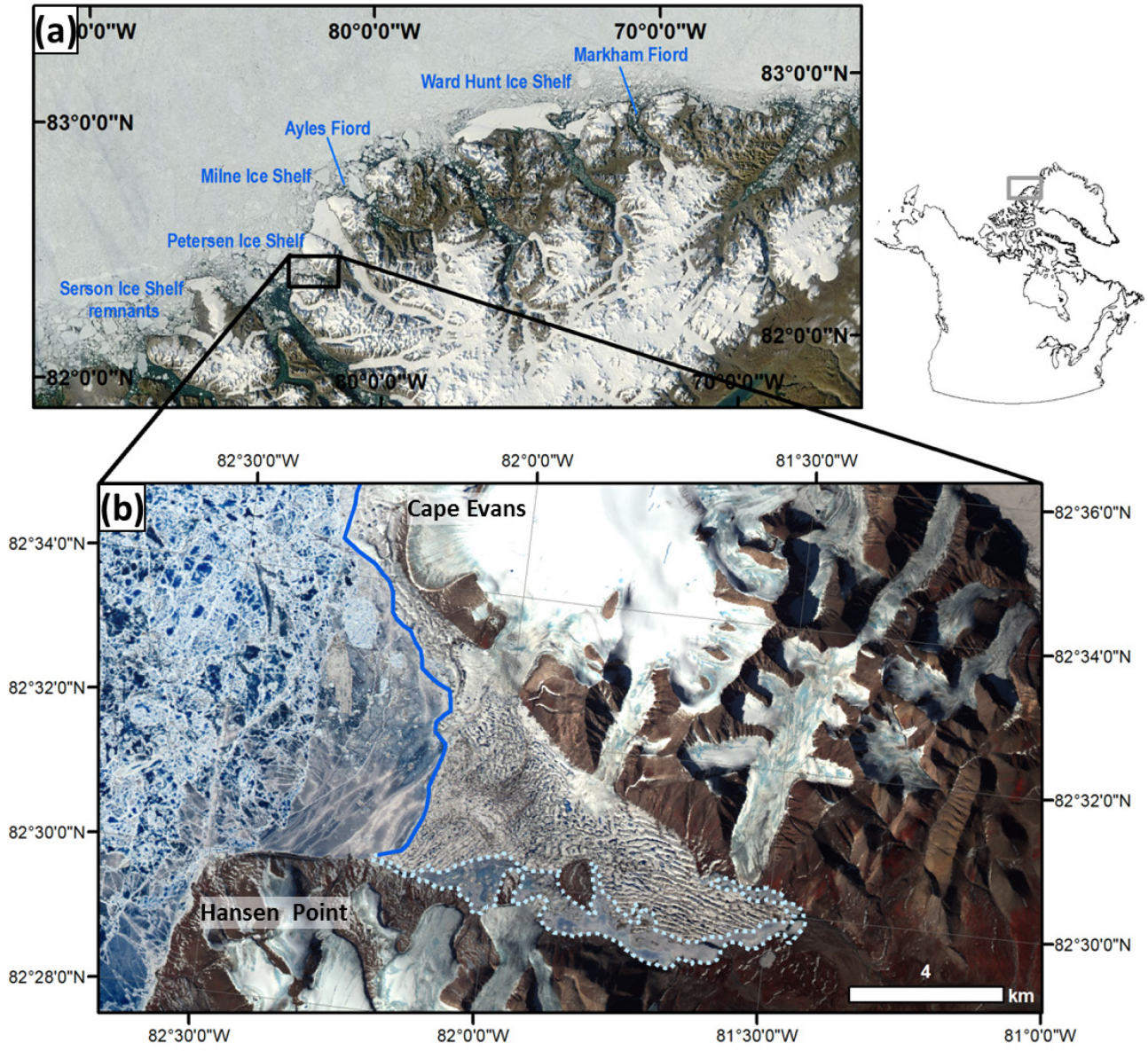

Figure 3.2: (a) MODIS scene (2011-08-01) of the northern coast of Ellesmere Island with annotated locations of the remaining ice shelves as of August 2011 (b) ASTER Terra scene (2009-07-16) showing Petersen Bay, the Petersen Ice Shelf (extent in 2009) and the Petersen Bay lake area (dotted line).

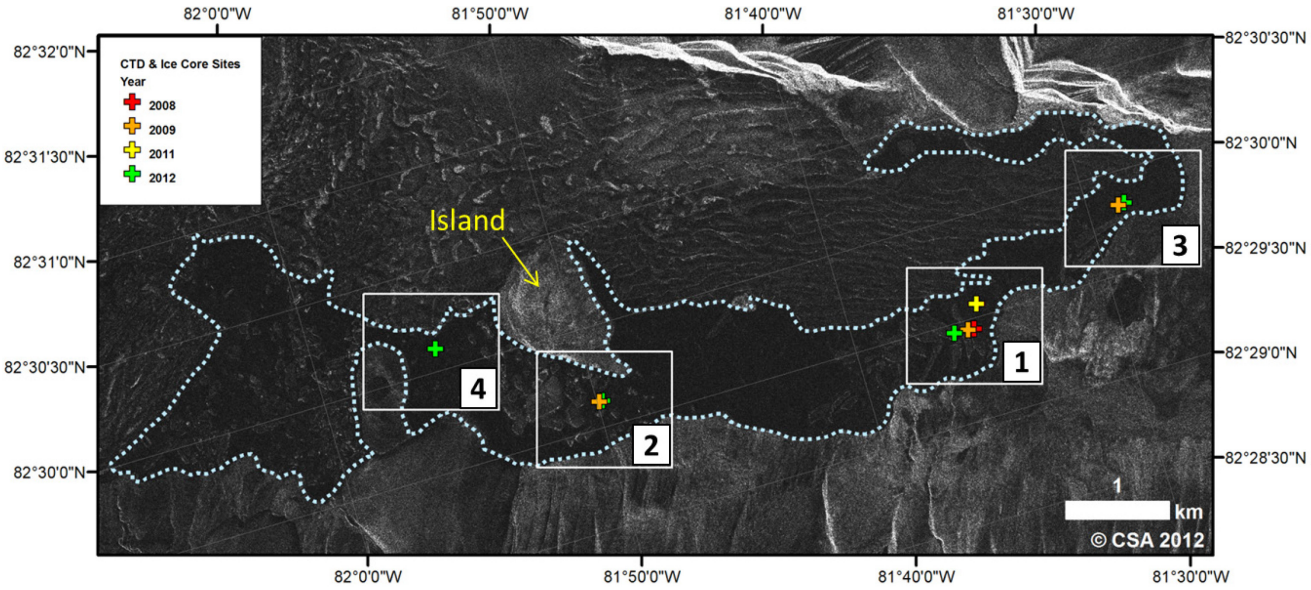

Figure 3.3: Annotated Radarsat-2 Ultrafine Wide HH scene from 2012-02-03, denoting the location of each CTD and ice coring site across the Petersen Bay epishelf lake. A CTD and ice core was collected from each site and in each year except for 2008, when only a CTD profile was collected. White boxes denote the study areas.

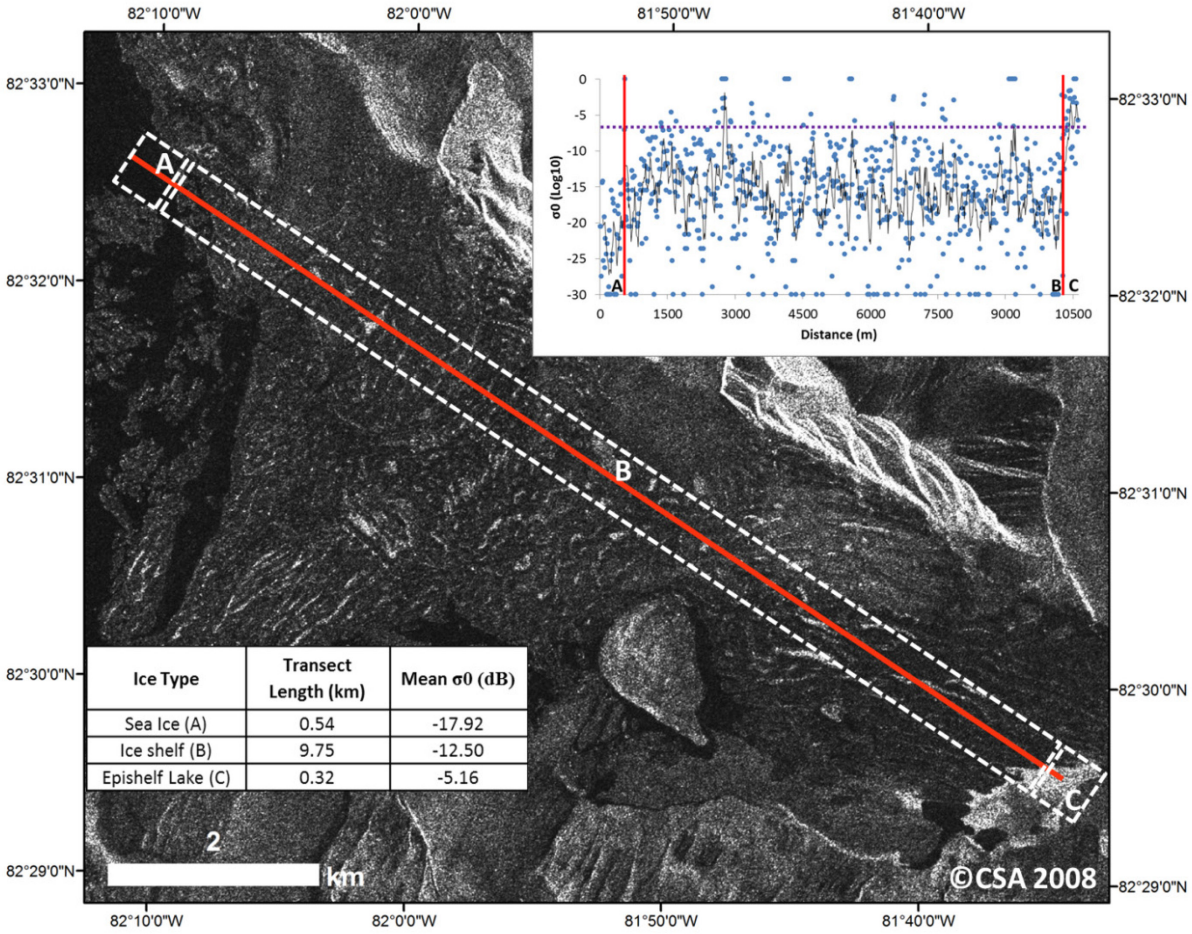

Figure 3.4: Radarsat-1 fine beam satellite image (2008-02-14) showing the transect (in red) used to extract sigma nought values from different ice types: (A) sea ice, (B) ice shelf, (C) epishelf lake ice. Inset graph: sigma nought values extracted from the transect, separated by ice type (red line): (A) sea ice, (B) ice shelf, (C) epishelf lake ice. The dotted purple line represents the -6 dB threshold. Inset table: transect length and mean sigma nought value for each ice type.

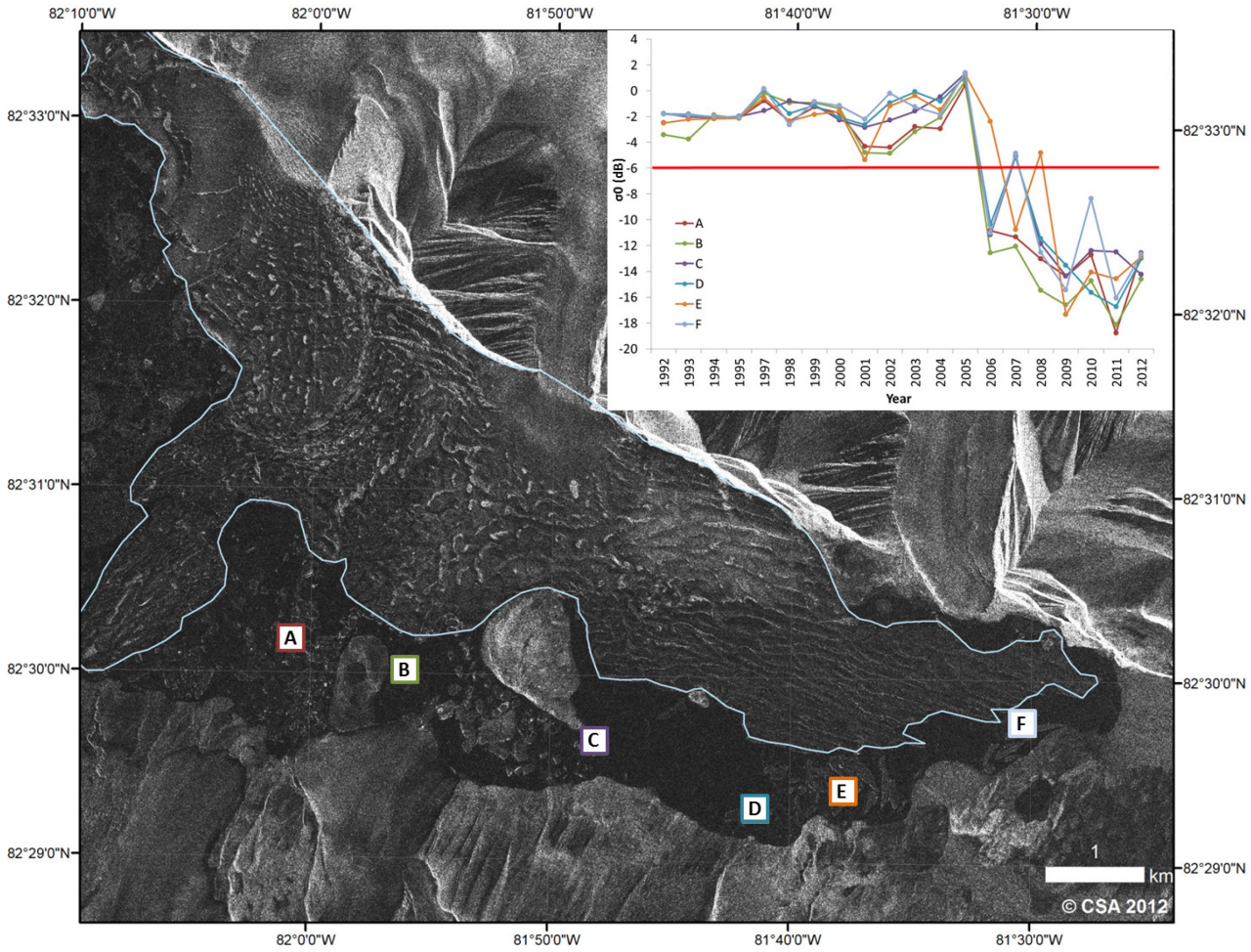

Figure 3.5: The six sites selected for sub-regional backscatter analysis within the Petersen Bay lake area, overlaid on an Ultrafine Wide Radarsat-2 HH scene (2012-02-03). Inset: Graph of the mean sigma nought value extracted from the six sites (colour of the box for each site corresponds with the graph). The red line denotes the -6 dB threshold associated with the presence of an epishelf lake.

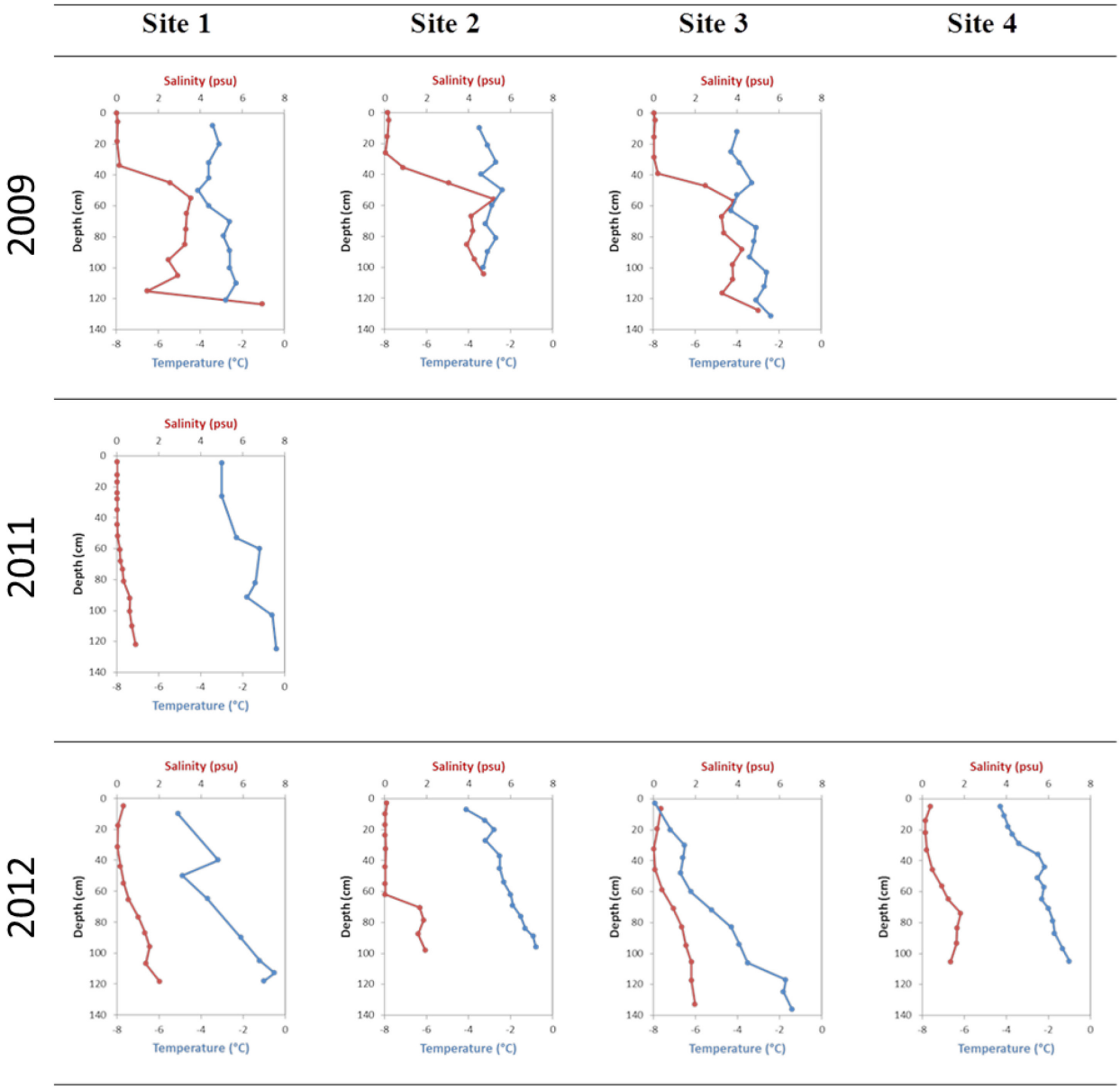

Figure 3.6: Ice core conductivity and temperature measurements collected across the Petersen Bay epishelf lake in May 2009, May 2011 and May 2012. All ice cores penetrated the full lake ice thickness (See Figure 3.3 for location of sites).

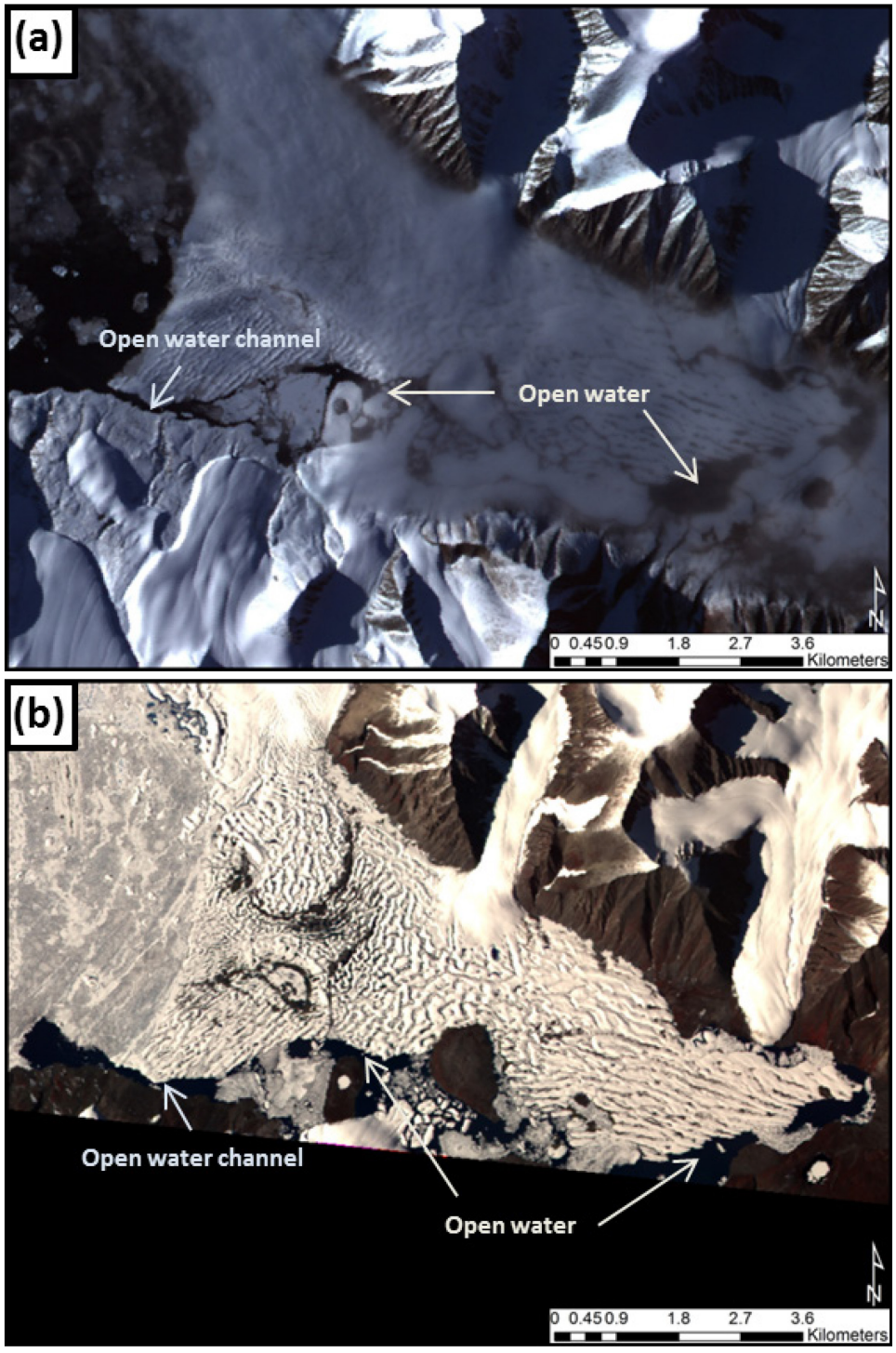

Figure 3.7: Open water in the Petersen Bay lake area visible in ASTER imagery from (a) 2008-08-22; and (b) 2010-07-19. These open water events indicate that an epishelf lake is no longer viable in this area due to the exposure to wind mixing and an open water channel along the southern coast.

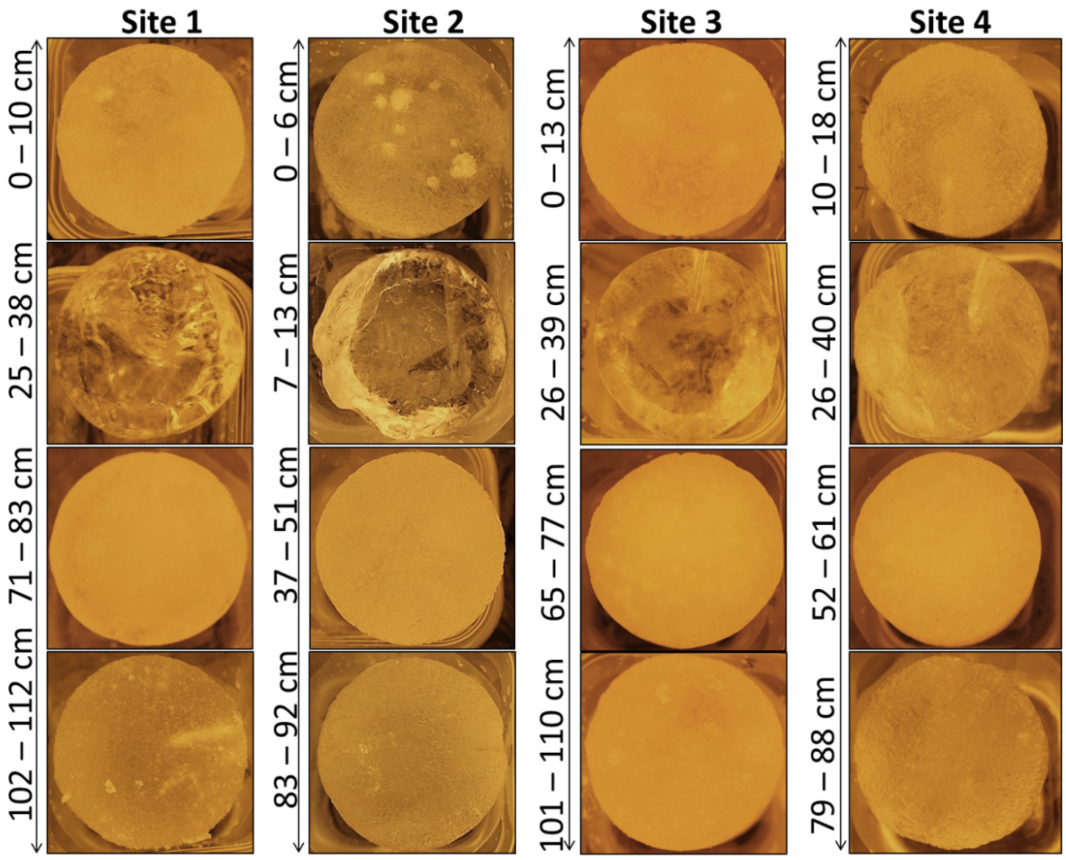

Figure 3.8: Photographs of the core segments extracted from sites 1, 2, 3, and 4 in May 2012 from the Petersen Bay lake area (See Figure 3.3 for site locations). Measurements refer to distance of core segments below the surface.

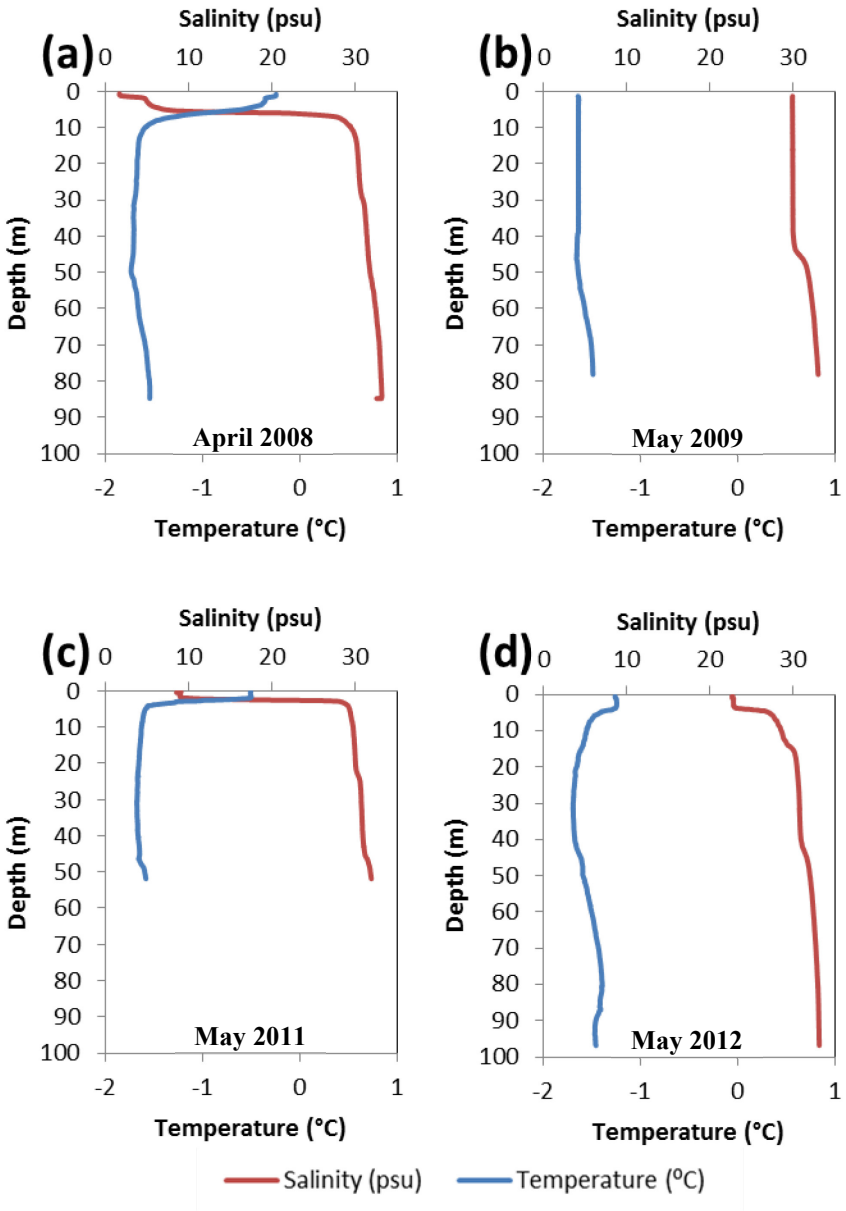

Figure 3.9: CTD (conductivity-temperature-depth) profiles showing the fluctuation in salinity and temperature through the depth of the lake area at site 1 (ephemeral region) in (a) April 2008; (b) May 2009; (c) May 2011; (d) May 2012.

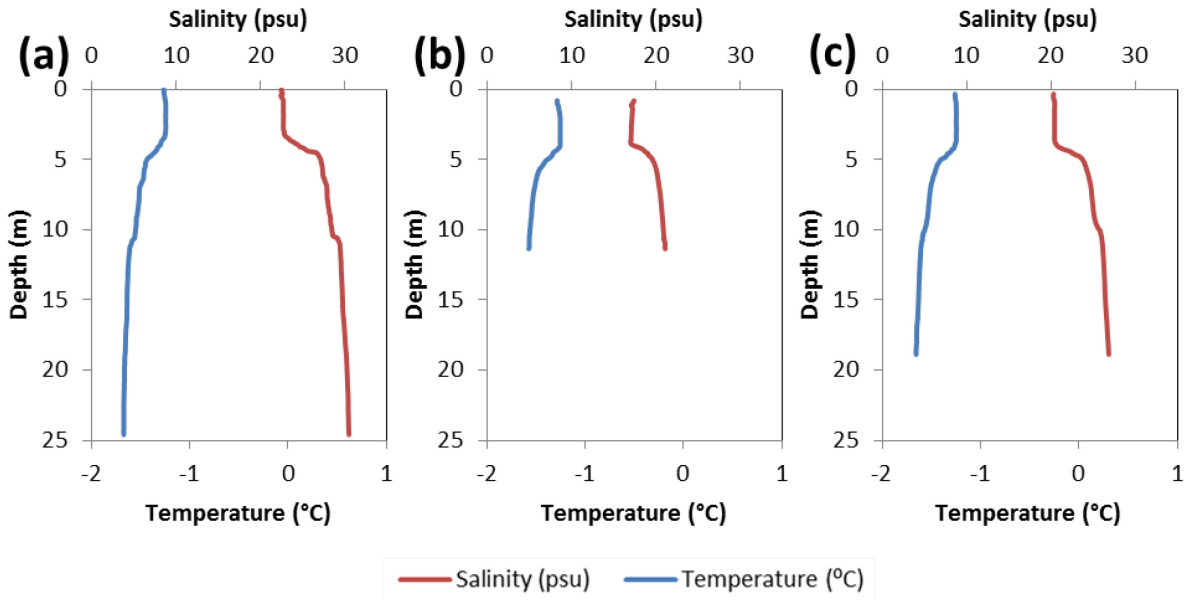

Figure 3.10: CTD (conductivity-temperature-depth) profiles showing the fluctuation in salinity and temperature through the depth of the lake area in May 2012 at (a) site 2; (b) site 3; (c) site 4. See Figure 3.3 for measurement locations.

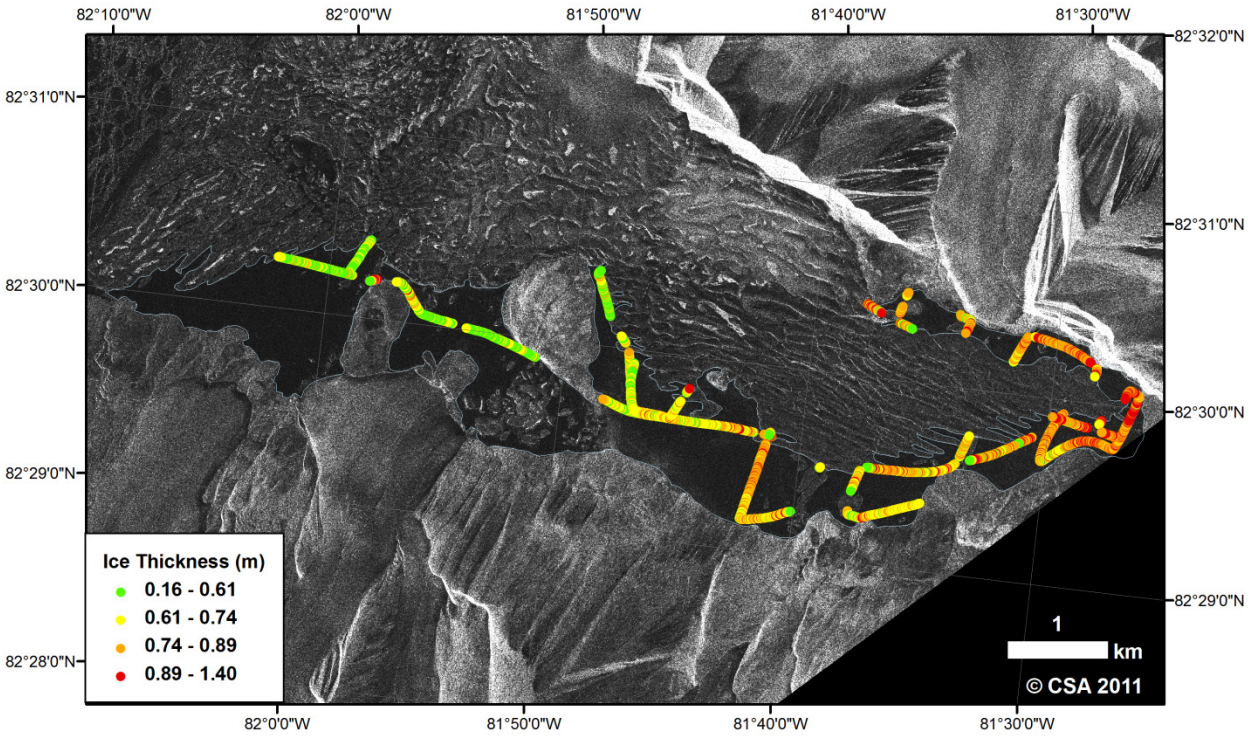

Figure 3.11: GPR measurements showing ice cover thickness (overlain on a Radarsat-2 Ultrafine HH scene, 2011-04-01) across the Petersen Bay lake area in May 2011. Ice thickness was up to 1.40 m, with the greatest thicknesses at the back of the bay (east side).

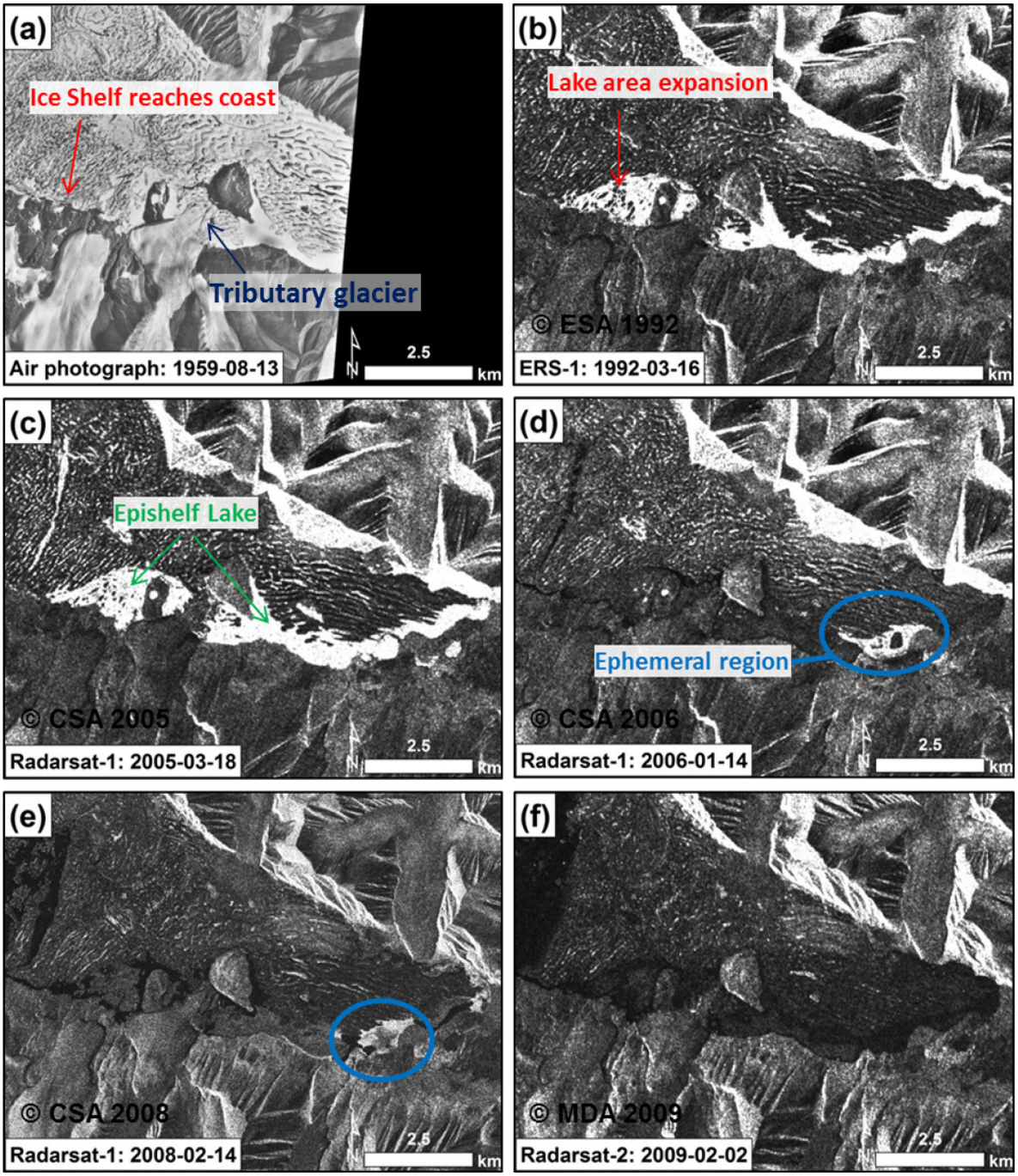

Figure 3.12: Aerial photography (1959) and SAR imagery showing: (a) extent of the lake in 1959; (b) expansion of epishelf lake to the west of the islands in March 1992; (c) evidence for the epishelf lake as bright backscatter across the bay, adjacent to the Petersen Ice Shelf in March 2005; (d) loss of epishelf lake area, but remaining ephemeral freshwater regions identified by higher backscatter in January 2006; (e) ephemeral region of freshwater in February 2008, present since 2006; (f) low backscatter across entire southern coast in February 2009 indicates complete loss of any epishelf lake. The regions of high backscatter on the northern side of the ice shelf are due to layover and foreshortening of the SAR image (i.e. an artifact) and therefore this area was not considered in the backscatter analysis.

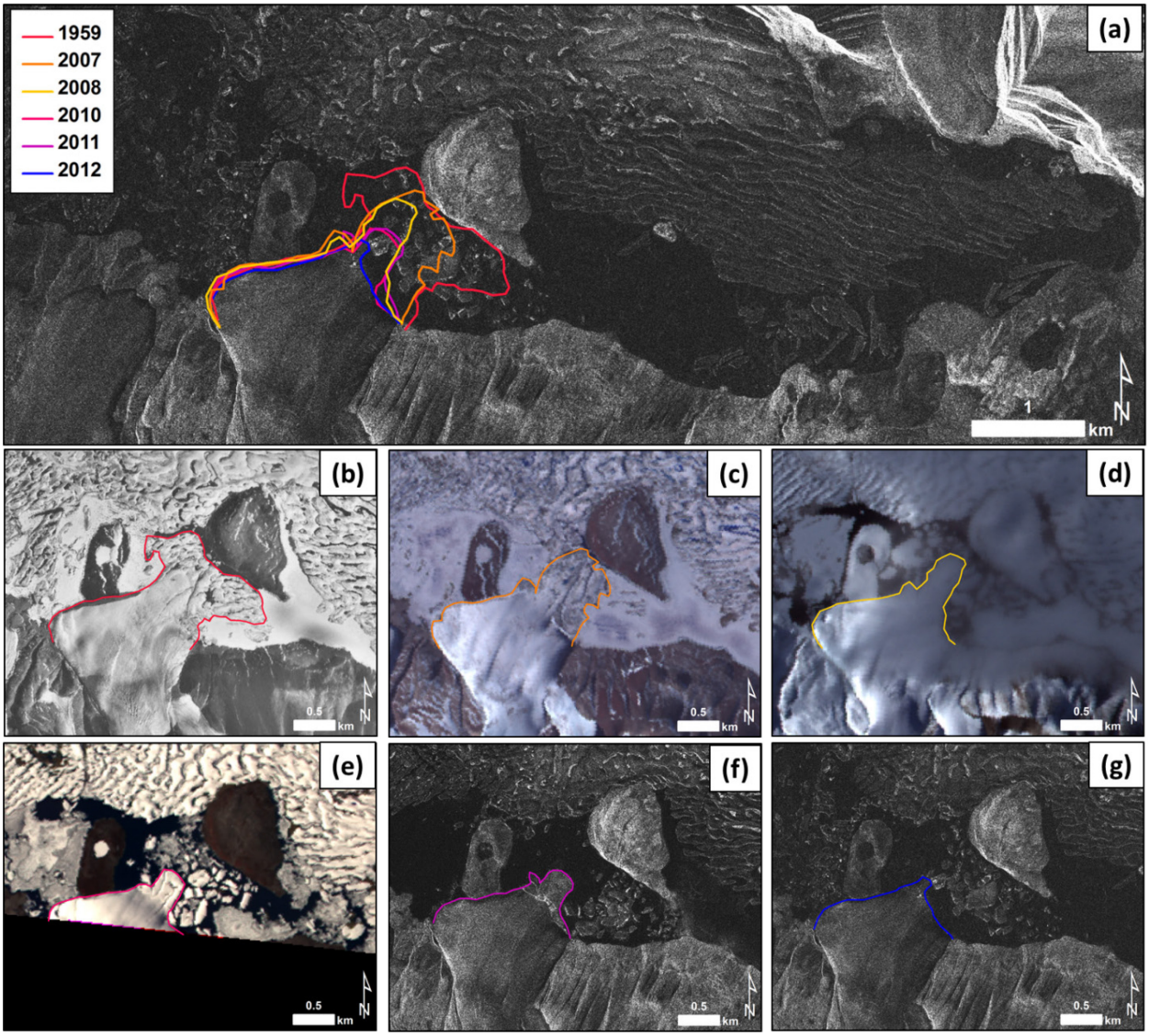

Figure 3.13: Aerial photography and satellite imagery highlighting changes in the tributary glacier flowing from the southern coast into Petersen Bay and the dispersal of icebergs. (a) Ultrafine Wide Radarsat-2 HH from February 3, 2012; (b) Aerial photography mosaic from August 13, 1959; (c) ASTER L1B scene acquired July 7, 2007; (d) ASTER L1B scene acquired August 22, 2008; (e) ASTER L1B scene acquired July 19, 2010; (f) Ultrafine Radarsat-2 HH scene acquired July 19, 2011; (g) Ultrafine Wide Radarsat-2 HH scene acquired February 3, 2012.

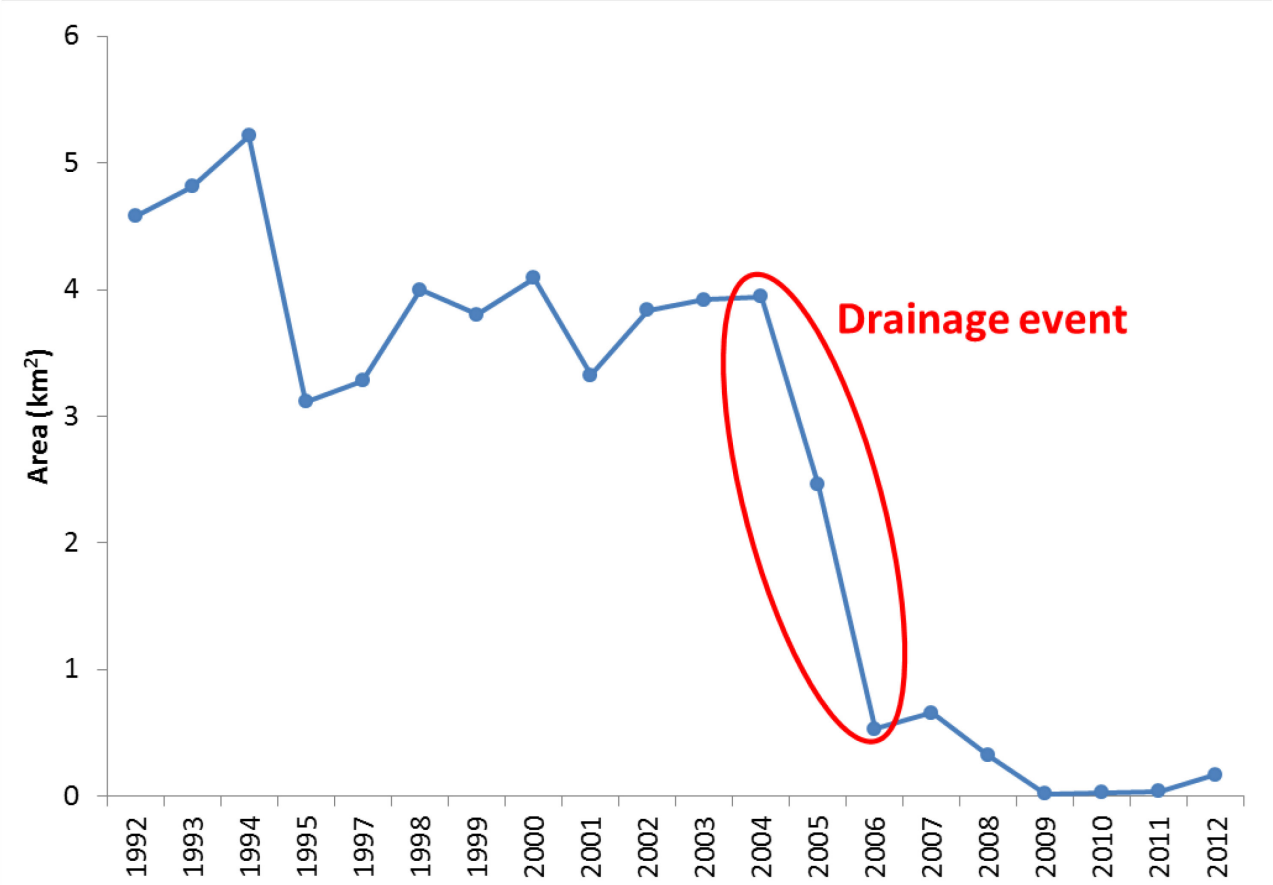

Figure 3.14: Changes in freshwater lake area determined through backscatter thresholding (values >-6 dB) from 1992 to 2012. The drop in freshwater area from 2005 to 2006 likely marks a drainage event coincident with the first major break up of the Petersen Ice Shelf. From 2006 onwards, the freshwater area remained low with no sign of recovery.

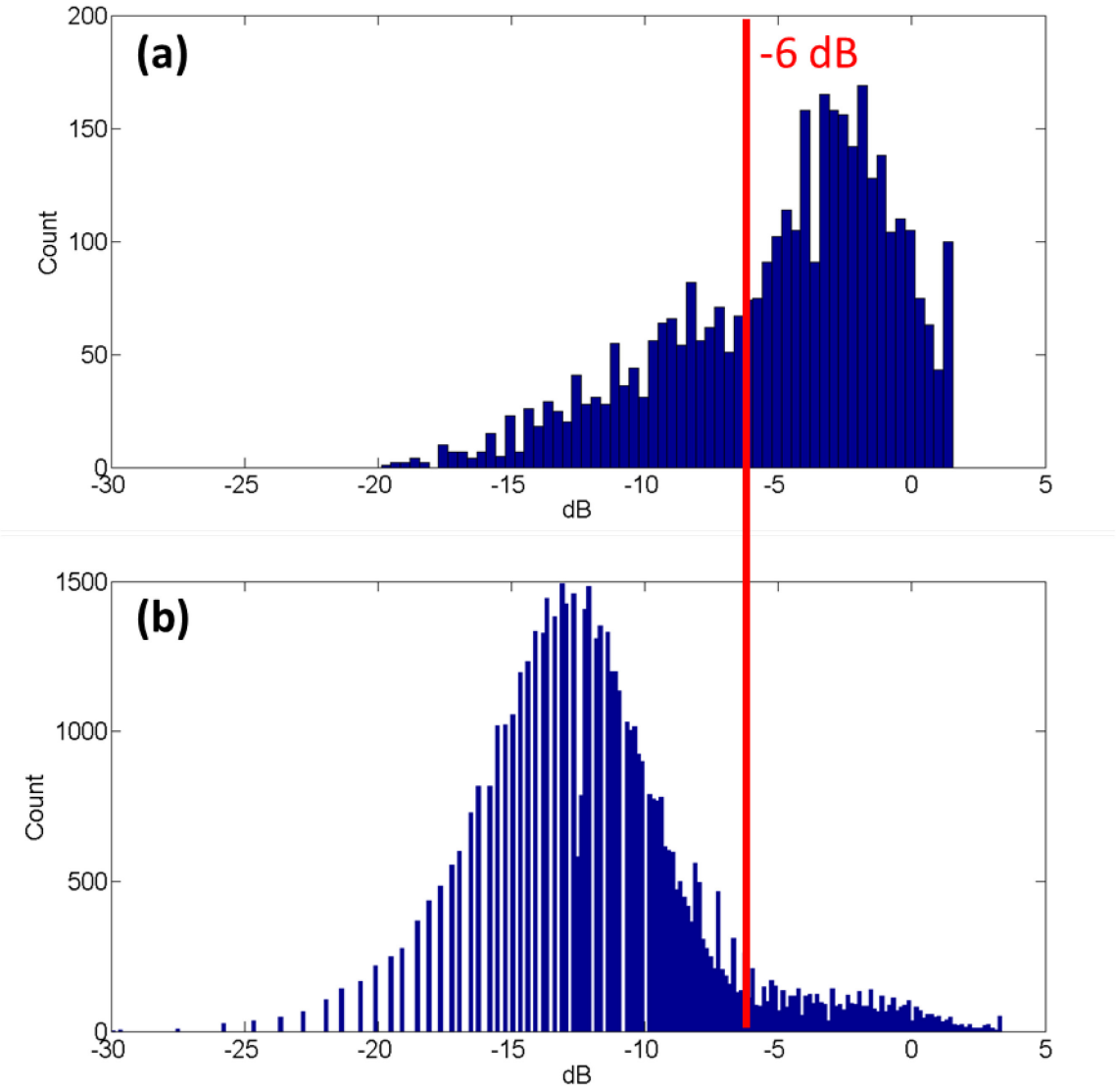

Figure 3.15: Histograms indicating the change in distribution of backscatter before and after the first major break up of the Petersen Ice Shelf in 2005, in (a) 2004 and (b) 2006. In 2004 the backscatter was predominantly >-6.0 dB, while post-break up, the backscatter dropped below the -6.0 dB threshold.

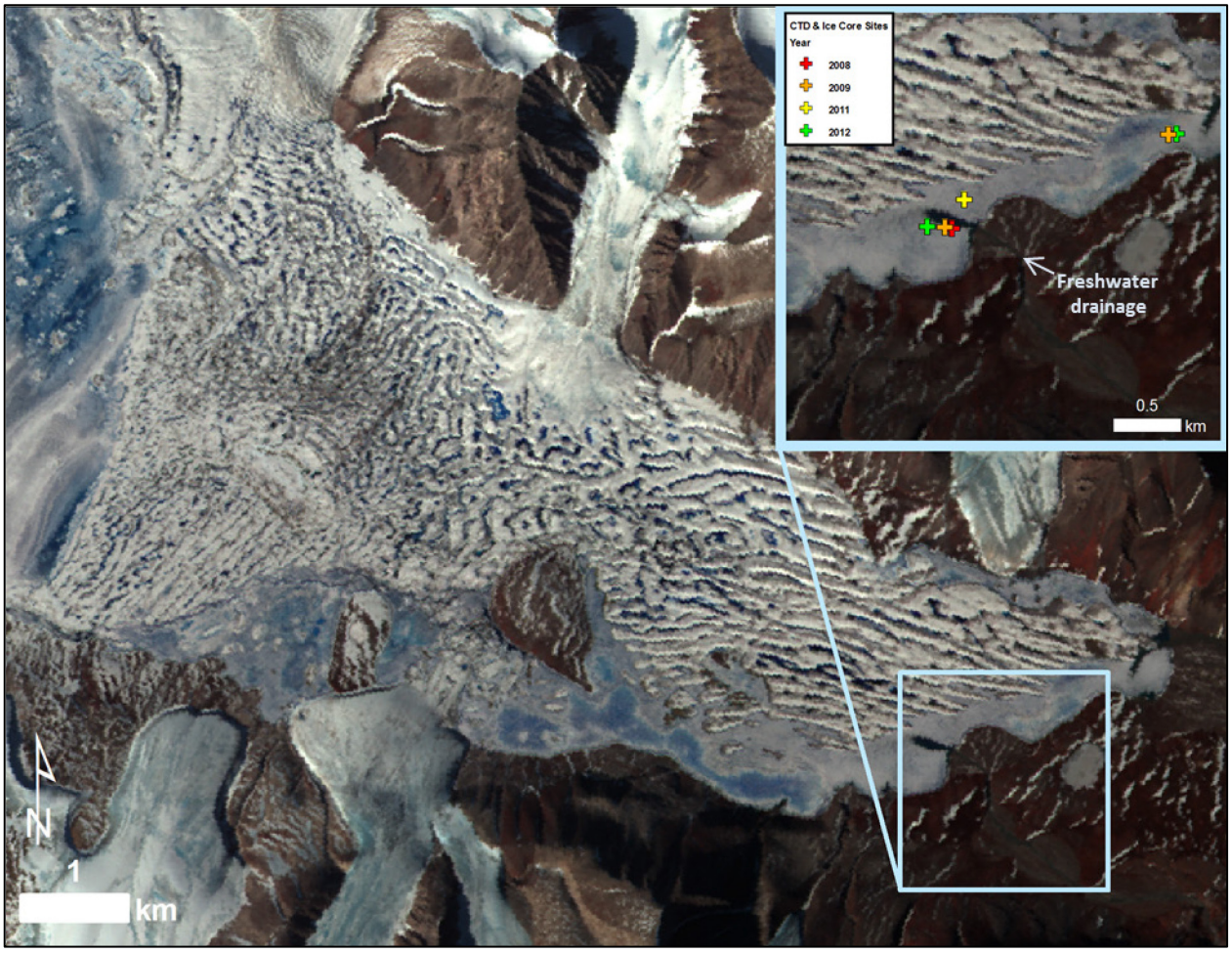

Figure 3.16: ASTER L1B satellite image (2009-07-14) of Petersen Bay with inset showing the pathway of major terrestrial freshwater drainage and an alluvial fan along the coast of the lake area.

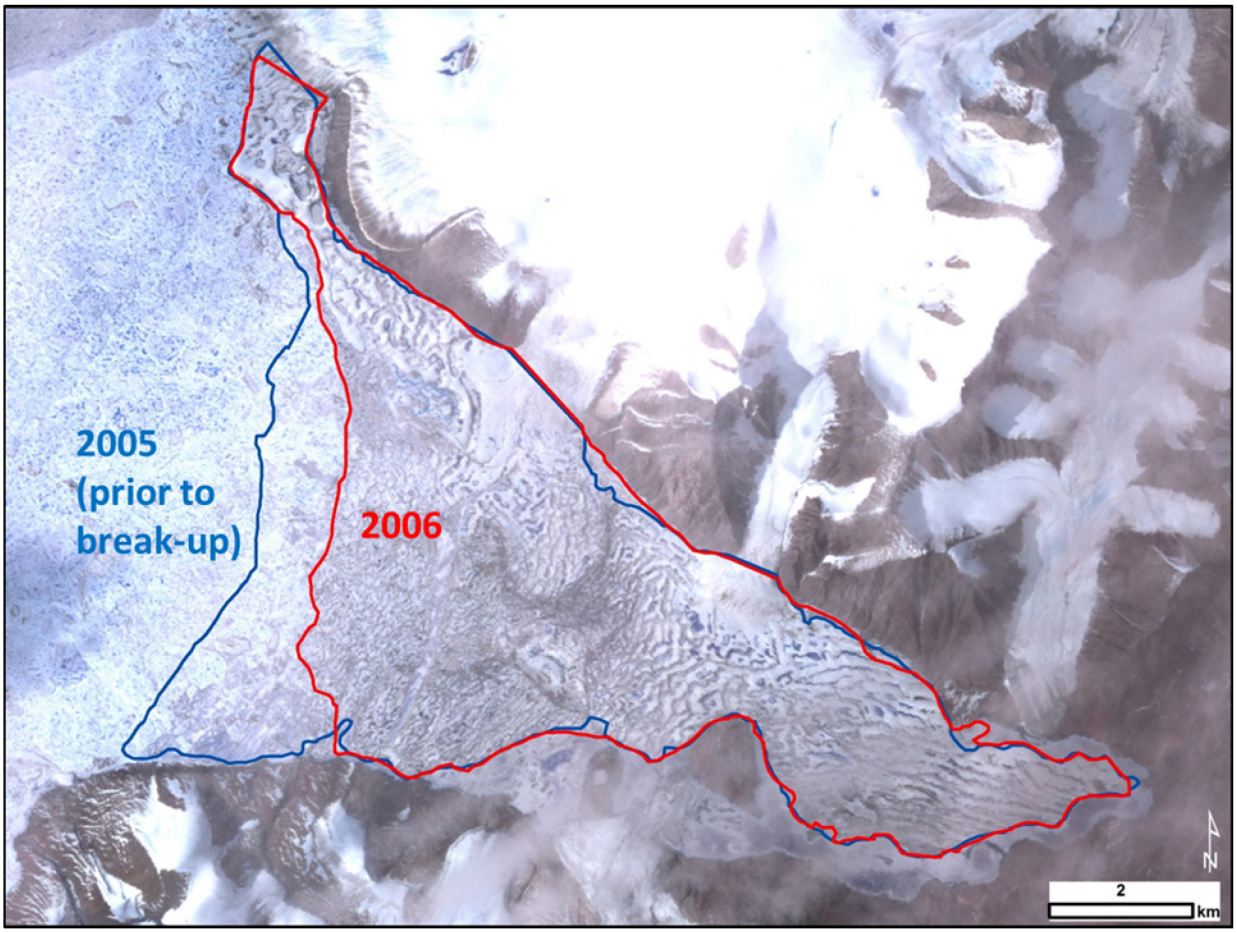

Figure 3.17: ASTER image (2006-07-24) showing the extent of the Petersen Ice Shelf before and after the 2005 breakup which accounted for a loss of 8.1 km^2.

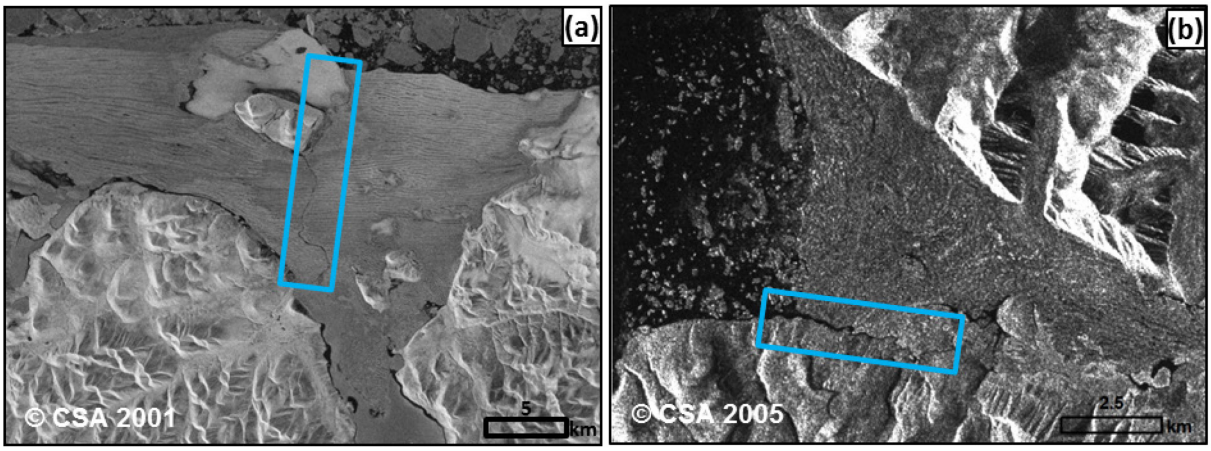

Figure 3.18: Fractures through ice shelves which provide a conduit (shown within blue rectangle) by which freshwater is lost: (a) Radarsat-1 scene from August 2002 showing the drainage channel from Disraeli Fiord through the Ward Hunt Ice Shelf; (b) Radarsat-1 scene from August 2005 showing the drainage channel along the southern coast of Petersen Ice Shelf.

4. Conclusions

The studies presented here provide the first comprehensive assessment of the Petersen Ice Shelf and epishelf lake, including their current physical characteristics and recent changes. Between the late 1950s and early 2005 the Petersen Ice Shelf remained relatively stable with a minor cumulative area increase of 1.5 km^2. Since this time, however, three major break-ups have occurred in the summers of 2005, 2008, 2011, and 2012 with losses of 8.07 km^2, 8.99 km^2, 5.48 km^2, and 5.49 km^2 respectively. The first break-up in summer 2005 coincided with the loss of 690 km^2 of MLSI from adjacent Yelverton Bay, which had originally provided a buffer across the front of the Petersen Ice Shelf, protecting it from the effect of winds, waves and collisions with pack ice. Upon loss of this buffer the ice shelf front became vulnerable to these factors, likely facilitating its break-up. The 2005 break-up also coincided with the complete loss of the nearby Ayles Ice Shelf, which Copland et al. (2007) attributed to the loss of MLSI at the ice shelf front, long-term climate warming and exceptional weather conditions associated with high winds and warm air temperatures. The break-ups of the Petersen Ice Shelf in 2008, 2011 and 2012 were similarly accompanied by unusually warm temperatures and open water conditions across the ice shelf front. The losses during these years also coincided with losses from other ice shelves along the northern coast of Ellesmere Island including the Ward Hunt, Markham, and Serson ice shelves in 2008, the Serson and Ward Hunt in 2011, and Ward Hunt in 2012. Furthermore, the 2008 break-up of the Petersen also occurred in tandem with further loss of MLSI from Yelverton Bay.

Based on SAR backscatter analysis, the southern portion of Petersen Bay likely contained an epishelf lake until 2005. During the 2005 calving event from Petersen Ice Shelf, a channel formed between the southern coastline and the ice shelf, providing a conduit through which freshwater likely drained. This sequence of events is similar to those observed at the Ward Hunt Ice Shelf, where break-up and fracturing of the ice shelf were followed by the drainage of the freshwater epishelf lake from Disraeli Fiord in 2002 (Mueller et al., 2003). From 2006 to 2008, ephemeral regions of freshwater occurred towards the back of the Petersen Ice Shelf. However, regeneration of the epishelf lake was prevented by summer open water events and continued drainage along the southern coast. The southern coast of Petersen Bay currently contains marine water with a MYI cover with a mean thickness of 0.86 m. Below

sea ice, ~3 m of brackish water overlays the marine water below. While freshwater likely continues to feed into this area from surface runoff and nearby terrestrial sources, the increased frequency of open water summers prevents permanent stratification.

Based on field measurements, the mean thickness of the Petersen Ice Shelf was 29 m in May 2011, with thinner regions (<20 m) along its southern coast and both east and west margins. Although these thin areas do not meet the 20 m thickness required for the technical definition of an ice shelf, they are still connected to thicker areas well over the 20 m threshold (Dowdeswell & Jeffries, In press). These thicker regions (>100 m) were detected at the front of a main tributary glacier that flows in from the north (Glacier 2), indicating the importance of glaciers as input to Petersen Ice Shelf. Surface velocities determined via speckle tracking of imagery acquired in spring 2012, combined with the thickness measurements, provide the means to estimate the mass flux from the two tributary glaciers that feed into the ice shelf from the northern coast. When averaged over the February 2005 ice shelf area of 24.8 km^2, these glaciers input 7.89 to 13.55 cm yr^{-1} equivalent ice thickness per year to the ice shelf. The input from these glaciers, however, is offset by a mean surface ablation of 1.30 m yr^{-1} recorded at two stakes over the period 2011-2012. If this ablation rate is extrapolated across the entire ice shelf area (30.3 km^2 in April 2011), this equates to a mass loss of 3.54×10^7 to 3.71×10^7 m^3 yr^{-1} and a complete loss of the ice shelf by the year 2034-2036 (assuming no losses via calving, no basal melt or accretion and no changes to the rate of surface lowering). This estimate is in line with the prediction by Hattersley-Smith et al. (1955) that the northern Ellesmere ice shelves would be completely lost by 2035.

An investigation of spatial variability in GPR bed reflection strength showed that strong basal reflections were prevalent in thicker regions of the ice shelf, but that basal reflections were often absent in thinner regions, particularly in the eastern part of the ice shelf. A 13.24 m deep ice core extracted from the eastern region confirmed the presence of saline ice (>2 psu) at a depth of 5-6 m, followed by an exceptionally high salinity (>79 psu) slush layer between 11 m and 13 m. The presence of saline ice is likely the cause of signal attenuation, as was also found in past studies on the Ward Hunt Ice Shelf (Jeffries and Sackinger, 1988). Traces along the Petersen Ice Shelf that were less affected by signal attenuation were used in

combination with dGPS data to examine the relationships between surface and basal topography. Based on this analysis the ice was found to be thinner below surface troughs and thicker below surface ridges, which supports the theory by Hattersley-Smith et al. (1955) that the undulating surface of Arctic ice shelves is in isostatic equilibrium with its basal ice topography.

In summary, the Petersen Ice Shelf and epishelf lake have undergone extensive changes since 2005, including a ~63% loss of the June 2005 area between June 3, 2005 and August 24, 2012, and the complete drainage and replacement of the epishelf lake with sea ice. Under the current and projected climate, the long-term outlook for Petersen Ice Shelf is poor. Surface melt alone suggests complete loss by 2034-2036, but when combined with the frequency of recent calving events it's unlikely that the ice shelf will survive for more than a decade.

References

Adams, W.P. and Roulet, N.T. (1980) Illustration of the roles of snow in the evolution of the winter cover of a lake. *Arctic*, 33(1), 100-118.

Alt, B. and Wilson, K. (2006) A case study of old-ice import and export through Peary and Sverdrup Channels in the Canadian Arctic Archipelago: 1998-2005. *Annals of Glaciology*, **44**, 329-338.

AMAP (2011) Snow, Water, Ice and Permafrost in the Arctic (SWIPA): Climate Change and the Cryosphere. Arctic Monitoring and Assessment Programme (AMAP), Oslo, Norway, 538 pp.

Anisimov, O.A., D.G. Vaughan, T.V. Callaghan, C. Furgal, H. Marchant, T.D. Prowse, H. Vilhjálmsson and J.E. Walsh, 2007: Polar regions (Arctic and Antarctic). *Climate Change 2007: Impacts, Adaptation and Vulnerability. Contribution of Working Group II to the Fourth Assessment Report of the Intergovernmental Panel on Climate Change*, M.L. Parry, O.F. Canziani, J.P. Palutikof, P.J. van der Linden and C.E. Hanson, Eds., Cambridge University Press, Cambridge, 653-685.

Antoniades, D., Francus, P., Pienitz, R., St. Onge, G. and Vincent, W.F. (2011) Holocene dynamics of the Arctic's largest ice shelf. *Proceedings of the National Academy of Sciences of the United States of America*, **108**(47), 18899-18904. doi: 10.1073/pnas.1106378108.

ArcGIS (2009) Spatial Analyst: IDW. *ArcGIS Desktop Help*.

Bogorodsky, V.V., Bentley, C.R. and Gudmandsen, P.E. (1985) *Radioglaciology*, D. Reiedel Publishing Co., Dordrecht, Netherlands, 272 pp.

Braun, C., Hardy, D.R., and Bradley, R.S. (2004) Surface mass balance of the Ward Hunt Ice Rise and Ward Hunt Ice Shelf, Ellesmere Island, Nunavut, Canada, *Journal of Geophysical Research*, **109**. doi: 10.1029/2004JD004560.

Comiso, J.C., Parkinson, C.L., Gersten, R. and Stock, L. (2008) Accelerated decline in the Arctic sea ice cover. *Geophysical Research Letters*, **35**(L01703). doi: 10.1029/2007GL031972.

Copland, L. (2009) *Review of Recent Changes in Canadian Ice Shelves*. University of Ottawa, Report prepared for Canadian Ice Service, 21 pp.

Copland, L. and Sharp, M. (2001) Mapping thermal and hydrological conditions beneath a polythermal glacier with radio-echo sounding. *Journal of Glaciology*, **47**(157), 232-242.

Copland, L., Mueller, D.R. and Weir, L. (2007) Rapid loss of the Ayles Ice Shelf, Ellesmere Island, Canada. *Geophysical Research Letters*, **34**. doi: 10.1029/2007GL031809.

Crary, A.P. (1960) Arctic ice island and ice shelf studies: Part II. *Arctic*, **13**(1), 32-50.

Dowdeswell, J.A. (In press) Eurasian arctic ice shelves and tidewater ice margins. In L.Copland & D.R. Mueller (Eds.), *Arctic Ice Shelves and Ice Islands*. Dordrecht: Springer SBM.

Dowdeswell, J.A. and Jeffries, M.O. (In press) Arctic ice shelves: An introduction. In L. Copland and D.R. Mueller (Eds.), *Arctic Ice Shelves and Ice Islands*. Dordrecht: Springer SBM.

Duguay, C.R., Pultz, T.J., Lafleur, P.M. and Drai, D. (2002) RADARSAT backscatter characteristics of ice growing on shallow sub-Arctic lakes, Churchill, Manitoba, Canada. *Hydrological Processes*, 16(8), 1631-1644.

England, J.H., Lakeman, T.R., Lemmen, D.S., Bednarski, J.M., Stewart, T.G. and Evans, D.J.A. (2008) A millenial-scale record of Arctic Ocean sea ice variability and the demise of the Ellesmere Island ice shelves. *Geophyscial Research Letters*, **35**. doi: 10.1029/2008GL034470.

Fofonoff, P. and Millard Jr, R.C. (1983) *Algorithms for computation of fundamental properties of seawater*. UNESCO Technical Papers in Marine Science 44, 58 pp.

Gibson, H.A.E. and Andersen, D.T. (2002) Physical structure of epishelf lakes of the southern Bunger Hills, East Antarctica. *Antarctic Science*, **14**(3), 253-261.

Hattersley-Smith, G. (1957) The rolls on the Ellesmere Ice Shelf, *Arctic*, **10**(1), 32-44.

Hattersley-Smith, G. (1966) Note on ice shelves off the north coast of Ellesmere Island. *The Arctic Circular*, **XVII**(1), 13-14.

Hattersley-Smith, G., Crary, A.P. and Christie, R.L. (1955) Northern Ellesmere Island, 1953 and 1954. *Arctic*, **8**(1), 3-36.

Hattersley-Smith, G., Fuzesy, A. and Evans, S. (1969) *Glacier Depths in Northern Ellesmere Island: Airborne Radio Echo Sounding in 1966*. Defence Research Establishment Ottawa, Technical Note **69**(6), 23 pp.

Jeffries, M. (1982) The Ward Hunt Ice Shelf, spring 1982. *Arctic*, **35**(4), 542-544.

Jeffries, M.O. (1986) Ice Island calvings and ice shelf changes, Milne Ice Shelf and Ayles Ice Shelf, Ellesmere Island, NWT. *Arctic*, **39**(1), 15-19.

Jeffries, M.O. (1987) The growth, structure and disintegration of Arctic ice shelves. *Polar Record*, **23**(147). doi: 10.1017/S0032247400008342.

Jeffries, M.O. (1991) Massive, ancient sea ice-strata and preserved physical-structural characteristics in the Ward Hunt Ice Shelf. *Annals of Glaciology*, **15**, 125-131.

Jeffries, M.O. (1992a). Arctic ice shelves and ice islands: origin, growth and disintegration, physical characteristics, structural-stratigraphic variability, and dynamics. *Reviews of Geophysics*, **30**(3), 245-267.

Jeffries, M.O. (1992b) The source and calving of ice island ARLIS-II. *Polar Record*, **28**(165), 137-144.

Jeffries, M.O. (2002) Ellesmere Island Ice Shelves and Ice Islands. In R.S. Williams, Jr. and J.G. Ferrigno (Eds.), *Glaciers of Canada*. U.S. Geological Survey Professional Paper 1386-J-1, Washington D.C.: U.S. Geological Survey.

Jeffries, M. and Serson, H. (1983) Recent changes at the front of Ward Hunt Ice Shelf, Ellesmere Island, N.W.T. *Arctic*, **36**(3), 289-290.

Jeffries, M.O., Sackinger, W.M., Krouse, H.R. and Serson, H.V. (1988) Water circulation and ice accretion beneath Ward Hunt Ice Shelf (Northern Ellesmere Island, Canada) deduced from salinity and isotope analysis of ice cores. *Annals of Glaciology*, **10**, 68-72.

Jeffries, M.O., Morris, K., Weeks, W.F. and Wakabayashi, H. (1994) Structural and stratigraphic features and ERS 1 synthetic aperture radar backscatter characteristics of ice growing on shallow lake in NW Alaska, winter 1991-1992. *Journal of Geophysical Research*, 99(C11), 459 -471.

Johnston, M.E. and Timco, G.W. (2008) *Understanding and Identifying Old Ice in Summer*. Ottawa: Canadian Hydraulics Centre, National Research Council, 236 pp.

Johnston, M., Frederking, R. and Timco, G. (2003) Property changes of first-year ice and old ice during summer melt. Technical Report, CHC-TR-010, 55 pp.

Jungblut, A.D., Mueller, D.R. and Vincent, W.F. (In press) Arctic Ice Shelf Ecosystems. In L. Copland and D.R. Mueller (Eds.), *Arctic Ice Shelves and Ice Islands*. Dordrecht: Springer SBM.

Kealey, C., Mueller, D. and Copland, L. (2011). *Canadian Ice Shelves Breaking up at High Speed*. [press release], September 27, 2011.

Keys, J.E. (1977) *Water Regime of Ice-Covered Fiords and Lakes*. PhD thesis, Marine Sciences Centre, McGill University, 75 pp.

Koenig, L.S., Greenaway, K.R., Dunbar, M. and Hattersley-Smith, G. (1952) Arctic Ice Islands. *Arctic*, **5**(2), 66-103.

Kovacs, A. and Morey, R. (1978) Radar anisotropy of sea ice due to preferred azimuthal orientation of the horizontal *c*-axis of ice crystals. *Journal of Geophysical Research*, **83**(C12), 6037-6049.

Lemmen, D.S., Evans, D.J.A. and England, J. (1988) Ice shelves of Northern Ellesmere Island, NWT. *The Canadian Geographer*, **32**(4), 363-367.

Lesins, G., Duck, T.J. and Drummond, J.R. (2010) Climate trends at Eureka in the Canadian High Arctic. *Atmosphere-Ocean*, **48**(2), 59-80. doi: 10.3137/AO1103.2010.

Lyons, J.B., Savin, S.M. and Tamburi, A.J. (1971) Basement ice, Ward Hunt Ice Shelf, Ellesmere Island, Canada. *Journal of Glaciology*, **10**(58), 93-100.

McBean, G., Alekseev, G., Chen, D., Førland, E., Fyfe, J., Groisman, P. Y., King, R., Melling, H., Vose, R. and Whitfield, P.H. (2005) Arctic Climate: Past and Present. *Arctic Climate Impact Assessment* (ACIA). Cambridge: Cambridge University Press, 40 pp.

Mortimer, C. (2010) Quantification of changes for the Milne Ice Shelf, Nunavut, Canada, 1950-2009. M.Sc. thesis, Department of Geography, University of Ottawa.

Mortimer, C., Copland, L. and Mueller, D.R. (2012) Volume and area changes of the Milne Ice Shelf, Ellesmere Island, Nunavut, Canada, since 1950. *Journal of Geophysical Research*. **117**(F04011). doi: 10.1027/2011JF002074.

Mueller, D. R., Vincent, W.F. and Jeffries, M.O. (2003). Break-up of the largest Arctic ice shelf and associated loss of an epishelf lake. *Geophysical Research Letters*, 30(20), 2031. doi: 10.1029/2003GL017931.

Mueller, D.R., Vincent, W.F. and Jeffries, M.O. (2006) Environmental gradients, fragmented habitats, and microbiota of a northern ice shelf cryoecosystem, Ellesmere Island, Canada. *Arctic, Antarctic, and Alpine Research*, **38**(4), 593-607.

Mueller, D.R., Copland, L., Hamilton, A. and Stern, D. (2008) Examining Arctic ice shelves prior to the 2008 breakup. *EOS, Transactions American Geophysical Union*, **89**, 502-503.

Mueller, D.R., Van Hove, P., Antoniades, D., Jeffries, M.O. and Vincent, W.F. (2009) High Arctic lakes as sentinel ecosystems: Cascading regime shifts in climate, ice cover, and mixing. *Limnology and Oceanography*, **54**(6, part 2), 2371-2385.

Narod, B.B., Clarke, G.K.C. and Prager, B.T. (1988) Airborne UHF radar sounding of glaciers and ice shelves, northern Ellesmere Island, Arctic Canada. *Canadian Journal of Earth Science*, **25**, 95-105.

Nyland, D. (2004) Profiles of floating ice in arctic regions using GPR. *The Leading Edge*, **23**, 665-668.

Onstott, R.G. and Shuchman, R.A. (2004) Chapter 3. SAR measurements of sea ice. In C.R. Jackson and J.R. Apel (Eds.), *Synthetic Aperture Radar Marine User's Manual*. Washington, DC: National Oceanic and Atmospheric Administration, 464 pp.

Paterson, W.S.B. (1994) The Physics of Glaciers, Third Edition. Elsevier Science, Birlington, MA, 481 pp.

Peary, R.E. (1907) *Nearest the Pole: A Narrative for the Polar Expedition of the Peary Arctic Club in the S. S. Roosevelt, 1905-1906*, Hutchinson, London, U.K, 411 pp.

Pope, S., Copland, L. and Mueller, D. (2012) Loss of multiyear landfast sea ice from Yelverton Bay, Ellesmere Island, Nunavut, Canada, *Arctic, Antarctic, and Alpine Research*, **44**(2), 210-221.

Prager, B.T. (1983) Digital signal processing of UHF radio echo sounding data from northern Ellesmere Island. M.Sc. thesis, Department of Geophysics and Astronomy, University of British Columbia, 97 pp.

Sensors & Software (2003) EKKO_View Enhanced & EKKO_View Deluxe User's Guide. Sensors & Software Inc, Mississauga, ON.

Serreze, M.C., Holland, M.M. and Stroeve, J. (2007) Perspectives on the Arctic's Shrinking Sea-Ice Cover. *Science*, **315**(5818), 1533-1536.

Short, N.H., and Gray, A.L. (2004) Potential for Radarsat-2 interferometry: glacier monitoring using speckle tracking. *Canadian Journal for Remote Sensing*, **30**(3), 504-509.

Short, N.H. and Gray, A.L. (2005) Glacier dynamics in the Canadian High Arctic from RADARSAT-1 speckle tracking. *Canadian Journal for Remote Sensing*, **31**(3), 225-239.

Spedding, L.G. (1977) *Ice Island Count, Southern Beaufort Sea 1976, Report IPRT-13ME-77, Arctic Petroleum Operations Association Project 99*, 50 pp.

Stroeve, J., Holland, M.M., Meier, W., Scambos, T. and Serreze, M. (2007) Arctic sea ice decline: faster than forecast. *Geophysical Research Letters*, **34**(L09501). doi: 10.1029/2007GL029703.

Van Hove, P., Swadling, K.M., Gibson, J.A.E., Belzile, C. and Vincent, W.F. (2001) farthest north lake and fjord populations of calanoid copepods *Limnocalanus macrurus* and *Drepanopus bungei* in the Canadian high Arctic. *Polar Biology*, **24**, 303-307. doi: 10.1007/s003000000207.

Van Wychen, W., Copland, L., Gray, L., Burgess, D., Danielson, B. and Sharp, M. (2012) Spatial and temporal variation of ice motion and ice flux from Devon Ice Cap, Nunavut, Canada. *Journal of Glaciology*, **58**(210), 657-664.

Veillette, J., Mueller, D.R., Antoniades, D. and Vincent, W.F. (2008) Arctic epishelf lakes as sentinel ecosystems : Past, present and future. *Journal of Geophysical Research*, 113 (G04014). doi: 10.1029/2008JG000730.

Veillette, J., Lovejoy, C., Potvin, M., Harding, T., Jungblut, A.D., Antoniades, D., Chénard, C., Suttle, C.A. and Vincent, W.F. (2011) Milne Fiord epishelf lake: a coastal arctic ecosystem vulnerable to climate change. *Ecoscience*, **18**(3), 304-316.

Vincent, W.F., Gibson, J.A.E. and Jeffries, M.O. (2001) Ice shelf collapse, climate change, and habitat loss in the Canadian high Arctic. *Polar Record*, 37(201). doi:10.1017/S0032247400026954.

Wadhams, P. (2000) *Ice in the Ocean*. Gordon and Breach Science Publishers, Amsterdam, 351 pp.

World Data Center A for Glaciology [Snow and Ice] (1978) *Arctic Sea Ice. Report*. Colorado: Institute of Arctic and Alpine Research, University of Colorado, Boulder, Colorado, Report No.: GD-2. 127 pp.